Thin films for Healthcare Acquired Infections (HAIs) prevention: materials preparation, testing and characterization.

THÈSE N^{O} 7121 (2016)

PRÉSENTÉE LE 29 JUILLET 2016

À LA FACULTÉ DES SCIENCES DE BASE

GROUPE PULGARIN

PROGRAMME DOCTORAL EN CHIMIE ET GÉNIE CHIMIQUE

ÉCOLE POLYTECHNIQUE FÉDÉRALE DE LAUSANNE

POUR L'OBTENTION DU GRADE DE DOCTEUR ÈS SCIENCES

PAR

Sami RTIMI

acceptée sur proposition du jury:

Dr H. Pick, président du jury
Prof. C. Pulgarin, directeur de thèse
Prof. S. Pillai, rapporteur
Prof. D. Dionysiou, rapporteur
Prof. P. Bowen, rapporteur

ÉCOLE POLYTECHNIQUE
FÉDÉRALE DE LAUSANNE

Suisse
2016

To the soul of my mother
To my father
To my brothers and sisters

قل إن صلاتي ونسكي ومحياي ومماتي لله رب العالمين ﴿.

Acknowledgements

First of all, I would like to thank Prof. César Pulgarin for having accepted me in his group to carry my research projects. These 4 years altogether were like a treasured journey for me. I would like to thank him for the lessons I learned from him. His lessons of science and his high experience in life changed my vue to the world.

I really feel very lucky to work and discuss jointly with Dr. PD John Kiwi. I really like his stories full of moral and experience. His advises and guidance helped me to build my scientific personality. Another person that marked my scientific carrier in Physics: the very professional Dr. Rosendo Sanjines, many thanks Sir.

I deeply thank Prof. Paul Bowen, Prof. Suresh Pillai and the big brain Prof. Dionysios Dionysiou for their tricky, inspiring and yet enjoyable questions during my thesis defense brilliantly presided by Dr. Horst Pick. I deeply appreciate our discussions during and after the exam. A special thank to Paul for his valuable carrier advices.

I would like to thank my friend Stefanos Giannakis, the tall guy with crazy diets, for all fun we had during our PhD time. I can not forget Oualid Baghriche (the crazy guy) Jelena Nesic (the Yugoslavian girl), Francesca Petronella and her nice Italian-English, Stefanos Papoutsakis for the challenging stories of strange competitions, the sensitive Laura Suarez, Cristina Ruales the bee of the lab, Juliette Ndounla the "Queen" and la "tonta" Alba Camarasa (a strange Catalan girl !!). I am starting a new sentence to thank Myriam Ballo, the Phd student with whom I share this project. We enjoyed together many parties and send-off parties of trainees and external collaborators…To all the GPAO people, the ones actually around or the people that passed through this castle. To Evelyne Toubes, "la belle dame souriante" and to our administrative assistant Véronique Bauler many thanks for your support. I also thank the adorable Karin Juillerat and Nathalie Miazza for the shared social events.

I can not let this opportunity without thanking my compatriots: Nadia Baati, Eya Damergi, Emna Belghith, Idriss Hindaoui and many others.

I thank also the sympathic walking computer Yoann Dind… André Fattet "le chef des chefs" and all his helpful and professional team, really: "Chapeau bas Messieur!!" Also, I thank the sympathic guys from the electronic shop and the chemical store (magazine chimie).

To all the people that they don't like me (insulting me in the back), thank you for giving me one more reason to go ahead and tease you more.

I really met a lot of nice people at EPFL that I will never forget them, thank you all.

…

Préface

Les traitements de surface font maintenant partie de l'ingénierie des matériaux dans de très nombreux secteurs industriels. Parmi ceux-ci les dépôts par voie sèche, souvent appelés dépôts physiques, connaissent un développement important ces dernières décennies du fait qu'ils sont, dans l'ensemble, moins polluants que les traitements par voie humide. Ces dépôts permettent de satisfaire aux normes les plus sévères comme ISO 14000. Les traitements de surface par dépôt physique ont été en grande partie limités aux technologies avancées : espace, aéronautique, nucléaire et électronique. Ceci est dû au fait qu'ils sont contrôlés par de très nombreux paramètres.

De nos jours, les dépôts physiques représentent un chiffre d'affaires trop élevée et leur importance économique ne cesse de croître d'année en année. L'activité économique dans ce domaine est développée surtout par les industries de revêtement tandis que la recherche dans ce domaine est faite par les laboratoires universitaires et centres de recherche. Le développement d'un revêtement nouveau demande non seulement une bonne connaissance du procédé de dépôt et de son matériau mais aussi des techniques qui sont utilisées pour tester les propriétés des couches déposées.

Il y a plusieurs difficultés à présenter les dépôts physiques. D'abord, la science et la technologie des dépôts sont pluridisciplinaires. Bien que la science des matériaux semble être la plus proche, elle ne couvre pas le développement des procédés des dépôts qui est souvent lié avec le génie chimique, la mécanique de fluide ou la physique atomique. Une autre difficulté majeure vient d'un relatif cloisonnement des activités basées sur les couches minces (dépôts atomistiques) et les couches épaisses (dépôts granulaires et massifs). Ce cloisonnement empêche souvent de choisir la technologie de dépôt la plus appropriée au besoin industriel.

Aujourd'hui les dépôts physiques envahissent les domaines biomédicaux pour les rendre plus compatibles avec leur environnement. La conception d'une composantes/outil biocompatible fait appel à plusieurs interactions difficiles à les contrôler. Ces interactions sont en générale liées aux réponses physiologiques des êtres-vivants en liaison direct avec le dépôt. La pluparts des implants médicales sont couvertes par des couches minces aidant à l'adhésion cellulaire avec des indices de cytotoxicité/génotoxicité négligeables voire inexistantes. Une autre application des dépôts physique dans le domaine biomédical est la synthèse des couches minces, voir nanométriques, à activité antibactériennes, antivirales, antifongiques....

Abstract

This thesis addresses the preparation of antibacterial surfaces for hospital facilities taking biomedical thin polymer films, textiles and catheter as probes. Magnetron sputtering is used to apply the coatings leading to fast bacterial inactivation in the dark and under low intensity light on the selected substrates. These coating are designed and prepared to achieve fast bacterial inactivation to avoid biofilm formation on textiles and polymer films and later on the catheter surface. The infection due to catheters is one of the major problem leading to catheter associated infections (CAIs). The design, preparation, testing and the characterization of the surface properties of uniform and adhesive TiO_2,TiO_2/Cu, Ag, Cu-films presenting fast bacterial inactivation kinetics on textiles and catheters by up to date HIPIMS and DCMS/DCPMS has been addressed very sparsely until now mainly on 3D objects. No evidence for Ag-Cu coating applied by sputtering covering uniformly the entire catheter surface has been reported up to this date. A modification of the sputtering unit was carried out to coat 3D objects and is one of the main novelties reported in this thesis.

The antimicrobial activity was tested on antibiotic resistant bacteria Methycillin resistant *Staphylococcus aureus* (MRSA) and *Escherichia coli* (*E. coli*) alone or jointly representing an important focus of infection by themselves or in the form of pathogenic biofilms in hospital facilities.

The bacterial inactivation kinetics was investigated in details under low intensity light and in the dark. The active part of the catheter remains under the patient skin (in the dark). Ag/Cu-has been selected since fast bacterial inactivation proceeds in with a quasi-instantaneous kinetics inducing a cytotoxicity below the limit authorized by the sanitary regulations for mammalian cells. These coatings are also well tolerated by osteoblasts. The sputtered films leading to fast bacterial inactivation and showing low cytotoxicity consisted mainly of TiO_2, Cu-TiO_2, and Ag/Cu films on 2D surfaces and on catheters with 3D-geometry. This is the first report for materials of this kind, their evaluation and surface properties.

Keywords: Biomedical textile, Catheters, Hospital Acquired Infections (HAIs), Ag/Cu-sputtering, 3D-geometry, Bacterial inactivation in the dark, Oligodynamic effect.

Table of content

Abbreviations

- HAIs: Hospital acquired infections
- CAIs : Catheter acquired infections
- *MRSA :* Methicillin Resistant *Staphylococcus Aureus*
- *E. coli: Escherichia coli*
- Ag: Silver
- Cu: Copper
- O_2: oxygen
- CVD: Chemical Vapor Deposition
- PVD: Physical Vapor Deposition
- CHUV: The University Hospital at Lausanne
- DNA: Deoxyribonucleic acid
- PE: Polyethylene
- LDPE: Low density polyethylene
- PES: Polyester
- HIPIMS: High Power Impulse Magnetron Sputtering ()
- DCMS : Direct Current Magnetron Sputtering
- DCPMS : Direct Current Pulsed Magnetron Sputtering
- UV: ultraviolet
- Vis: visible light
- TiO_2: Titanium dioxide
- TiO_2-CuOx: co-sputtered TiO_2 and CuOx
- TiO_2/Cu: sequentially sputtered TiO_2 followed with Cu
- FTIR: Fourier transform infrared spectroscopy
- Ar: Argon
- H_2O_2: Hydrogen peroxide
- cb: Conduction band
- vb: Valence band
- SC: Semi-conductor
- CFU: colony forming unit
- NPs: Nanoparticles
- ppb: parts per billion
- ZrN: Zirconium nitride
- Amps: Ampers
- XPS: X-ray photoelectron spectroscopy
- XRF: X-ray Fluorescence
- XRD: X-ray diffraction
- DRS: diffuse reflectance spectroscopy
- ICPMS: Inductively coupled plasma mass spectrometry
- HPLC: High performance liquid chromatography

- Weight: wt
- RF-plasma: Radio-frequency plasma
- Ra: roughness
- kJ: Kilojoule
- N_2: nitrogen

List of figures

Chapter 2

Chapter 3

Chapter 4

Chapter 5

Chapter 6

Chapter 7

List of tables

Chapter 1

Objectives and thesis structure

1.3. Objectives

During the last decade, there has been a growing interest in the design, synthesis and characterization of more efficient bactericide coatings due to the increasing resistance of toxic bacteria to antibiotics. This is a growing problem for human health with its associated higher health care costs. For instance, methycillin-resistant *Staphylococcus aureus* (MRSA) and *P. aureginosa* are the major causes for nosocomial hospital acquired infections (HAI) accounting for 70% of the bacteria infecting the people contracting with hospital acquired infections (HAIs) [1-5]. Antibacterial coatings are drawing attention in many industrial applications related to medicinal devices, food processing, water treatment, impregnation textiles and implants [6-9]. Biofilm formation on surfaces spreading bacteria on a continuous basis is considered the most dangerous source of toxic pathogenic infections.

The antibacterial and antiviral/fungicide surfaces containing Ag, Cu and Ti on highly resistant surfaces deposited from colloids and adhered to the substrate materials by calcination have been reported [10, 11]. Sol-gel commercial methods are used to prepare TiO_2 and Ag thin films on heat resistant substrates. However, the thickness of these sol-gel deposited films is not reproducible, they are not mechanically stable and they exhibit low adhesion since they can be wiped off by a cloth or thumb [12]. Colloid deposition on substrates require temperatures of few hundred degrees for an adequate adherence to the selected substrate. This calcination cannot be applied on low thermal resistant substrates like the polyester, polyethylene or polyurethane. The synthesis of uniform, adhesive, robust and effective bactericide films on 2D and 3D surfaces having a low thermal resistance like polymer films, textile and catheters is the objective of this thesis work.

Using Chemical Vapor Deposition (CVD) the bactericide precursors are heated in vacuum until decomposition. The released atoms/species condense on the substrate being this surface at a lower temperature mainly on heat resistant materials. The

disadvantages of the CVD deposition are the high investment costs, the high temperatures needed precluding film deposition on textiles like the polyester and the amount of heat used requiring costly cooling systems. Ag-films with nanoparticulates sizes ranging from 6 to 50 nm have been reported leading to bacterial inactivation under UV/Vis light irradiation. By Chemical Vapor Deposition (CVD) Ag-films have been deposited by Page et al., [13,14], Dunlop et al., [15] and Wang et al., [16].

1.4. Structure of the Thesis

This thesis is structured comprising chapters. The chapters are focused along a common objective addressing the preparation, testing and characterization of innovative antibacterial coated polymer/textile 2D surfaces and 3D catheters. Non-coated commercial polymers used extensively in hospitals grow easily bacteria/fungi biofilms. These bacteria biofilms on polyethylene (PE), polyurethane (PU) and polyester (PES) spread pathogens in hospital facilities. In Chapter 2, the current state of the art in this area is reviewed. Chapters 3-6 address in a detailed way the work focusing on the design, synthesis, evaluation and characterization of innovative antibacterial films. Chapters 3 to 7 constitute the main part of the thesis reporting in a comprehensive and systematic way the results obtained.

Chapter 3 describes the preparation of TiO_2-Cu co-sputtered polyester (PES) leading to the fast kinetic bacterial inactivation of Gram-negative *Escherichia coli* and Gram-positive *Staphylococcus aureus*. Sequential deposition of TiO_2 followed by a Cu/CuOx layer was investigated [17]. Sequentially sputtered TiO_2/Cu on polyester led to bacterial inactivation in the minute range but with a slightly high Cu-release that may pose some problem if used in implants. This is why we moved to the co-deposition of both oxides (TiO_2 and CuOx, from now TiO_2-Cu) to reduce the release of Cu but conserving the fast bacterial inactivation obtained with Cu alone as reported by Baghriche et al., 2012 [17]. In addition, a systematic comparison between the (photo)-catalytic bacterial inactivation activity against gram-negative bacteria and gram-positive bacteria was explored in details.

Chapter 4 addressed and investigated the co-deposition of TiO_2-Cu on PES using an up-to-date sputtering technology: High Power Impulse Magnetron Sputtering (HIPIMS). In this chapter, we stress the fast kinetics of bacterial inactivation, the structural details of the TiO_2-Cu PES coatings comparing the structure and performance of the HIPIMS coatings with the TiO_2/Cu on PES coatings obtained by Direct Current Magnetron Sputtering (DCMS).

Chapter 5 presents TiO_2 coating of polyethylene (PE). Low density PE (LDPE) is a low cost thin polymer membrane widely available material, chemically inert, mechanically stable and flexible, UV-resistant and does not oxidize in air under sunlight. For this reason PE has been selected as the support for the TiO_2 film depositions by HIPIMS and DCMS sputtering. The PE-TiO_2 films increase the quantum yield for light induced processes due to their transparency. TiO_2-PE is a uniform, non-scattering film and transparent due to the low size of the TiO_2 particles uniformly distributed on its surface. LDPE as a substrate is a promising polymer for biomedical applications (e.g. meshes, artificial joints, catheters…) due to its excellent chemical resistance, lightweight and flexibility. The limitations of the use of LDPE are generally related to its low surface energy and the non-polar nature. This precludes coating involving chemical bonding at relatively low temperature ≤ 100°C. Surface pretreatment techniques were used to generate polar groups at the PE surface facilitating TiO_2 bonding.

Chapter 6 addresses the deposition by sputtering of antibacterial binary metal-oxides on 3D polyurethane catheters sputtered by DCMS. Infections in the hospitals induced by catheters have increased during the last two decades. This has triggered considerable interest to fight catheters associated infections (CAI's) in hospitals. Catheters associated infections account for many of the hospital acquired infections (HAIs) and the improvement of films precluding the bacterial colonization are urgently required nowadays in general and in particular in the CHUV-facilities in Lausanne with whom the EPFL shares a grant to look into this problem of growing concern. Bacterial antibiotic resistance has rapidly increased in the last years due to the drastic overuse of antibiotic and the adaptation of the pathogens to the traditional antibiotics used to neutralize them.

Chapter 6 presents in a detailed way innovative catheters coated with Ag/Cu films leading to controlled and a continuous release of Cu or Ag in the ppb range to comply with the biocompatibility limits set by sanitary regulations for these metals. The Cu/Ag films release their constituent metals far below the cytotoxicity level allowed for mammalian cells. Sputtering Ag/Cu from a mixed target was carried out and the coating evaluated taking *E. coli* and MRSA as the probe pathogens of choice. To find the optimized metal ratios leading to the fastest bacterial inactivation kinetics, different Cu/Ag ratios were sputtered: 50%-50%, 33%-67% and 25%-75% of Cu%-Ag%. Bacterial inactivation on Cu/Ag coated catheters led to a loss of viability within the minute range under actinic light irradiation as used in hospital facilities. Bacterial inactivation in the dark was also investigated due to the fact that the needle of the catheter will be inserted under the skin (dark condition). This was an unexpected observation occurring in less than 30 min. Ag/Cu lead to bacterial loss of viability below 30 min. The importance of bacterial inactivation processes in the dark is that the bacterial/fungi inactivation proceeds on a permanent and continuous basis not needing any activation energy involving considerable costs over long-operational periods.

Chapter 7 presents the microstructure and the the oxidative states leading to the fast bacterial inactivation seen in chapter 6 for Ag/Cu coated catheters. This microstructure seems to play a crucial role in the bacterial inactivation dynamics.

Finally, Chapter 8 summarizes the most important findings of the Thesis, the conclusions and outlook to address in future work by the people/readership active in this area.

Chapter 2

Antibacterial active surfaces: biomedical textiles and catheters as examples.

2.1. Introduction

Hospital acquired infections (HAIs) are in the rise in Europe infecting 5-7% of hospital patients staying ≥10 days with the consequent high cost for the necessary healing process [18,19]. About 40% of these infections are due to catheter-associated infections (CAIs) when the catheters tube is inserted in veins for more two days amounting [20].

Thirty years ago Domek et al., [21] reported the inactivation effect of Cu on coliform, later Keevil's group reported the Cu inactivation of *MRSA* [22] and *E. coli* [23]. The Cu-ions released from coated surfaces were reported to be biocidal. Antibacterial agents reaching bloodstream infections were recently reported by I. P. Parkin [24]. The disinfection in some cases seems to proceed via an olygodynamic effect due to ppb/ppm amounts of Cu or Ag released by the biocidal surfaces [25]. Cu-ions have been shown to complex proteins and break hydrogen bonds within the DNA opening the double helix [26].

Antimicrobial surfaces are the object of increased attention and are being more widely applied to avoid infections on implants and catheters [27-30]. Recently, Yates et al., [31], Foster et al., [32] and Page et al., [27] reported CVD-deposition of Cu-titania films being applied in single or multilayer's coatings. The C-residues after the disinfection process were monitored by ATR-FTIR. Innovative films against MRSA have been reported for packaging materials [33], for plastics [34] and for stethoscopes [35]. Boyce et al., [36] found MRSA contamination up to 65 % in the hospital staff gloves and uniforms. This happens by direct contact in hospital infected rooms/surfaces. Later, Bhalla et al., [37] showed that in the gloves/uniforms of hospital workers who had touched contaminated surfaces with MRSA were always infected in variable amounts. It was also seen that microbial colonization occurs after 24 hours of insertion of a vascular catheter into a patient. The microbial biofilms adhere tightly to the catheter surface [38]. For this reason biofilm formation has to be precluded in the first place. Catheters on the market

are impregnated with antibiotics and showed short-term effect [39,40]. This was attributed to the low stability of the coating containing the antibiotic from one hand and to the increasing bacterial resistance to antibiotics from the other hand [36,25,17].

Studies have shown rapid killing of bacterial cells when exposed to Cu-surfaces but the mechanism of the Cu-MRSA killing is still controversial. It seems that Cu does not affect membrane integrity of cells. The Cu- antimicrobial effect seems to comprise the cellular metabolism damaging cell DNA [41]. In a recent study, the uptake of Cu-ions by MRSA was fast and damaged the cell DNA, but the mechanism of this uptake remains unknown [41]. The weak points of Cu, Ag, antibiotic and antiseptic coated catheters are:

a) They are not effective over long-operational times,

b) They lose the biocidal properties within short-times,

c) In some cases they are not compatible with mammalian cells, and

d) Antibiotic impregnated catheters diffuse their components and by doing so induce microbial resistance in the blood stream.

In the past few years, the continuous exposure to antibiotics over long times has led to increased antibiotic resistance of bacteria. But at present only a few pathogens display resistance to Ag and Cu [18,19,25,30]. Consequently, the development of innovative antibacterial films and innovative biocidal catheters like Ag/Cu should be investigated and are addressed in this thesis [45-46]. The use of DCMS, DCPMS and HIPIMS sputtering to prepare active, highly adhesive, uniform and stable Cu, Ag [45-46] and TiO_2 [47] antibacterial film addresses the objective chosen for this Thesis work. The approach we use to prepare these antibacterial coatings uses up-to date thin film technology. The stability of the innovative Ag/Cu coatings and films does preclude any metal nanoparticles entering the blood stream. Antibiotics/antiseptics used currently rapidly detach from the carrier surface entering the blood stream. This decreases very rapidly their antibacterial performance currently in use.

Recently, Heidenau et al., [29,30] demonstrated that Cu possess the most favorable ratio Cu:Ag inactivating bacteria compared to other metal. These surfaces presented also acceptable in vitro compatibility. Recent work In our laboratory with Cu-sputtered surfaces induced a faster kinetic bacterial inactivation [43,44] compared to Ag-sputtered surfaces [48,49].

TiO_2 surfaces in the dark are ineffective against bacterial infection, but Cu addition to TiO_2 surfaces introduce an effective antibacterial action under light and in the dark on medical implants [50,51]. TiO_2 has been reported to increase the adhesion of Cu on glass and other surfaces [31-32, 52].

Recently, high power impulse magnetron sputtering (HIPIMS) has gained increasing attention to deposit metal films on a variety of surfaces due to the high pulse power densities applied (kW/cm^2 range). This leads to very thin coatings presenting very effective bactericide effects. A high degree of ionization is attained by HIPIMS close to 70% [54-56] compared to conventional DCMS [53] showing ionization of 1%-5% and the pulsed-DCMS ionization of about 10%. HIPIMS pulses range from 1 microsecond and up to seconds and generate current densities of $10^{18}/m^3$. This is 10^4 times higher than that obtained with conventional DC-sputtering. In the present work we investigated the sputtering of Ag/Cu nanoparticles on polyurethane (PU) 3D catheters. This is an area that has not been addressed until now [45-46].

2.8. Thin Films Deposition

Conventional deposition techniques e.g. sol-gel or films prepared via colloidal route enable the synthesis of materials presenting a high thermal resistance leading generally to coating thickness in the micrometer range. Commercial sol-gel method have reported TiO_2 and other thin films on heat resistant substrates. But the thickness of these sol-gel deposited films is not reproducible, they are not mechanically stable and they exhibit low adhesion due to the fact that they can be wiped off by a cloth or thumb [18-19,47]. These traditional colloidal coatings require temperatures of few hundred degrees for an adequate adherence to the selected substrate. This approach does not work on low thermal resistant substrates like the polyester, polyethylene or polyurethane used in this study.

During the last four decades, the sputtering of surfaces was used to protect the surface against external corrosion. Nowadays, thin coatings are used for many purposes like anti-reflective, self-cleaning and/or self-sterilizing among of others. More recently, reactive sputtering methods (in the presence of O_2) have been carried out to deposit thin metal oxides on non-heat resistant substrates like textiles at temperatures <130 °C out of our laboratory. DCMS, DCPMS) [48] and HIPIMS [54] have been used to graft Ag-metal/oxide nano-particulate adhesive films on a variety of polymer thin membranes and

textile fabrics. The bacterial inactivation performance by Ag textiles in the dark and under light has been recently reported [17]. The Scheme in Figure 2.1 shows plasma assisted deposition methods used on different substrates.

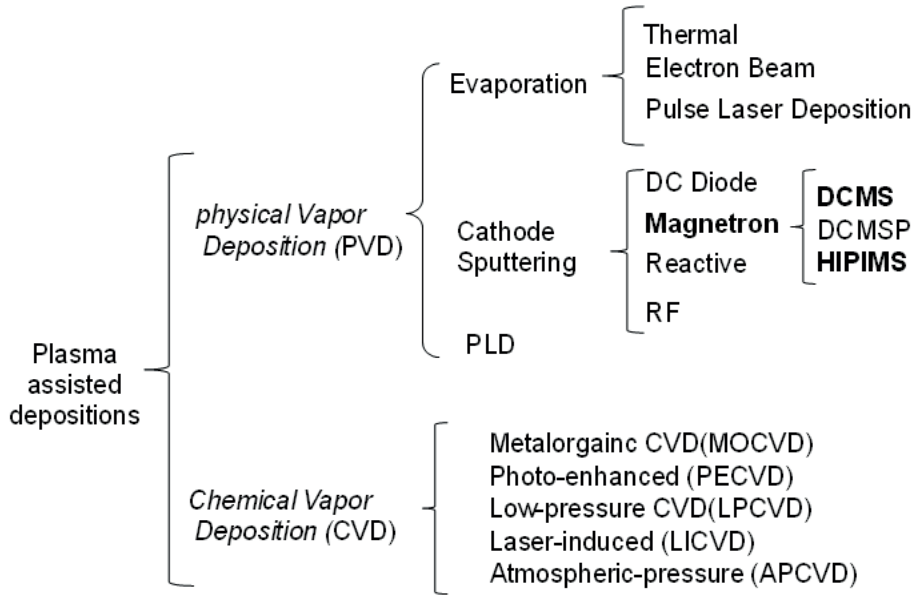

Figure 2.1. Plasma assisted deposition methods.

2.9. Physical vapor deposition coatings: Magnetron sputtering

Physical Vapor Deposition (PVD) is a coating process carried out in high vacuum at temperatures between 120 and 500°C. Solid coating materials (such as titanium, aluminum, zirconium) are either evaporated by heat or by bombardment with ions (sputtering) from a high-purity source called “target”. At the same time, a reactive gas (e.g. oxygen or Nitrogen) is introduced leading to a thin uniform adhesive metal/metal oxide film. In order to obtain a uniform coating thickness, the substrate is rotated at a pre-selected speed in a defined axe. The properties of the coating such as hardness, microstructure, chemical composition and adhesion can be accurately controlled. The PVD processes include arc evaporation, sputtering, ion plating, and enhanced sputtering. During the Thesis work, we will focus on the sputtering on non-heat resistant substrates like textiles and thin polymer membranes.

Magnetron sputtering is a widely used PVD technique to deposit thin films. This technique is based on the generation of low-pressure magnetically enhanced glow discharge plasma so called magnetron discharge. Figure 2.2 shows: a) the magnetron-sputtering chamber, (b) the sputtering process and (c) the target emission of metal and ions during the sputtering process.

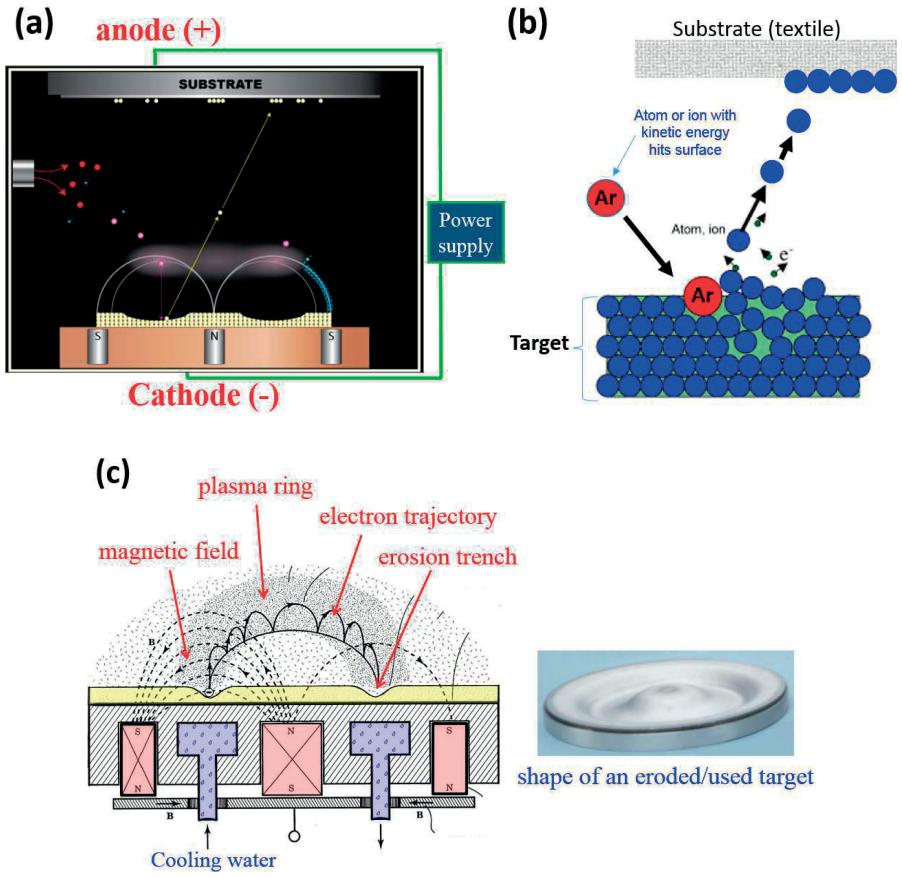

Figure 2.2. (a) Magnetron sputtering chamber and (b) sputtering process and (c) an eroded target.

The anode comprises the substrate used to fix the metal, metal-ions and composites coming from the target and the walls of the deposition chamber. After evacuation of the deposition chamber, the inert working plasma gas is introduced in the sputtering chamber. Argon (Ar) is typically chosen as the inert working gas. The name "argon" is derived from the Greek word “αργον”, neuter singular form of “αργος” meaning "lazy" or "inactive", as a reference to the fact that the element undergoes almost no chemical reactions. When

the plasma is established between the electrodes, positive ions from the plasma are accelerated towards the cathode. When the ions strike the cathode, momentum transfer results in the ejection of neutral atoms and secondary electrons. The neutral atoms travel to the substrate anode, where they are deposited, whereas the secondary electrons have an added ionizing effect on the plasma gas.

2.9.1. Direct Current Magnetron sputtering (DCMS)

The low rate deposition for a direct current deposition is proportional with the applied power to the target. To overcome this disadvantage, electromagnets can be placed behind the target(s) and the corresponding process is referred to as direct current magnetron sputtering (DCMS). As shown in Figure 2.2, the orientation of the electric and magnetic fields forces the electrons to follow a hopping trajectory close to the target leading to more collisions with the gas atoms. As consequence, a higher ions-flow is produced in the direction of the target. Increased ion flux leads to increase the deposition flux increasing the deposition rate.

2.9.2. Direct Current Pulsed Magnetron sputtering (DCPMS)

To prevent arc formation during the deposition, pulsed discharges can be introduced by neutralizing the surface charges. Positive charges accumulate near the target hindering the deposition. Periodic interruption of the negative DC-voltage eliminate the accumulated positive charges on the target. This process is called direct current pulsed magnetron sputtering (DCPMS). Kelly et al., [57] showed that enhanced film properties were achieved through the use of pulsed sputtering processing. This process is attractive because it offers stable arc free operating conditions during the deposition of functional films on architectural and automotive glass, or antireflective/antistatic coatings and displays [57].

2.9.3. High Power Impulse Magnetron Sputtering (HIPIMS)

By the application of HIPIMS to coat surfaces in the car and plane industries the anticorrosive Fe-Cr coatings applied at a high energy per pulse led to high-density coatings. In part this was due to the increased ionization of the sputtered species. Also, HIPIMS improved the direction of the flow of the metal-ions in the sputtering chamber. Furthermore, the plasma density of the conventional magnetron discharges increases with the applied power to the cathode. The maximum applied power to the cathode is limited

by the heat resistance threshold of the target during the pulse during the HIPIMS sputtering.

Nonetheless, to avoid the heating limitation the duration of the high power pulses can be shortened. A dead recovery period is introduced in a repetitive way that is sufficiently long so that the heat accumulated on the surface of the target can be removed. The HIPIMS sputtering requires a time consuming calibration before it can be applied (see annex 1 and 2). This technique has been reviewed by Helmersson et al. [58-59-60].

Sputtering processes of surfaces lead to an enhanced film uniformity, film adherence and compactness [43,48,52]. HIPIMS present an important development in the PVD field [57] and is gaining acceptance in many applications for surface treatments of metallic surfaces due to its high plasma density of $10^{19}/m^3$ compared to $10^{14}/m^3$ for DCMS and $10^{16}/m^3$ for DCPMS [52,57,60]. The inconvenience of HIPIMS is its slow rate of deposition.

2.10. Antibacterial surfaces

2.10.1. Catalytic/photocatalytic property of Silver and Copper surfaces

The bactericidal properties of Ag thin layers involve release of Ag^+-ions reacting with the bacteria cell wall, damaging the outer bilayers and translocating Ag-ions to the cytoplasm. Ag-ions are capable of penetrating the cell wall and interacting with the DNA. But there are still many open questions regarding the Ag- antibacterial mechanism [43,61-62]. Some reports showed that only Ag-ionic species present meaningful bactericide action compared to the metal-Ag [63].

Another biocide material is Cu/CuOx. This metal is found in the structure of many enzymes involved in electron transport and redox cycles in living microorganisms. CuOx can produce reactive oxygen species like H_2O_2 leading to the damage of the iron-sulfur enzymes or even DNA by generating free radicals [64]. The complete mechanism of bacterial inactivation by CuOx has not been completely worked out but it is suggested to be similar to the one suggested for the AgOx [65-68].

Borkow et al., [25], Sunada et al., [69] and Kiwi et al., [11,17,43,48,62,63] have recently shown that metal oxides of Ag and Cu play a major role in the antibacterial

behavior of powders and surfaces. They attributed this fact to the semi-conducting properties of the oxides formed by these metals in contact with air. These semi-conductors presenting narrow band-gaps are photo-activated by low intensity solar irradiation.

A semi-conductor (sc) is defined as a material that has an intermediate electrical conductivity between that of a conductor and an insulator. The excitation of a semiconductor is governed by the applied energy to its band- gap. When the applied energy is higher than the energy of the band-gap an electron is promoted from the valence band (vb) to the conduction band (cb) of the sc leaving a hole in the VB. Titanium dioxide (TiO_2) is one of the most used semi-conductors in catalysis/photocatalysis, water treatment, air treatment, self-cleaning and self-sterilizing processes due to its stability, lack of corrosion, and chemical inertness.

The intrinsic light absorption by TiO_2 induces the transition 2p (O) $\rightarrow$3d (Ti). The photo-generated electrons and holes interact with surface adsorbed molecules such as water and oxygen to form active radicals so called reactive oxygen species (ROS) [47]. The catalytic reaction of the TiO_2 involves the water, dissolved oxygen and the catalyst surface groups. Indeed, they are summarized in equations 1 and 2:

$$H_2O + h^+_{vb} \rightarrow {}^\circ OH + H^+ \qquad (2)$$

$$O_2 + e^-_{cb} \rightarrow O_2{}^{\circ -} \qquad (2)$$

At the molecular level, the photo-generated electrons tend to reduce Ti^{4+} to Ti^{3+} and the holes react with the bridging oxygen sites leading to oxygen vacancies and free °OH-radicals. Water molecules heal the oxygen vacancies producing OH-groups on the surface leading to the oxidation of Ti^{3+} into Ti^{4+} [47].

The performance of a TiO_2 can be improved as to increase the light absorption in the visible region by doping. Kiwi et al., recently reported that associating Ag and/or Cu oxides with other metal oxides hinders the photo-generated charges recombination through the introduction of intra-gap energy level midway between the cb and vb of TiO_2 facilitating the indirect transition of the electron trough the forbidden band [70].

2.10.2. Hospital acquired infections, bacterial resistance to antibiotics and antibacterial catheters

Hospital Acquired Infections (HAIs) has become a great challenge during the last decades. Statistics revealed deteriorating situation in developed countries like UK and European countries. About 1.7 million HAIs occurred leading to almost 99,000 deaths in 2002. This makes HAIs the sixth leading cause of death in the USA and Europe. Recently Peleg and Hooper [71] reported that gram-negative (gram-) bacteria are responsible for more than 30% of HAIs, and these bacteria predominate in cases of ventilator-associated pneumonia (47%) and urinary tract infections (45%) and account for about 70% in intensive healthcare units. Figure 2.3 shows the surfaces (textiles, polyethylene and catheters) in contact with the pateient in a healthcare room susceptible to host/bring infections. The preparation, characterization and antibacterial performance of these surfaces will be the focus of the present thesis.

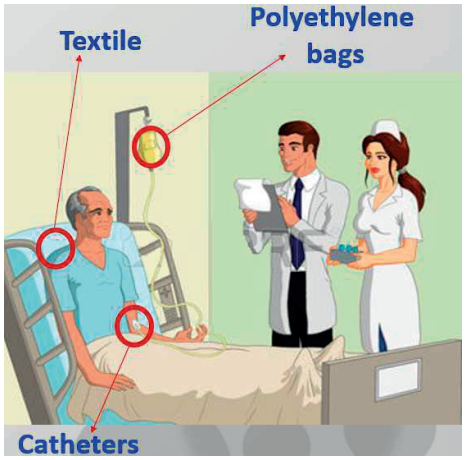

Figure 2.3. Surfaces hosting bacteria in hospital facility.

Gram negative bacteria have been described to be highly efficient at up-regulating or acquiring genes that code for mechanisms of antibiotic drug resistance. There are different modalities of acquisition of the antibiotic resistance for gram negative bacteria. This will not be discussed further during the presentation of this thesis.

The level found for a variety of infectious bacteria in many UK hospitals is higher than the allowed level for the hospital rooms. For example, the contamination of 10^5 CFU/cm^2 was observed in a diabetic wound dressing. But in the vicinity of the patient, a

microbial density of about 10^2 CFU/cm^2 was found. The use of Ag-textiles previously reported [48,63] should be sufficient to decrease significantly the room bacterial concentration, since we do not deal with a high bacterial concentration to start with. Research in this area for more effective antibacterial surfaces presenting a faster bacterial inactivation precluding the formation of biofilms is warranted. To eliminate the Ag-leaching during the textile washings [72] and keep at the same time a meaningful Ag-disinfection performance is one of the objectives when searching for more adhesive Ag-textiles. Ag reaching drinking and natural water bodies through furtive emissions is a recurrent problem due to the increasing amounts of Ag being used in different industrial processes.

Sputtered surfaces should in principle be able to reduce/eliminate the contamination of public hospitals from *E. coli* and MRSA. This is why we have focused our work on the sputtering of Cu/Ag-surfaces [62] presenting new Ag/Cu surfaces with almost no leaching of Cu/Ag. This is not the case for Ag-surfaces prepared by sol-gel methods used in wound pads and in disinfecting fabrics [62,72]. Ag-hydrophilic textiles like cotton are used to disinfect presenting a large uptake of water. The cotton provides an effective brewing media for bacterial colonization [73].

Inhibiting bacterial adhesion is essential to prevent implant-associated infection, because biofilm are extremely resistant to both the immune system and antibiotics [71]. To avoid bacterial colonization/adhesion, we coated catheters with Ag/Cu leading to continuous release of Cu or Ag-ions in the ppb range below the cytotoxicity limits allowed by sanitary regulations for mammalian cells. Sputtering Ag/Cu from mixed targets with different atomic ratios was determined to a) find the optimal amount of Ag/Cu to achieve the fastest bacterial inactivation kinetics and b) find the most suitable ratio between Ag and Cu for faster bacterial disinfection [45-46].

Commercial catheters impregnated with antibiotics or antiseptics or combination of both last for short operational lifetime. Microbial colonization on the catheter surface has been observed after 24 hours after insertion of a vascular catheter in the CHUV, Lausanne. The microbial biofilms attach tightly to the catheter surface [38] and this is the reason why biofilm formation has to be precluded in the first place.
The actual state of the art can be resumed as:

- Antibiotics impregnated as an adhesive layer on catheters present only a short-term effect. Gentamicin-sulfate on hydroxyapatite layers (Synthacer) elute up to 350 micrograms for up to 5 days and stops the release of the antibiotic after 10 days [40]. As effective drug carriers gentamicin [40] and amikacin [74] have worked towards the covalent bonding on vascular prostheses extending the release of the drugs with respect to less sophisticated grafting methods
- Minocycline-rifampin coated intravascular catheters showed a 0.3% intravascular infection ratio [75] but induce a drug a decrease in the resistance towards antibiotics over the years.
- Ag-coatings have been used widely to preclude the microbial colonization on catheters [27,28,18,19]. Ag-polyurethane catheters releasing Ag hinder microbial colonization and decreased by >50% microbial infections compared to catheters not coated with Ag for periods beyond 5 days [76].
- Catheters impregnated with antiseptics like chlorhexidine and Ag-sulfadiazine have been shown to be effective but present significant antimicrobial activity lasting for shorter times than the catheter action is required on the patient [77].
- Anti-adhesive films like hydrogels [8] and antimicrobial polymers [78] show also antibacterial action, but the adhesion and the uniformity of the antimicrobial agents does not reach the concentration needed to be highly effective.

Studies to date have shown rapid killing of bacterial cells when exposed to Cu-surfaces but the mechanistic action of Cu on MRSA remains controversial. Cu-surfaces induce a rapid antimicrobial effect comprising cellular metabolism and DNA damaging [44,18]. In a recent study, the uptake by MRSA of Cu-ions was reported, but the mechanism of this uptake remains unknown [44,18-19]. Ag-ions were investigated since they present a long effective operational time against bacterial colonization. Recent research explored oligodynamic effect of Ag-ions leading to bacterial inactivation occurring at ppb levels Ag-nanoparticles [79]. The antibacterial properties of Ag and Cu-ions eluting from Ag/Cu coated surfaces prepared by sputtering [18-20, 41-44] and took into consideration:

a) the wide antibacterial spectrum of Ag and Cu being nano-particles with a high oxidation potential,

b) Ag and Cu in the ppb range (micrograms) are only necessary to inactivate bacteria/fungi/virus. The ppb-release is believed to depend on the coating network and the surrounding biological medium. In many cases Ag and Cu fast bacterial inactivation proceed with a low cytotoxicity below the standards allowed in mammalian cells.
c) Ag and Cu coatings have shown acceptable inactivation kinetics in minutes/hours ranges,
d) The long-term bio-compatibility (from 5 to 30 days) is not known at the present time and will not be monitored as part of this thesis [31-32].

Cu-Ag coated surfaces offer an innovative way for preventing catheter-associated infections [16,47,52] against *E. coli*, MRSA, *P. Aeruginosa* and fungi. No catheter Cu-coated surfaces showing stable long-term effective antibacterial performance has been reported so far.

The Cu-induced bacterial inactivation kinetics work recently reported [46,17] used as initial bacterial concentration 10^8 CFU/ml. The level of contamination found in public hospitals in the UK of ~10^5 CFU/cm^2 in a diabetic wound dressing and it is much above the level found in a common hospital room of 10^2 CFU/cm^2. Therefore, Cu-sputtered surfaces should be able to eliminate bacteria in the presence of a low bacterial concentration as found in hospital facilities [34].

During the last few years, Prof. Pulgarin's laboratory have addressed the bacterial inactivation of *E. coli* by Cu/CuOx-textiles prepared using Rf-plasma Magnetron sputtering [43], DCMS [80], DCPMS [81] and HIPIMS technologies [82,83]. The performed experiment during these studies followed the standard methods to determine the *E. coli* concentration described in reference [49] (ISO 27 447: 2009) and for the evaluation of the MRSA inactivation was recently described [44].

The work described in this thesis involves reactive and non-reactive magnetron sputtering offering many advantages such as the uniformity of the coating, the high adhesion to the substrate and the relatively low-temperature of deposition on low thermal resistant substrates. This approach is less aggressive compared to CVD, and it is easily scaled-up for industrial applications. The use of energetic-ions and controlled-ion

bombardment can modify the nucleation process, improve the film adhesion, change the grain size and crystallite preferential orientation and achieve an effective antibacterial action employing very thin films [48,52]. The correlation between roughness and bactericide inactivation has been recently reported for Ag-ZrN surfaces [49].

In general, when a semi-conductor (e.g. TiO_2, Ag_2O, CuOx…) is photoexcited, electron-hole pairs are generated and separated at the semi-conductor surface. In the case of photoexcited TiO_2, the electrons in the conduction band tend to reduce Ti^{4+} to Ti^{3+} and the photo-generated holes (in the valence band) react with oxygen generating oxygen vacancies and free OH-radicals. Adsorbed water molecules react with the oxygen vacancies producing OH groups and oxidizing Ti^{3+} into Ti^{4+}.

2.11. Set-up optimization for deposition on 3D shape catheters

More effective and stable coated antibacterial catheters are needed now to prevent intravascular infections. For this reason, during the last 2 years at the EPFL, we modified the DCMS, DCPMS sputtering equipment to coat effectively Cu on the 3D cylindrical catheter surface. This modification is shown in Figure 2.4. The metal targets are in the lower part of the deposition chamber, in positions (1) and (2). In the case of standard substrate holder (3), the position of the metal-targets with respect to the flat substrate makes the ions follow the direction of the axis perpendicular to the metal-target until they reach the sample. Since the ionization degree attained by DCMS is around 1-5%, the attachment of this positive plasma flow is effective only on the top of a negatively biased substrate. The new holder (4) can clutch cylindrical and more complex-shaped objects. The axial rotation of the holder (4) and the application of negative bias ensure a Cu-uniform distribution on the catheter tube surface.

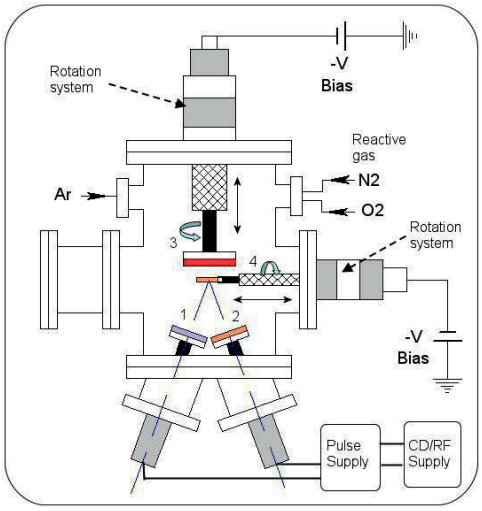

Figure 2.4. Schematic of the Pulsed Magnetron unit for catheter sputtering: (1) and (2) magnetron cathodes for Ti and Cu targets, (3) rotary substrate holder for flats surfaces with axial variable positioning possible (4) retractable axial rotary substrate holder for catheter. Both substrate holders can be biased.

2.12. Surface pretreatment of surfaces/textiles

To bind the Ag/Cu/TiO_2 layers on textiles, polyethylene (PE) and polyurethane (PU) surfaces sometimes it is hard to bind the coating to the substrate. Rf-plasma surface pretreatment introducing polar negative groups like carboxylate, peroxides –O-O- enhancing/modifying textile surfaces was reported by Kiwi et al., [85] This lead us to pretreat textiles by RF-plasma in the presence of residual O_2 to introduce the O-containing negative polar groups on the activated sustrate surfaces. These sites introduce additional bonding functionalities able to attach the Ag found in colloidal suspension.

2.12.1. RF-plasma pretreatment

Fabrics were pretreated in a RF-plasma cavity (Harrick Corp. 13.56 MHz, power 100 W). Generally for RF-plasma, low pressures are used to increase the capture length of the electrons generated in the electric field generated in the RF-chamber. The RF-plasma is created when a gas is exposed to an electromagnetic field within radio frequencies. Vacuum at 1 torr avoids the collisions between the electrons allowing the electrons to react with residual O_2. In the low temperature plasma, the gaseous ions present temperature ranges between ambient and few hundred degrees, but the electrons have transient energies corresponding to high temperature values. The system is not under

thermal equilibrium. The activated RF-plasma interacts with oxygen leading to atomic, excited O^*, anionic O^- and cationic O^+, giving rise to carboxyl, per-carboxylic, peroxides, lactam etc able to chelate/complex or/and attach by electrostatic attraction with the partial positive Ag-species. Without vacuum, the RF-plasma induces a localized heating breaking intermolecular H-bonds and generating for very short times temperatures >160°C able to segment the textile [85-89]. The introduction of additional O-containing air creates binding sites for metal/oxide binding at the textiles surface.

2.12.2. Functionalization of fibers by atmospheric or vacuum UVC

The textile polymer surface can also be functionalized by UVC light irradiation using the 185 nm line (6W) from a 25W (254 nm + 185 nm light) low-pressure mercury lamp (Ebara Corp. Tokyo, Japan). UVC activation having a lower energy than the RF-plasma, does not lead to cationic or anionic oxygen species in the gas phase. Only atomic (O) and excited oxygen (O^*) species under UVC are obtained. The energy necessary for the $O_2 \rightarrow 2O^*$ reaction is at the wavelength 241 nm (495 kJ/mole). The absence of cationic or anionic oxygen species when pre-treating with UVC leads to a more uniform TiO_2 layer of the textile surfaces and has been reported in the literature [30].

The O_2 cross section is 10^{-20} cm^2 and the molar absorption coefficient εO_2 (185 nm) ~26 M/cm^{-1} [47,85]. The cross section of N_2 is about 10 times smaller than for O_2 at this wavelength. Therefore, the εN_2(185 nm) would be negligible. At 185 nm the extinction coefficients of O_2 and N_2 are so low, that practically no UVC-radiation is lost in the optical pathway between the light source and the sample even at atmospheric pressures. Figure 2.5 below shows a schematic for oxygen activation by RF-plasma or UVC. The negative polar groups like: COO-, -O-O- and other -O-C- were obtained by surface pretreatment (RF-plasma or UVC) and were identified/quantified using X-ray photo-electron spectroscopy (XPS) or titrated with a base.

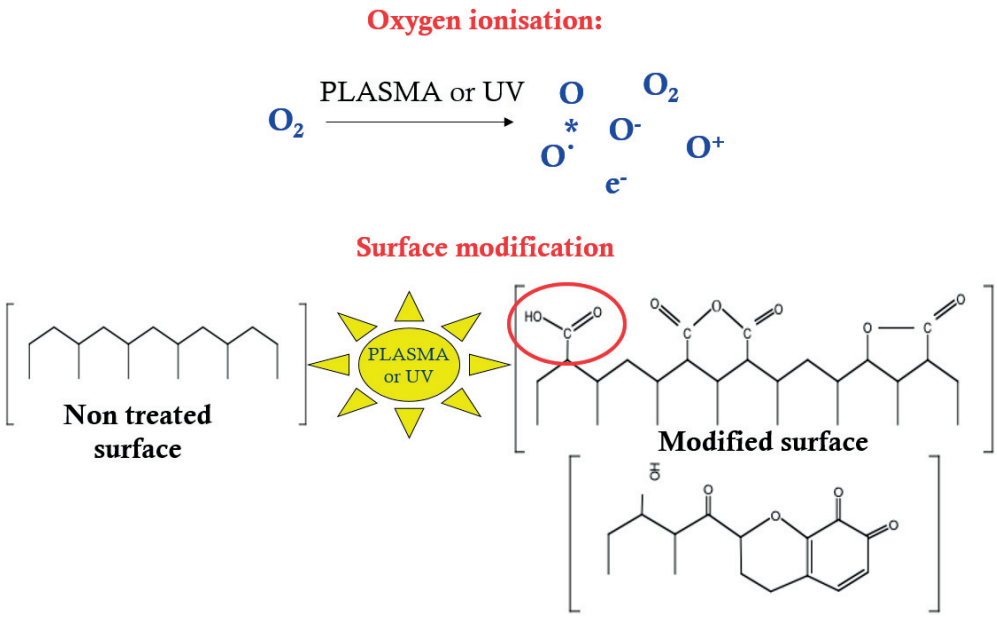

Figure 2.5. Schematic of surface pretreatment by Rf-plasma and UVC to generate surface functionalities.

Chapter 3

Co-sputtered polyester showing duality in the *E. coli and* MRSA bacterial inactivation under actinic light

This chapter is based on the following publication: S. Rtimi, M.K.S. Ballo, D. Laub, C. Pulgarin, J.M. Entenza, A. Bizzini, R. Sanjines, J. Kiwi, Applied Catalysis A: General 498 (2015) 185–191 (Reproduced with permission of Elsevier, Copyright 2015).

3.1. Introduction

Recently, some laboratories [1,90,5,15], have reported antibacterial Ag, Cu and TiO_2 coatings on glass and polymer films depositing the metal/oxides by CVD and sputtering techniques. Studies on the photo-activated TiO_2 and Cu-TiO_2 mediated bacterial inactivation have been reported [10,91-92]. There is a need for active, uniform and adhesive surfaces to decrease more effectively environmental risks associated with HAIs. In this chapter we report DCMS co-sputtering of TiO_2 and Cu films leading to uniform, adhesive and robust layers on polyester (PES) at temperatures not exceeding 120-130°C. This approach allows the sputtering of antibacterial films on textiles and polymers presenting a low thermal resistance.

Recent studies [93-96] report the preparation of Cu and TiO_2/Cu films by sol-gel methods inducing significant bacterial inactivation under UV-visible light. Nevertheless, the sol-gel films are not mechanically stable, nor reproducible, present low uniformity and little adhesion [12]. This moved us to work on the preparation of sputtered antibacterial films to overcome the shortcomings of colloidal loaded films.

Escherichia coli (*E. coli*) and MRSA inactivation on Cu-sputtered polyester (Cu-PES) [95,18] have recently been reported by our laboratory [44]. This study is a continuation of previous work on TiO_2/Cu surfaces leading to *E. coli* [49] reduction, focusing on new aspects to show: a) the bacterial reduction on novel TiO_2/Cu co-sputtered PES, b) the differential effect of the applied actinic/visible light (400-700 nm) on the bacterial reduction kinetics of *E. coli* and MRSA, c) the stabilizing effect of TiO_2 on the Cu release from the co-sputtered surfaces during bacterial reduction/inactivation compared to Cu sputtered

individually, d) by inductively coupled plasma mass spectrometry (ICP-MS) to account for the Cu-oligodynamic effect leading to bacterial reduction and finally e) the effect of a co-sputtered catalyst TiO_2/Cu-PES on the bacterial reduction kinetics of Gram+ and Gram- bacteria, as well as the effect of actinic/visible intensity on bacterial reduction.

The novelty of this work is the preparation of highly performing, uniform, adhesive and robust TiO_2/Cu on PES textile using magnetron sputtering. Co-sputtering TiO_2 and Cu/CuOx simultaneously led to fast bacterial inactivation kinetics with a surprisingly low release of Cu compared to Cu sputtered alone on PES.

3.2. Experimental Section

3.2.1. Catalyst Preparation

The PES used corresponds to the EMPA test cloth sample No 407. It is a polyester Dacron polyethylene terephthalate, type 54 spun, 130 microns thick, plain weave ISO 105-F04. Direct current magnetron sputtering deposition of Ti and Cu was carried out in a CMS-18 Vacuum system from Kurt Lesker Ltd. evacuated to $5.8x10^{-3}$ mbar by a turbo-molecular pump. The Cu as well as the Ti target were 2 inches in diameter, 99.99% pure from K. Lesker Ltd. UK. Co-sputtering was carried out at 300 mA. The Ti and Cu targets used for the co-sputtering were positioned at 10 cm of the PES substrate. The nominal calibration of the film thickness was carried out on the Si-wafers and the film thickness was determined with a profilometer (Alphastep500, TENCOR).

3.2.2. Catalyst Characterization:

3.2.2.1. Surface loading and ions release during bacterial inactivation

The X-ray fluorescence (XRF) determination of the Ti and Cu on PES was evaluated in a PANalytical PW2400 spectrometer. A Finnigan™ ICP-MS (Inductively Coupled Plasma-Mass Spectrometry) was used to determine the Ti and Cu release during the bactericidal cycles with a resolution of $1.2x10^5$ cps/ppb and detection limit of 0.2 ng/L. A washing solution of the TiO_2/Cu samples were digested with nitric acid 69% (1:1 HNO_3 + H_2O) to remove the organics in the solution and to guarantee that there were no remaining ions adhered to the flacon wall. The samples droplets were introduced to the ICP-MS trough a peristaltic pump to the nebulizer chamber at ~7700°C allowing the evaporation

and ionization of the elements in the sample. The Cu and Ti found in the nebulizer droplets were subsequently quantified by mass spectrometry.

3.2.2.2. Diffuse reflectance spectroscopy (DRS)

Diffuse reflectance spectroscopy (DRS) was carried out in a Perkin Elmer Lambda 900 UV-VIS-NIR spectrometer within the wavelength range of 200-800 nm. The rough UV–Vis reflectance data cannot be used directly to assess the absorption of the TiO_2/Cu/CuO-PES samples because of the large scattering contribution of the PES fabric to the DRS spectra. Normally a weak dependence is assumed for the scattering coefficient S on the wavelength. The spectra were plotted in Kubelka-Munk (KM) units.

3.2.2.3. High-resolution transmission electron microscopy (HRTEM) and stereomicroscopy

The transmission electron microscopy (TEM) required the PES fabrics embedding in epoxy resin (Embed 812) and cross-sectioned with an ultra-microtome (Ultracut E) up to a thin section of 70 nm for TEM images. The used microscope was a CM12 (120 kV).

The fluorescence stereomicroscopy was carried out on samples inoculated with 10^8 CFU of *E. coli* and incubated for 2 hours in a humidification chamber. This method uses a fluorochrome-based staining procedure from Filmtracer™ LIVE⁄DEAD® Biofilm Viability Kit (Molecular Probes, Invitrogen). The kit contains a combination of the SYTO 9® green fluorescent nucleic acid stain and propidium iodide fluoro-chromes for the staining of live and dead cells, respectively. The sample fluorescence was monitored in a fluorescence stereomicroscope (Leica MZ16 FA, Leica Microsystems GmbH Wetzlar, Germany) and the images were processed using the LAS v.1.7.0 build 1240 software from Leica Microsystems CMS GmbH. Adhesion of bacteria to the sputtered PES was allowed for 2 min before washing the sample with sterile Milli-Q water to remove non-adherent bacteria.

3.2.2.4. X-ray-photoelectron spectroscopy (XPS)

The XPS of the samples was carried out in an AXIS NOVA unit (Kratos Analytical, Manchester, UK) equipped with monochromatic AlK_α ($h\nu$ = 1486.6 eV) anode and the deconvolution software CasaXPS-Vision 2. The carbon C1s line with position at 284.6 eV was used as a reference to correct the charging effects. The surface atomic concentration of some elements was determined from the peak areas and known sensitivity factors [97-98]. Spectrum background was subtracted using the program of the Kratos unit. The

etching depth induced by the Ar-ions was referenced to the etching of Ta of 15 atomic layers per minute equivalent to ~3 nm/min.

3.2.3. Catalytic tests

3.2.3.1. Bacterial reduction and irradiation sources

Unsputtered and sputtered PES samples were sterilized in 70% ethanol and dried overnight at room temperature (RT). Cultures for the preparation of the MRSA ATCC 43300 and *E. coli* K12 inoculum were prepared by picking a single bacteria colony from the agar plate and incubated in tryptic soy broth at 37ºC overnight. Overnight cultures of the microorganisms were washed two times in 0.9% NaCl and lately diluted to the selected concentration.

E. coli K12 strain was obtained from the Deutsche Sammlung von Mikroorganismen und Zellkulturen GmbH (DSMZ) ATCC23716, Braunschweig, Germany, to test the antibacterial activity of the co-sputtered samples. The PES fabrics were sterilized by autoclaving at 121°C for 2h. The 20 µL culture aliquots with an initial concentration of ~10^6 CFU mL^{-1} in NaCl/KCl (pH 7) were placed on coated and uncoated (control) PES fabric. Samples were then placed on Petri dishes provided with a lid to prevent evaporation. After each determination, the fabric was transferred into a sterile 2 mL Eppendorf tube containing 1 mL autoclaved NaCl/KCl saline solution. This solution was subsequently mixed thoroughly using a Vortex for 3 min. Serial dilutions were made in NaCl/KCl solution. A 100 µL aliquot was pipetted onto a nutrient agar plate and then spread over the surface of the plate using standard plate method. Agar plates were incubated lid down, at 37°C for 24h before colonies were counted. Three independent assays were done for each sputtered sample during the course of this study. To verify that no re-growth of *E. coli* occurs after the first bacterial inactivation cycle, the TiO_2/Cu-film was incubated for 24 hours at 37°C. Then, the bacterial suspension of 100 µL was deposited on three Petri dishes to obtain replicates. The samples were incubated at 37°C for 24 h. No bacterial re-growth was observed for these samples.

For MRSA testing, PES samples (4 cm^2) were inoculated with 20 µl of cell culture and incubated for 30, 60 and 120 min in a humidified chamber at room temperature (RT) in the dark or under light. The temperature inside the light box was maintained (20-23 °C).

Bacterial loss of viability on TiO_2/Cu-PES samples was then evaluated by direct agar transfer plate (incubated at 37 °C).

3.2.3.2. Irradiation sources

The irradiation of the *E. coli* and MRSA bacteria on the co-sputtered samples was carried by a Philips Master TLD-18W/865 actinic lamps as used in hospital facilities with an emission between 400 and 720 nm with different light doses between 1.01 mW/cm^2 up to 4.65 mW/cm^2.

3.3. Results and discussion

3.3.1. Surface characterization of sputtered TiO_2/Cu-PES

Co-sputtering Ti and Cu for 3 min in Ar-O_2 atmosphere led to a coating thickness of ~135 nm (equivalent to ~700 atomic layers). The Cu, TiO_2 and TiO_2/Cu content were determined by X-ray fluorescence (XRF) and are reported in Table 3.1. The amounts of Cu, and TiO_2 are seen to increase with sputtering time as expected.

Table 3.1. Cu, TiO_2 and TiO_2/Cu determined by X-Ray Fluorescence (XRF) as a function of the DC-sputtering time.

Sample	%wt Cu/wt PES	%wt CuO/wt PES	%wt Ti/wt PES	%wt TiO_2/wt PES
Cu (5 min)	0.19	0.24	--	--
Cu (3 min)	0.16	0.20	--	--
Cu (1 min)	0.05	0.07	--	--
TiO_2 (5 min)	--	--	0.18	0.20
TiO_2 (3 min)	--	--	0.12	0.14
TiO_2 (1 min)	--	--	0.09	0.10
TiO_2/Cu (5 min)	0.09	0.11	0.11	0.17
TiO_2/Cu (3 min)	0.06	0.07	0.10	0.14
TiO_2/Cu (1 min)	0.02	0.04	0.02	0.03

It is important to note that TiO_2 sputtered for ~2 min has an equivalent to the amount of TiO_2 co-sputtering TiO_2/Cu for 3 min. CuO sputtered for ~1 min deposited Cu equivalent to a Cu/TiO_2 film co-sputtered for 3 min.

The diffuse reflectance spectra (DRS) show an increase in the optical absorption as a function of the co-sputtering time in Kubelka-Munk units up to 3 min as shown in figure 3.1.

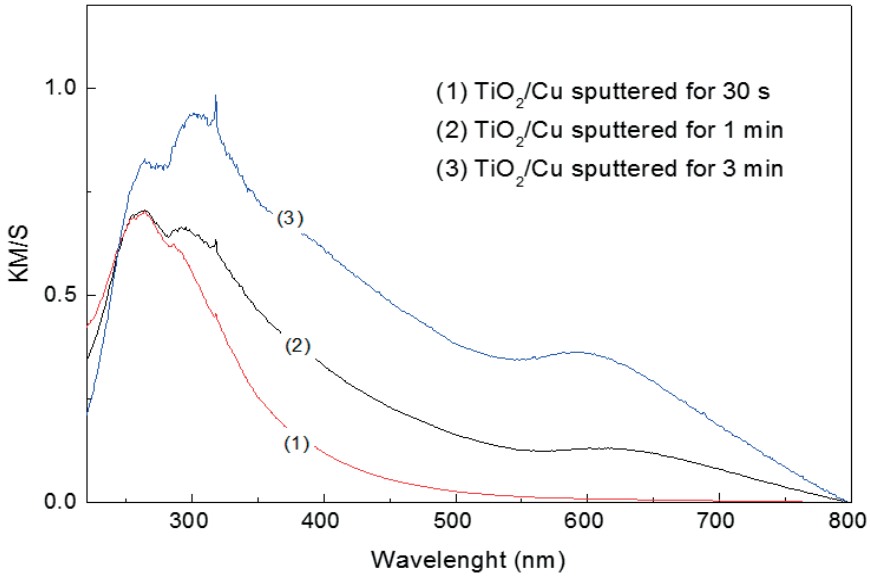

Figure 3.1. Diffuse reflectance spectroscopy (DRS) of co-sputtered TiO_2/Cu on PES for the times: 1) 30 s, 2) 1 min and 3) 3 min.

The wide spectral range for Cu(I)/Cu(II)-species between 200 and 800 nm extending allows a considerable absorption of the actinic light between 400 and 700. The optical absorption between 500 and 600 nm is due to the inter-band transition of Cu(I) and the absorption between 600 to 720 nm is attributed to the exciton band and the Cu(II) d-d transition [98,95].

Figure 3.2 shows the transmission electron microscopy (TEM) of TiO_2/Cu co-sputtered for 3 min on PES. The more dense Cu-clusters presented diameters between 16 and 20 nm while the TiO_2 clusters revealed smaller sizes between 5 and 10 nm. The TiO_2/Cu coating of 120 to 160 nm thick (500 to 800 atomic layers) presented a close contact between the TiO_2 and Cu-nanoparticles.

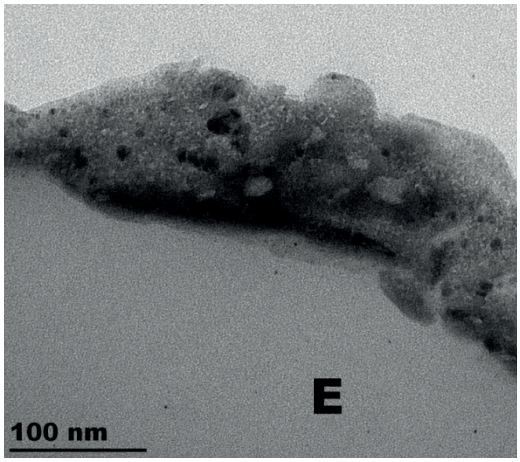

Figure 3.2. Transmission electron microscopy (TEM) of TiO_2/Cu co-sputtered for 3 min on PES. E stands for the epoxide that is required to embed the sample during the preparation of the TEM image.

3.3.2 Evaluation of the *E. coli* reduction and effects of the applied light doses

Figure 3.3 shows the bacterial reduction by TiO_2/Cu-PES under actinic light irradiation and in dark as a function of TiO_2/Cu co-sputtering times. PES by itself in the dark and actinic light does not reduce *E. coli.* But in the dark, *E. coli* bacterial reduction proceeds within 120 min in the dark on TiO_2/Cu-PES. The mechanism of TiO_2/Cu mediated *E. coli* inactivation under light irradiation has been reported in detail and for this reason it will not be addressed in the present study [95,93]. Reduction in the dark as shown in Figure 3.3, trace 4 proceeds through a mechanism involving the reaction of O_2 (air) with the Cu^0/Cu-ions. It will be discussed below in the XPS section and to suggest a possible reaction mechanism. Figure 3.3, trace 1 shows the complete bacterial reduction under visible light within 30 min for TiO_2/Cu samples co-sputtered for 3 min. In this case, sufficient amount of TiO_2 and Cu was coated on the PES leading to a number of exposed catalytic sites inducing the fastest *E. coli* load reduction (see Table 3.1).

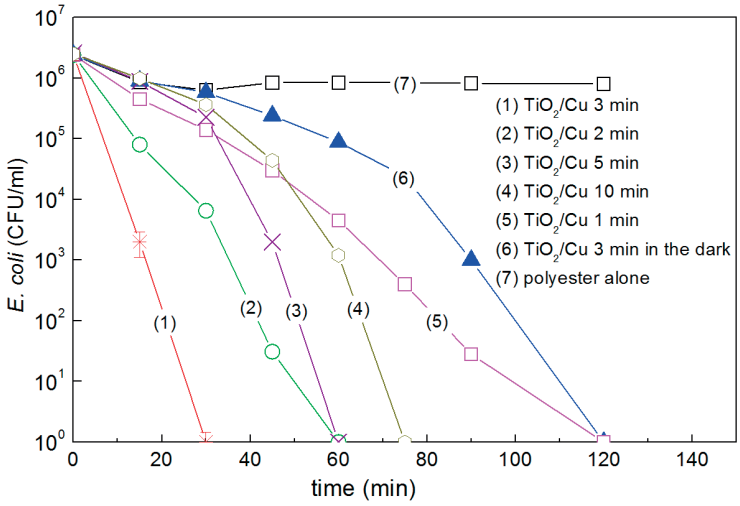

Figure 3.3. *E. coli* inactivation on TiO_2/Cu co-sputtered for different times on PES as indicated in the traces: (1) 3 min, (2) 2 min, (3) 5 min, (4) 10 min, (5) 1 min (6) 3 min in the dark and (7) PES-alone. The bacterial reduction under light irradiation used a lamp Philips Master-18W/865 (4.65 mW/cm^2).

Co-sputtering for 1 and 2 min (Figure 3.3, traces 2 and 5) did not attain the necessary TiO_2 and Cu active sites to induce fast bactericidal activity. Co-sputtering TiO_2/Cu for 5 and 10 min (Figure 3.3, traces 3 and 4) led to longer bacterial inactivation kinetics compared to TiO_2/Cu (3 min). This may be due to the inward charge diffusion [17,3]. In addition, longer sputtering times facilitate the TiO_2 inter-particle growth decreasing the TiO_2 contact surface with bacteria [47,52]. Figure 3.3, trace 6 shows the complete bacterial reduction in the dark. This is an important result showing that even in the absence of light (dark/actinic light switched off), the bacterial reduction continue to proceed. The effect of Cu on bacteria has been associated with the ingestion of copper leading to adverse reactions with transport-proteins of enzymes regulating the respiratory chain [30,93,98-101].

Figure 3.4 show that TiO_2/Cu-PES surfaces damage the *E. coli* cell wall more than the TiO_2 surface under light and in the dark due to the added effect of cytotoxic Cu. This suggests that *E. coli* damage is located at the cell wall [47] in contact with the bactericide TiO_2/Cu-PES surface in Figures 3.4. TiO_2 and Cu on PES proceeded with a similar trend in the bacterial reduction kinetics in Figure 3.4. Increased Cu-loading on PES led to faster bacterial inactivation kinetics, but this effect was not observed in the case of TiO_2 (Figure

3.4). Figure 3.4 also presents the effect of the actinic light intensity on the *E. coli* reduction mediated by TiO_2/Cu-PES surface at different light intensities.

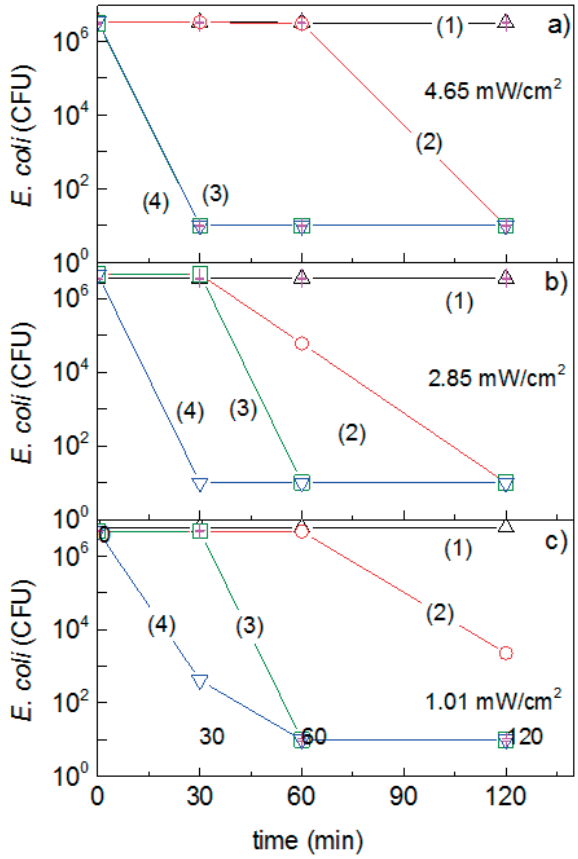

Figure 3.4. *E. coli* reduction under Philips Master-18W/865 (4.65 mW/cm²) light irradiation: (1) PES alone (2) TiO_2 sputtered on PES for 2 min, (3) TiO_2/Cu-PES sputtered 3 min and (4) Cu sputtered on polyester for 1 min. Error bars: standard deviation (n=5%)

At the highest light dose of 4.65 mW/cm² the PES by itself does not lead to *E. coli* reduction (Figure 3.4a, trace 1). TiO_2 sputtered samples for 2 min are seen to inactivate *E. coli* within 120 min (Figure 3.4a, trace 2). Figure 3.4a, trace 4 indicate that Cu sputtered for 1 min with the same surface content of Cu found in TiO_2/Cu co-sputtered for 3 min reduced *E. coli* as TiO_2/Cu-samples co-sputtered for 3 min. A similar trend was observed for the *E. coli* bacterial reduction applying intensities of 2.85 mW/cm² (Figure 3.4b) and 1.01 mW/cm² (Figure 3.4c). Under light irradiation TiO_2/Cu is a p-type semiconductor with band gap of 1.7 eV, a flat-band potential of -0.3 V vs SCE (pH 7) and a valence band of +1.4 V SCE [102].

Figure 3.4a shows that the bacterial reduction on TiO_2 (trace 2) is far below the bacterial reduction induced by Cu (trace 4). TiO_2 is acting as a semiconductor generating highly oxidative species under light irradiation. But Cu induces toxicity in the sputtered films that more effectively inactivate bacteria. The interfacial charge transfer (IFCT) [95] from CuO to TiO_2 inhibits the O_2 reduction by Cu_2O/CuO since cb electrons are injected into the TiO_2 decreasing the amount of electrons available to reduce O_2 by Cu_2O/CuO that subsequently would lead more effectively to HO_2° and °OH.

The effect of the light dose in Figure 3.4 shows that the density of active sites on the TiO_2/Cu-PES surface leading to *E. coli* reduction is higher than the photon/cm^2 reaching the TiO_2/Cu-PES surface. A higher light dose led to light saturation on the photocatalyst accelerating bacterial reduction (Figure 3.4). Cu/CuO/NPs-ions and other heavy metals have been reported to denature bacteria proteins by binding to reactive groups resulting in their precipitation and inactivation through an oligodynamic effect [103-105]. This last effect will be accounted in the section below providing the data for the Cu released in ppb quantities during bacterial reduction as monitored by ICP-MS,

3.3.3. Repetitive bacterial reduction and Ti and Cu-release during disinfection: mechanistic implications

Repetitive bactericidal cycles of *E. coli* were carried out by TiO_2/Cu-PES under light irradiation and showed a stable repetitive performance. The time necessary for the complete bacterial reduction up to the 5^{th} cycle was about 40 min and increased by a small amount during the last repetitive recycling. After each cycle, the co-sputtered samples were washed thoroughly with sterilized MQ-water, vortexed for 3 min and dried. No bacteria remained on the TiO_2/Cu-PES sample. This observation motivated us to assess the Cu- and Ti-release from the TiO_2/Cu-PES during bacterial reduction. The metal released during the bacterial reduction cycles when sputtering separately Ti (2 min) and Cu (1 min) on PES is shown on Table 3.2.

Table 3.2. Metal-ions released during bacterial loss of viability cycles when sputtering TiO_2 or Cu on PES compared to ions release in co-sputtered TiO_2/Cu-PES.

		First cycle	Third cycle	Fifth cycle
TiO_2-PES (2 min)	Ti (ppb/cm^2)	14	11	8
Cu-PES (1 min)	Cu (ppb/cm^2)	11	5	9
Co-sputtered TiO_2/Cu-PES (3 min)	Ti (ppb/cm^2)	7	3	2
	Cu (ppb/cm^2)	6	4	4

Table 3.2 shows the Cu, Ti release at the end of the bacterial reduction when both metals were co-sputtered for 3 min. The release of Ti and Cu decreases to 2 and 4 (ppb/cm^2) respectively after the fifth bacterial reduction cycle. Table 3.2 shows that the Cu and TiO_2 released during the cycles leading to complete reduction on samples co-sputtered for 3 min are significantly below the Cu and TiO_2 amounts released from samples loaded independently with similar amounts of Cu and TiO_2 on PES. A slower release of Cu allows a longer operational lifetime for the TiO_2/Cu-PES samples and this is important for any practical application of these films.

The copper toxicity toward mammalian cells have been reported with a median of lower effective concentration at 50% e.g. (L(E)C50 of 25 mg/L for mammalian cells [99-101]. The low release Cu of 4 ppb/cm^2 < 25 ppb/cm^2 shown in Table 3.2 is well below the Cu-cyto-compatible level [95,99]. Cu-levels of 4 ppb/cm^2 inducing bacterial reduction provide disinfection through an effective oligodynamic [79,95]. The Cu-ions have been reported to bind S, N and COO^- and other electron donor negative groups of the bacteria cell wall or entering the bacteria cytoplasm. Copper in the blood exists in two forms: bound to ceruloplasmin (85–95%), and the rest "free Cu" loosely bound to small molecules, protein, lipids and DNA.

The small amounts of toxic Cu NP's below 25 ppb/cm^2 released by the Cu-polyester allow for a higher cytocompatibility compared to a similar Ag-concentration as reported for mammalian cells. Cu is a metabolizable agent compared to Ag remaining in the body after ingestion increasing the Ag-serum levels [99-104].

3.3.4. Ar etching of TiO_2/Cu-PES film and Ti, Cu depth profile determined by XPS

By XPS the depth of Cu deposition on PES was investigated as well as the state of oxidation of the Ti- and Cu-species during bacterial reduction. The surface atomic percentage composition of C, O, N, Cu, and Ti is shown in Table 3.3 at time zero and after 30 min bacterial reduction of *E. coli* as shown in Figure 3.3, trace 1.

Table 3.3. Surface atomic percentages determined by XPS of TiO_2/Cu-PES co-sputtered for 3 min as detected by XPS.

	C	O	N	Cu	Ti
Before bacterial loss of viability	31.8	22.1	0.7	19.3	26.1
After bacterial loss of viability	39.0	19.4	0.9	16.6	24.1

Table 3.3 shows a small increase in the C-content due to bacterial decomposition residues besides the C-absorbed from the atmosphere during the bacterial reduction. A small decrease in the Cu and Ti-surface concentration after 30 min bacterial reduction was observed and was triggered by the increase of C on the topmost layers as described in the preceding paragraph.

Figure 3.5a presents the Cu doublet at time zero and Figure 3.5b presents the changes in the XPS spectra after bacterial reduction. This doublet is attributed to the presence of the Cu^{2+}-oxidation state (Cu^{2+}) prevalent in the Cu-sputtered sample exposed to air [93,95]. The Cu/Cu_2O with BE 932.2 eV at time zero remains stable after bacteria reduction at 933.1 eV. The CuO deconvoluted peak at time zero shifts to 943.2 eV after bacterial reduction as shown in Figure 3.5b. A shift of > 0.2 eV is indicative of a change in the oxidation state in the XPS specie [97,98]. Redox catalysis seems to take place during the disinfection process. The redox chemistry is associated with the production of highly oxidative radicals for composites of TiO_2 and Cu-composites [93-95].

The Cu oxidation state at time zero was monitored to be 75.5% for Cu/Cu_2O and 24.3% for CuO. A significant change in the oxidation state was observed after bacterial reduction rendering Cu/Cu_2O 4.1% and 95.7 % for CuO. The Ti^{3+}/Ti^{4+} surface electron traps have been reported to enhance the O_2 chemisorption in the presence of Cu in TiO_2/Cu- more markedly than in the case of TiO_2 alone [47].

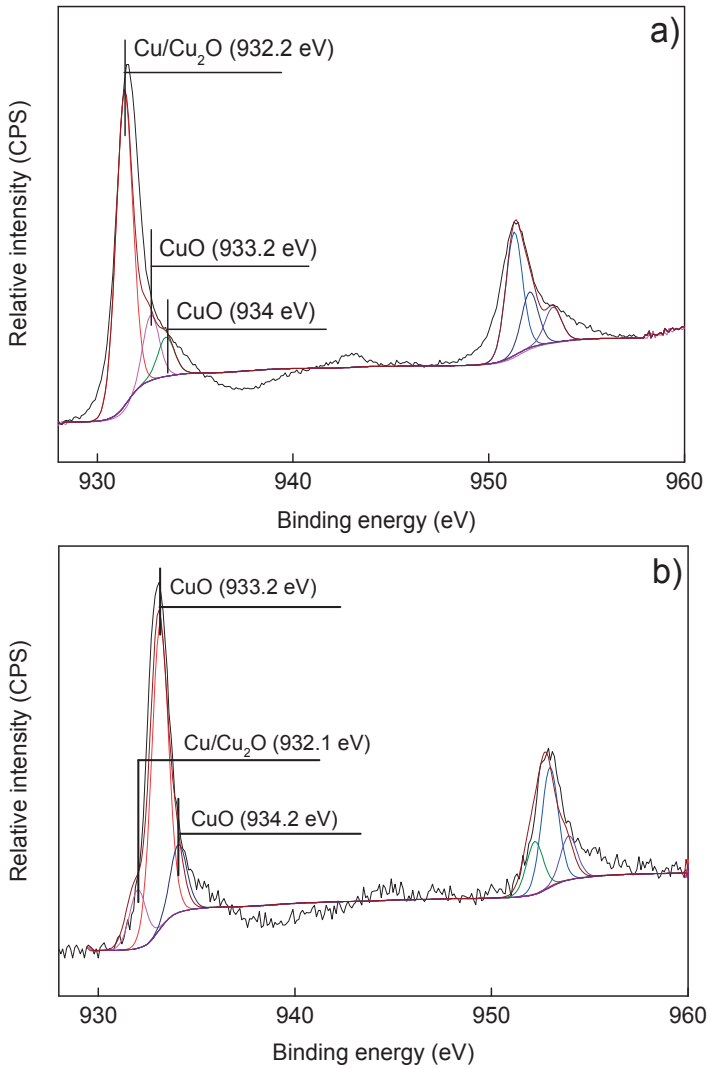

Figure 3.5a. XPS deconvolution of the Cu2p peak of co-sputtered TiO_2/Cu PES 3 min samples (a) before bacterial reduction of *E. coli.*

Figure 3.5b. XPS deconvolution of the Cu2p peak of co-sputtered TiO_2/Cu PES 3 min samples bacterial inactivation of *E. coli* under a Philips Master lamp irradiation18W/865 (4.65 mW/cm^2).

Production of reactive oxygen species (ROS) by the Cu-clusters on the PES leads to bacterial inactivation due to the interaction of the Cu-clusters with *E. coli* in the dark:

$$Cu^{+} + O_2{}^{\circ -} \leftrightarrow Cu^{\circ} + O_2 \qquad (1)$$

$$Cu^{0} + O_2 \leftrightarrow Cu^{+} + O_2{}^{-} \qquad (2)$$

The CuO (Cu^{2+}) is reduced

$$Cu^{2+} + e^{-}_{cb} \leftrightarrow Cu^{+} \qquad (3)$$

Or by a two electron transfer from Cu^{2+} leading to Cu° atoms

$$Cu^{2+} + 2e^{-} \leftrightarrow Cu^{0} \qquad (4)$$

The Cu-atoms then coalesce to Cu° nanoparticles settling in the Cu-network of the PES with E_{redox} = -0.34 V vs. NHE [105].

Figure 3.5c presents the deconvolution of the Ti and Cu, of TiO_2/Cu-PES samples co-sputtered for 3 min as a function of penetration depth of the Ar-ions. By following the decrease of the Ti2p doublet in Figure 3.5c it is readily seen that the Ti penetration into the PES reaches ~118 nm (or ~ 600 atomic layers).

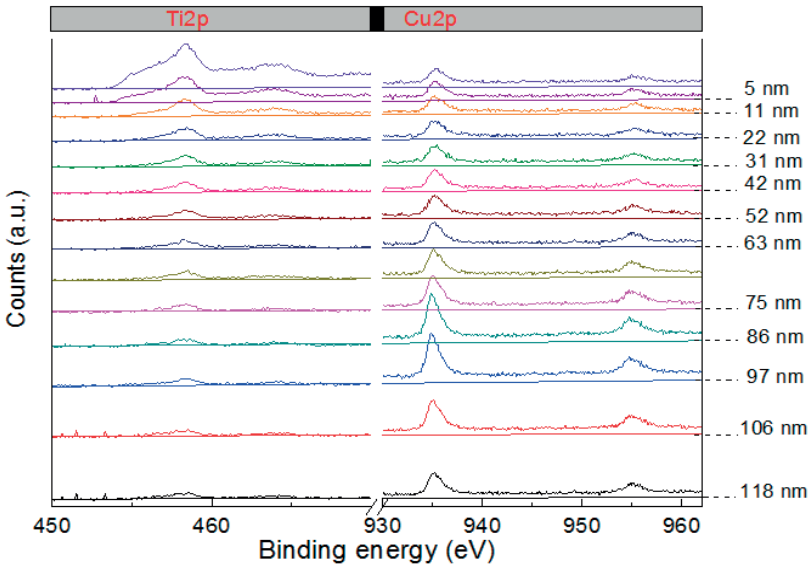

Figure 3.5c. XPS of the TiO_2/Cu-PES top-most layers for a sample co-sputtered for 3 min and etched by Ar^+-ions (5 KeV) up to a depth of 118 nm.

The penetration depth of Cu in Figure 3.5c on PES goes beyond 118 nm, since the Cu2p doublet is still present when the etching by Ar-ions has attained 118 nm. The etching of TiO_2/Cu-PES layers essentially takes off mostly the PES C-layers.

3.3.5 MRSA reduction as a function of initial CFU concentration and the effects of applied light intensity

Figure 3.6a shows the MRSA reduction as a function of the bacterial loading of the sample on: (1) PES alone (2) co-sputtered TiO_2/Cu-PES for 3 min in the dark with 10^8

CFU/ml, (3) co-sputtered TiO_2/Cu-PES for 3 min in the dark with 10^6 CFU/ml, (4) co-sputtered TiO_2/Cu-PES for 3 min in the dark with 10^5 CFU/ml.

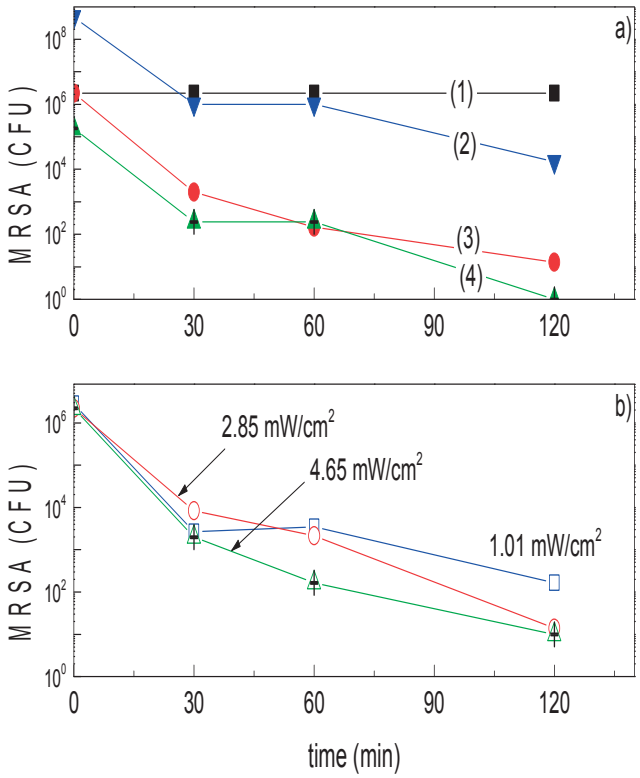

Figure 3.6a. Effect of initial bacterial concentration of MRSA loss of viability on: (1) PES alone (2) co-sputtered TiO_2/Cu-PES for 3 min tested in the dark, 10^8 CFU/ml, (3) co-sputtered TiO_2/Cu-PES for 3 min tested in the dark, 10^6 CFU/ml, (4) co-sputtered TiO_2/Cu-PES for 3 min tested in the dark, 10^5 CFU/ml. **Figure 3.6b.** Effect of light intensity irradiation on MRSA bacterial reduction on co-sputtered TiO_2/Cu-PES for 3 min under: 1.01 mW/cm^2, 2.85 mW/cm^2 and 4.65 mW/cm^2. Error bars: standard deviation (n=5%)

After initial optimization the co-sputtered TiO_2/Cu-PES (3 min) samples presented an MRSA bacterial reduction above the activity presented by co-sputtered TiO_2/Cu-PES samples sputtered for 1 and 2 minutes and are therefore the results presented in Figure 3.6. The bacterial reduction of MRSA in the dark is an important observation indicating the potential use of this catalyst in health facilities without any necessity of using photo-energy to activate the disinfection process.

Figure 3.6b shows the effect of light intensity on MRSA bacterial reduction by a TiO_2/Cu-PES sample co-sputtered for 3 min applying light intensities of 1.01 mW/cm^2,

2.85 mW/cm^2 and 4.65 mW/cm^2. Figure 3.6b shows that only a marginal increase in the MRSA bacterial reduction was observed with an increase in light intensity. We suggest that the MRSA reduction is predominantly controlled by the Cu/Cu-ions inherent toxicity and not by the reactive oxygen species (ROS) induced by light irradiation of the TiO_2/Cu-PES sample.

In the case of *E. coli* bacterial reduction under light shown in Figure 3.4a, the TiO_2/Cu-PES samples sputtered for 3 min (trace 3) reduced by a factor of two the *E. coli* reduction time when the light intensity was increased from 1.01 to 4.65 mW/cm^2. An accelerated reduction was observed for *E. coli*, but this was not the case for MRSA. The Gram- *E. coli* has a thinner peptoglycan cell wall compared to the Gram+ MRSA and containing additional bilayers with a high structural complexity [10,92]. The significant difference in wall thickness/wall microstructure between MRSA and *E. coli* lead to the different interaction for *E. coli* and MRSA with TiO_2/Cu-PES surface under light irradiation. MRSA is a Gram positive bacterium presenting a cell-wall ~ 40-80 nm thick with a peptidoglycan content > 50 %, a lipid content of < 3% and no lipo-polysaccharide content. *E. coli* is a Gram negative bacterium presenting a cell wall thickness of ~10 nm with a peptidoglycan content of 10-20%, a lipid content of < 58% and a lipo-polysaccharide content of 13%.

Kühn et al., [106] reported recently a fast bacterial reduction of *E. coli* and *P. Aeruginosa* compared to *Staphyloccocus aureus* presenting a thicker cell wall. Another important difference for the interaction of both types of bacteria with CuNP's is the strong electrostatic interaction of Cu NP's-positive-ions with the negative lipopolysaccharide (LPS) outer layer of *E. coli*. This is not the case for the interaction between MRSA and the Cu NP's positive-ions since both surfaces present similar charges. Cu-NP's absorption has been reported on the teichoic acid and the peptidoglycan outer MRSA cell wall [42]. For *E. coli* and MRSA the bacterial reduction has been reported to occur on several metal and oxide agents [104,107-108].

3.3.6. *E. coli* staining and viability on TiO_2/Cu-PES samples

Live and dead *E. coli* bacteria were determined by the staining with the dye fluorochrome that enters the cell and stains the cell DNA only if the cell wall membranes

are damaged [109]. To test the time at which *E. coli* cells suffer destabilization/damage leading ultimately to cell dead (red dots indicate membrane damage), the cells were incubated on PES in the dark and in parallel for 60 and 120 min on TiO_2/Cu-PES (See Annex 1). *E. coli* cells kept alive (green dots) on PES alone up to 120 min of incubation. But for cell incubated for 60 and 120 min on TiO_2/Cu-PES, the loss of viability was observed to become faster as the incubation time increases leading to membrane damage and cell death [110].

3.4. Conclusions

Visible light induced bacterial reduction kinetics of *E. coli* and MRSA on TiO_2/Cu-PES were shown in this chapter to be different. There seems to be a significant stabilizing effect of the TiO_2/Cu-PES on the release of Cu during bacterial reduction compared to Cu alone as monitored by ICP-MS. An oligodynamic effect seems to be responsible for the bacterial reduction of *E. coli* and MRSA occurring at ppb levels of Cu. This effect seems to be beneficial during repetitive bacterial reduction processes in processes related to long-operational lifetimes.

During this chapter, sputtering at conventional energies led to adhesive coatings. It has been shown in the literature that high energies applied to the sputtering target lead to more ionization in the plasma phase. This is why we thought about exploring the high power impulse magnetron sputtering unit to depose TiO_2 and Cu/CuOx on textiles and investigate the bacterial inactivation kinetics and the film microstructure as it will be shown in chapter 4 hereafter.

Chapter 4

TiO_2/Cu films prepared by HIPIMS showing accelerated bacterial loss of viability

This chapter is based on the following publication: Sami Rtimi, Oualid Baghriche, Cesar Pulgarin, Jean-Claude Lavanchy, John Kiwi, Surface & Coatings Technology 232 (2013) 804–813 (Reproduced with permission of Elsevier, Copyright 2015).

4.1. Introduction

Antimicrobial surfaces can reduce/eliminate hospital-acquired infections (HAI) acquired on contact with bacteria surviving for long times in hospital facilities [2,111]. To preclude/decrease viral, nosocomial infections and antibiotic resistant bacteria Borkow and Gabbay [112] introduced Cu into textile fabrics. Recently Sunada et al., [69,91], Torres et al., [43] Akhavan et al., [113-115] among others [11,116-119] have reported the preparation of the Cu and TiO_2/Cu films by sol-gel methods with materials absorbing in the visible range. Films obtained by DCMS/DCPMS as reported to avoid the disadvantages of films prepared by sol-gel methods [43,120] since they deposit uniform and adhesive metal films showing robust mechanical structures at temperatures compatible with low resistant polymer/textiles < 120-130°C.

In recent years, CVD has been used to produce antimicrobial films by condensation of a vaporized precursor onto the substrate at relatively high temperatures. The disadvantages of the CVD deposition approach are the high investment costs, the high temperatures needed precluding film deposition on textiles besides the large amount of heat used requiring costly cooling systems. HIPIMS has been used recently to prepare films by applying strong electrical pulses leading to sputter layers presenting superior resistance against corrosion and oxidation [55-56]. Surface presenting a high roughness is one of the main problems encountered when depositing uniform Cu-films by DCMS/DCPMS [56].

We address in this study HIPIMS sputtering on 3-D substrates leading to ultrathin uniform films showing an accelerated bacterial deactivation due to high amount of –metal-ions (M^+) produced in the magnetron chamber. The HIPIMS plasma high energy allows the generation of a high density of metal-ions. These ions interact strongly with the higher applied bias voltage on the substrate applied in the HIPIMS chamber compared to DCMS/DCPMS. This chapter presents the work on Cu and TiO_2/Cu films sputtered by HIPIMS describing the deposition parameters, the loss of bacterial viability under light and providing a detailed surface characterization. The results obtained will be compared to Cu and Cu/TiO_2 layers sputtered by DCMS and DCPMS [81,83,121,95]. The TiO_2/Cu polyester samples described in this study present the potential to be practical candidates to avoid biofilm formation due to their fast bacterial inactivation kinetics [111,2,25,43,12].

The novelty of this work is the use of advanced sputtering plasma technology (High Power Impulse Magnetron Sputtering, HIPIMS) to prepare robust, uniform and highly adhesive TiO_2/Cu films applying high energies leading to higher ionization compared to conventional sputtering. These films showed fast bacterial inactivation kinetics. HIPIMS has shown to depose denser films compared to DCMS leading to high adhesion to the substrate and a lower release of Cu-species [17,52].

4.2. Experimental section

4.2.1. Sputtering parameters, film thickness, sample composition and determination of the Cu and Ti by ICP- during bacterial inactivation

HIPIMS deposition of Ti and Cu was carried out in a CMS-18 Vacuum system from Kurt Lesker Ltd. evacuated to 5.8×10^{-3} mbar by a turbomolecular pump. The Cu- and the TiO_2 targets were 50 mm in diameter, 99.99% pure from K. Lesker Ltd. UK. The TiO_2/Cu target was 2 inches in diameter and had a composition of 60/40 atomic % in TiO_2 and Cu respectively. The HIPIMS was operated at 500 Hz with pulses of 100 microseconds separated by 1.9 ms, leading to a deposition rate for TiO_2/Cu of 15.3 nm/min. The average power was 87.5 W (5 A x 350 V) and the power per pulse of 100 microseconds was 1750 W. The 5 A current is the current at one pulse, the voltage at one pulse is 350V and the pulses had a rectangular shape since the pulse duration was 100 microseconds with an off period of 1900 microseconds (See Annex 2 & 3).

In the case of DCP, 622 V and 0.3 A were applied during the 3 pulses of 10 microseconds each within a 50 microsecond period. This gives 187 W per period or 62.3 W/ pulse and an average power of 312 W/period.

The PES used was described in chapter 3. The calibration of the Cu-nanoparticulate film thickness by HIPIMS on the Si-wafers is shown in Figure 4.1a. The film thickness was determined with a profilometer (Alphastep500, TENCOR). The X-ray fluorescence (XRF) determination of the Ti/Cu samples was evaluated in a PANalytical PW2400 spectrometer.

Inductively coupled plasma spectrometry (ICP-MS) was used to determine the Cu since it is a sensitive analytical technique because due to the low background and high ion transmission. The Finnigan^{TM} ICPMS used was equipped with a double focusing reverse geometry mass spectrometer able of a resolution of $1.2x10^5$ cps/ppb, detection limit of 0.2 ng/L. The solutions were then diluted 10 times to reach the volume necessary for the ICP-MS analyses.

4.2.2. *E. coli* loss of viability evaluation

Antibacterial activity of sputtered PES fabrics was carried out according to previous work reported by our laboratory [121]. The counting data reported were replicated three times. To verify that no re-growth of *E. coli* occurs after the total inactivation observed in the first disinfection cycle, the samples were incubated for 24 hours at 37 °C. Then bacterial suspension of 100 microliters was deposited on 3 Petri dishes to obtain replicates of the bacterial counting. These samples are incubated at 37 °C for 24 h. No bacterial re-growth was observed. Statistical analysis of the results was performed on the bacterial CFU values for the runs showing the fastest bacterial inactivation reporting standard deviations. The average values were compared by one-way analysis of variance and with the value of statistical significance.

4.2.3. Diffuse reflectance spectroscopy (DRS), electron microscopy (TEM, HAADF) and XRD of samples

Diffuse reflectance spectroscopy was carried out using a Perkin Elmer Lambda 900 UV-VIS-NIR spectrometer provided for with a PELA-1000 accessory within the

wavelength range of 200-800 nm and a resolution of 1.0 nm. The absorption of the samples was plotted in Kubelka-Munk (KM) arbitrary unit *vs* wavelength.

Transmission electron microscopy was carried out in a FEI Tecnai Osiris instrument microscope at 200 kV was used to measure grain size of the TiO_2/Cu films. The textiles were embedded in epoxy resin 45359 Fluka and the fabrics were cross-sectioned with an ultramicrotome (Ultracut E) and at a knife angle at 35°. High-Angle Annular Dark-Field (HAADF) imaging was used to map the scanning electron microscopy (STEM). These images (Z-contrast images) are obtained by collecting the scattered electrons passing through the objective provided with an annular dark-field detector.vCrystal structures were characterized by X-ray diffraction (XRD) and recorded on an X'Pert MPD PRO from PANalytical equipped with a secondary graphite (002) monochromator and an X'Celerator detector operated in Bragg–Brentano geometry. A step size of 0.0081 was chosen and an acquisition time of 2 min per degree.

4.2.4. X-ray photoelectron spectroscopy (XPS) and detection of highly oxidative radicals in the sputtered samples

An AXIS NOVA photoelectron spectrometer (Kratos Analytical, Manchester, UK) equipped with monochromatic AlK_α ($h\nu$ = 1486.6 eV) anode was used during the study. The electrostatic charge effects on the samples were compensated by means of the low-energy electron source working in combination with a magnetic immersion lens. The carbon C1s line with position at 284.6 eV was used as a reference to correct for charging effects. The XPS spectra for the Cu-species were analyzed by means of spectra deconvolution software (CasaXPS-Vision 2, Kratos Analytical UK). The surface atomic percentage concentration of some elements was determined by fitting of the peak areas using known sensitivity factors [97,122]. Spectrum background was subtracted according to the Shirley subtraction GL(30) program attached to the Kratos unit [122].

The detection of the oxidative species (mainly OH-radicals) in the TiO_2/Cu sputtered samples was carried out according to Ishibashi et al., [123]. Terephthalic acid 99% was an ACROSS reagent. The fluorescence spectrum of the 2-hydroxyterephthalic acid generated by the reaction of terephthalic acid with OH was measured on a Perkin Elmer LS-50B fluorescence spectrometer.

4.3. Results and discussion

4.3.1 Sample film thickness bacterial loss of viability, diffuse reflectance spectroscopy (DRS) and determination of elusive Cu

Figure 4.1a shows the results of the thickness calibration for HIPIMS sputtered Si-wafers at 5A for Cu, TiO_2 and TiO_2/Cu 60%/40% target. The fastest bacterial inactivation leading to complete inactivation was observed when the polyester sputtered for 150 s with the TiO_2/Cu target (Figure 4.1b) depositing a composite film 38 nm thick.

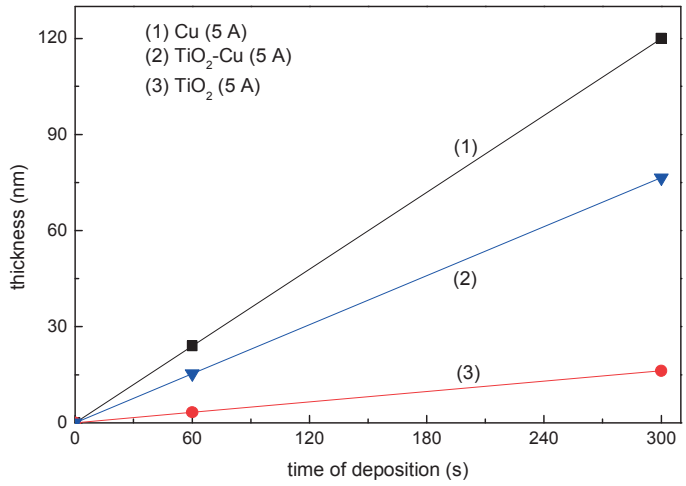

Figure 4.1a. Thickness calibration of: (1) Cu, (2) TiO_2-Cu and (3) TiO_2 HIPIMS-sputtered under current intensity of 5 A.

This is equivalent to ~190 layers 0.2 thick nm with 10^{15} atoms/cm^2 and deposited at a rate of 15.3 nm/min or 7.6x10^{16} atoms/cm^2/min. X-ray fluorescence in Table 4.1 shows the content of TiO_2 and CuO with increased sputtering time. When using the TiO_2/CuO 60%/40% target a ratio of TiO_2/CuO of 4-5 times was observed for the different sputtering times.

Table 4.1. TiO_2 and Cu loadings determined by X-ray fluorescence for the HIPIMS sputtered polyester samples used in this study

Samples	% wt CuO/wt polyester	% wt TiO_2/wt polyester	Current intensity
TiO_2 (30 min)	--	0.513	5 A
TiO_2 (20 min)	--	0.382	
TiO_2 (10 min)	--	0.192	
TiO_2 (4 min)	--	0.042	
TiO_2 (1 min)	--	0.039	
TiO_2 (30 s)	--	0.025	
Cu (60 min)	0.340	--	5 A
Cu (30 s)	0.189	--	
Cu (15 s)	0.144	--	
TiO_2/Cu (300 s)	0.107	0.570	5 A
TiO_2/Cu (150 s)	0.088	0.446	
TiO_2/Cu (60 s)	0.063	0.317	
TiO_2/Cu (30 s)	0.060	0.243	

The bacterial loss of viability in Figure 4.1b, trace 6 shows that no bacterial loss of viability occurs on polyester alone under light irradiation. Runs the dark for samples sputtered for 150 s induced a slow loss of bacterial viability within 120 min, showing that the bacterial CFU reduction involves Cu-layers.

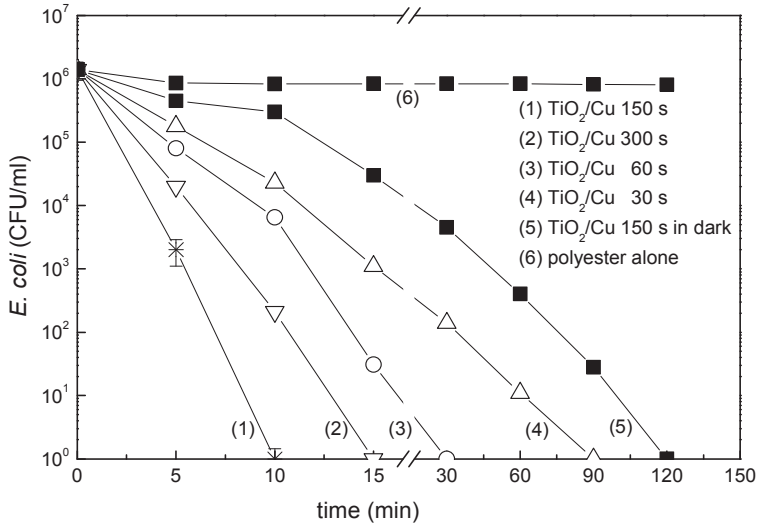

Figure 4.1b. *E. coli* survival on TiO_2/Cu HIPIMS-sputtered on polyester for different times in the dark and under Osram Lumilux 18W/827 actinic lamp (4mW/cm^2). Error bars: standard deviation (n=5%).

Under actinic light radiation, traces 3 and 4 indicate that sputtering times of 30 s and 60s induce faster bacterial loss of viability kinetics. A sputtering time of 150 s induced the shortest inactivation time (trace 1). Sputtering for 300 s induce bacterial inactivation taking longer times compared to samples sputtered for 150 s. Therefore, the amount of Cu^0 is not the main species leading to bacterial inactivation. A sputtering time of 150 s is seen to lead to the most favorable structure-reactivity for the Cu-polyester leading to the shortest *E. coli* inactivation. This sample presents the highest amount of Cu-sites held in exposed positions interacting on the surface or close to the polyester surface with *E. coli* leading to bacterial loss of viability [95]. The surface bactericide action seems to be due to a synergistic effect introduced by the TiO_2/Cu layers since longer times was observed when sputtering TiO_2 as shown next in Figure 4.1c.

Figure 4.1c shows the bacterial inactivation kinetics by the HIPIMS TiO_2 sputtered samples. As shown in Figure 4.1c no bacterial inactivation take place in the dark but the bacterial inactivation becomes faster for HIPIMS sputtering times between 1 min (trace 5) and 4 min (trace 2).

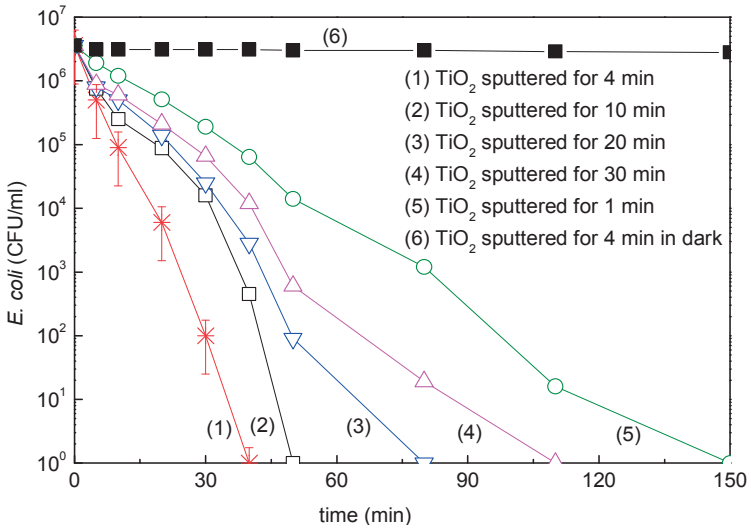

Figure 4.1c. *E. coli* survival on TiO_2 HIPIMS-sputtered (5 A) on polyester for different times in the dark and under solar simulated irradiation. Error bars: standard deviation (n=5%).

Longer deposition times between 10 and 30 min did not accelerate the loss of viability kinetics due to the fact that an increased TiO_2 thickness > 12 nm sputtered within 4 min leads to: a) bulk inward diffusion of the charge carriers generated on TiO_2 under light leading to highly oxidative radicals [124-125], and b) longer sputtering times facilitate the TiO_2 inter-particle growth decreasing the TiO_2 contact surface with bacteria [81,83].

Figure 4.1d shows the *E. coli* inactivation within 60 min for HIPIMS Cu-sputtered samples within 15, 30, and 60 s. This inactivation time is longer than the time reported in Figure 4.1b for TiO_2/Cu HIPIMS of 10 min suggesting a synergic effect between TiO_2 and Cu leading to a faster loss of viability.

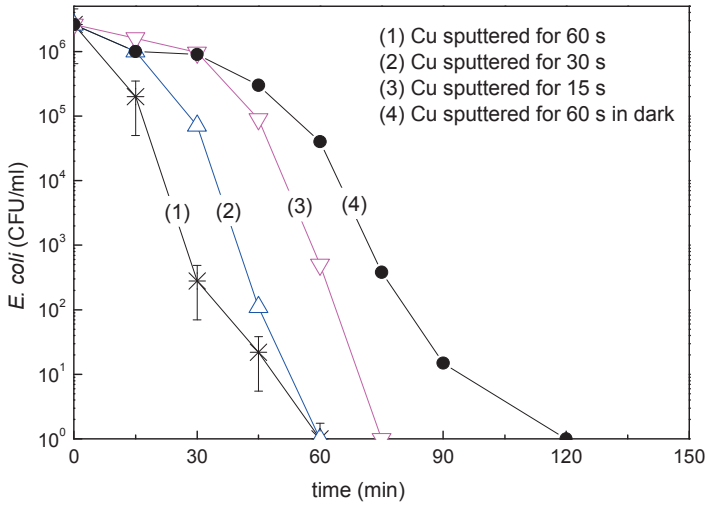

Figure 4.1d. *E. coli* survival on Cu HIPIMS-sputtered for different times in the dark and under Osram Lumilux 18W/827 actinic lamp (4 mW/cm^2). Error bars: standard deviation (n=5%).

Figure 4.1e presents the results for the diffuse reflectance spectroscopy (DRS) for the TiO_2/Cu samples used to evaluate the bacterial inactivation (Figure 4.1b). The absorption in Kubelka-Munk units shows agreement with the data reported for TiO_2 and Cu Table 4.1, showing that TiO_2 is the main surface element. The Cu/Cu_2O/CuO absorption increases with longer Cu-sputtering times up to 300s [102]. The weak absorption from 400 and 500 nm is due to the interfacial charge transfer (IFCT) from the TiO_2 to CuO. The optical absorption between 500 and 600 nm is due to the interband

transition of Cu_2O. The absorption between 600 to 800 nm has been attributed to the exciton band and the Cu (II) d-d transition.

The rough UV-Vis reflectance data cannot be used directly to assess the absorption coefficient of the sputtered polyester because of the large scattering contribution to the reflectance spectra. Normally, a weak dependence is assumed for the scattering coefficient S on the wavelength. The KM/S values for the samples in Figure 4.1e are proportional to the TiO_2/Cu absorption coefficient up to sputtering times of 150s and these values are in agreement with the trend observed for the inactivation kinetics reported (Figure 4.1b).

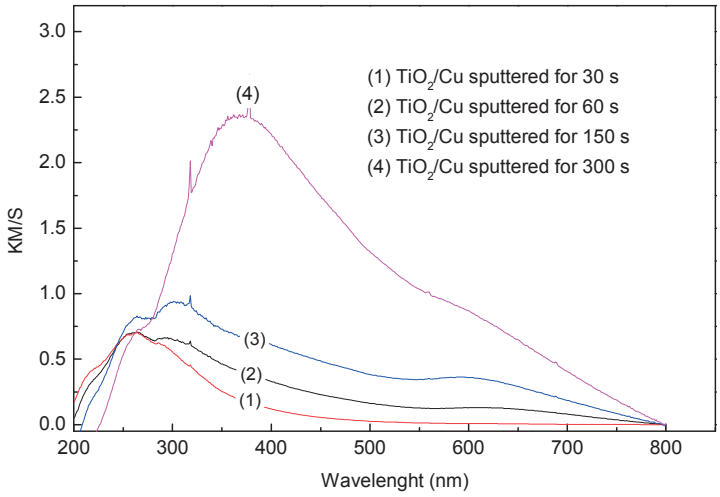

Figure 4.1e. DRS of TiO_2/Cu polyester samples sputtered by HIPIMS for different times at 5A.

Figure 4.1f shows that the loss of bacterial viability due to the TiO_2/Cu sample irradiated by three different light doses. The loss of bacterial viability with time is shown to be a function of the intensity of the applied light. The mechanism will be discussed below in the section describing the results presented in Figure 4.4.

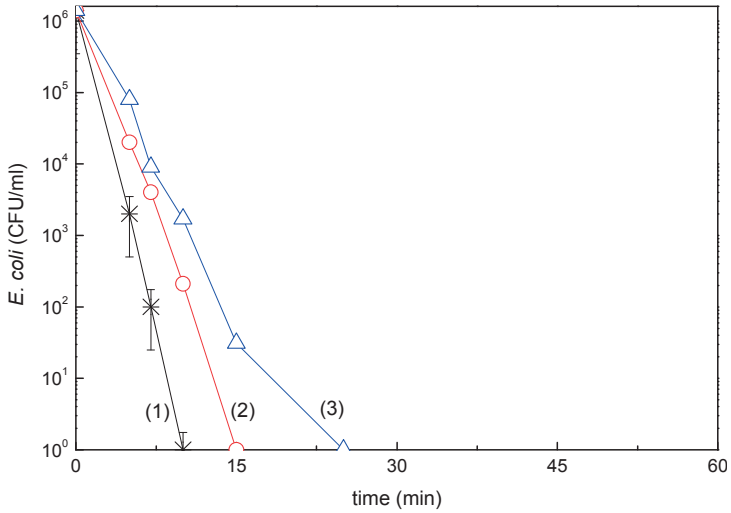

Figure 4.1f. *E. coli* survival on TiO_2/Cu HIPIMS-sputtered samples for 150s under different light intensities of 1) 5.0 mW/cm^2, 2) 3.5 mW/cm^2 and 3) 2.2 mW/cm^2. Error bars: standard deviation (n=5%).

Figure 4.1g shows the reuse cycles of the TiO_2/Cu (150 s) sample up to the 8th cycle. No loss in activity was observed in the sample during the sample recycling. The sample was thoroughly washed after each recycling run leading to the reuse of the sample since complete bacterial loss of viability was attained after each cycle. The chemical state and environment of the CuO/Cu-ions seem not to change after the bacterial loss of viability showing the stable nature of the TiO_2/Cu on the polyester fabric.

Figure 4.1h shows the release of Cu-ions inactivating *E. coli* as a function of catalyst recycling. Figure 4.1h shows the repetitive release of Cu-ions up to the 8th reuse cycle as measured by ICP-MS. The release of Cu- from the TiO_2/Cu samples shown in Figure 4.1h was ~8 ppb/cm^2. This value is lower compared to the Cu-release from the Cu-sputtered samples reaching up to ~18 ppb Cu/cm^2 at the end of the 8th cycle. In both cases the small amounts of Cu are considered not to be cytotoxic to mammalian cells and seems to proceed through an oligodynamic effect [79,95]. The Cu and TiO_2/Cu induced bacterial inactivation is carried out in a way that it is not toxic to human health.

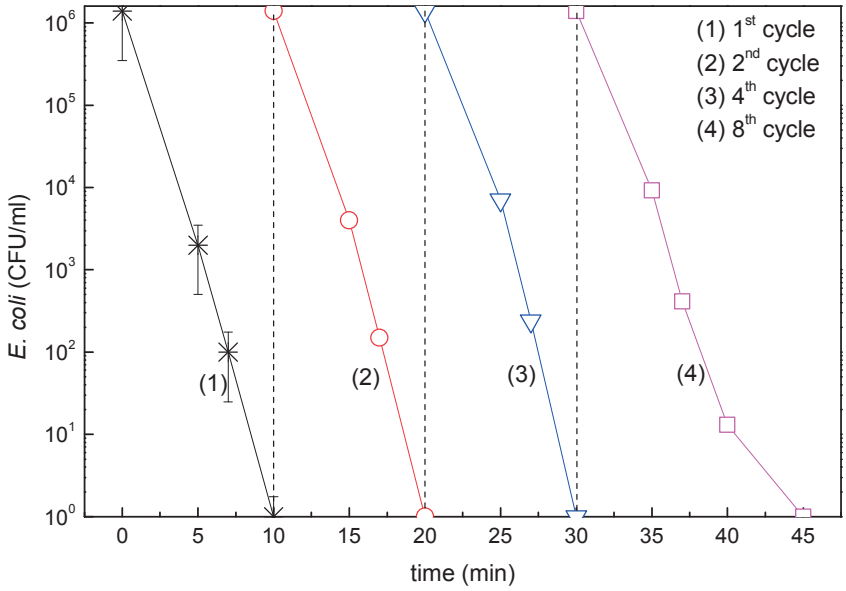

Figure 4.1g. *E. coli* survival on TiO_2/Cu HIPIMS-sputtered sample for 150 s under solar simulated light up to the 8th repetitive cycle. Error bars: standard deviation (n=5%).

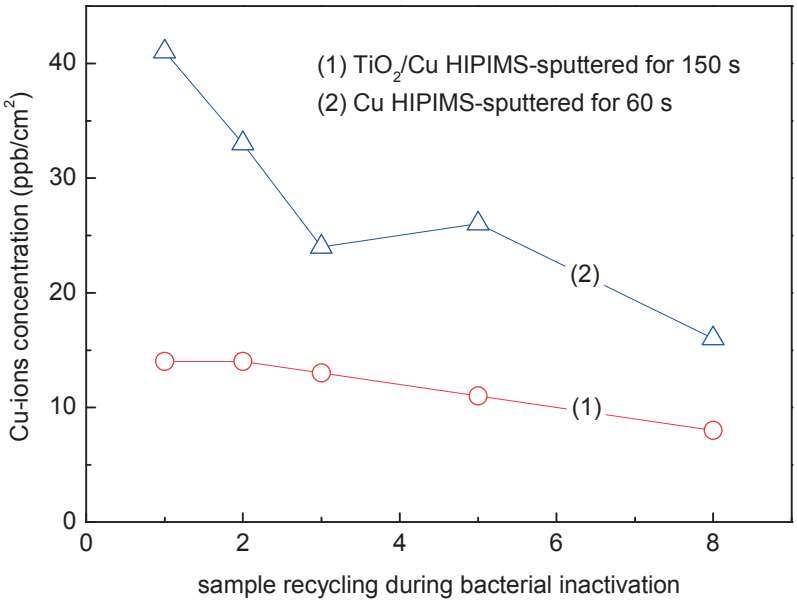

Figure 4.1h. Concentration of ions eluted into solution determined by ICP-MS up to the 8th recycling of TiO_2/Cu samples inactivating *E coli*.

4.3.2 Steric factors, transmission electron microscopy (TEM) and XRD of samples

The particle size of the film nanoparticulate and the hydrophobic-hydrophilic balance determine to great extent the surface photocatalytic properties. Samples sputtered for 30s show Cu-nanoparticles between 8-15 nm. The TiO_2 samples sputtered for 150 s present sizes between 8-12 nm, and the TiO_2/Cu samples sputtered for 150 s presented particles 5-10 nm (Figure 4.2a). The TiO_2 stabilize the Cu-clusters on the polyester surfaces.

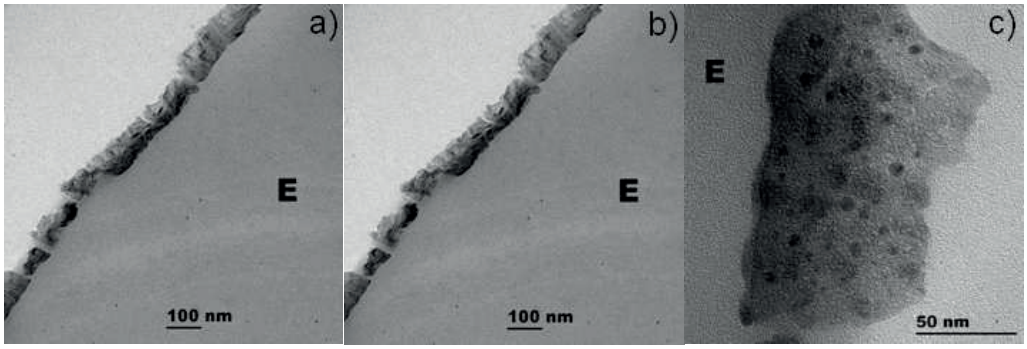

Figure 4.2a. Transmission electron microscopy (TEM) of: a) Cu sputtered for 150s by HIPIMS on polyester, b) TiO_2/Cu sputtered for 30s by HIPIMS on polyester and c) TiO_2/Cu sputtered for 150s on polyester

The nanoparticles small size accounts partly for the favorable bacterial inactivation kinetics due to the large surface area per unit mass [81,83,124,126]. The distribution of TiO_2 and Cu-nanoparticles on the polyester was found to be uniform not presenting any cracks. The uniformity of the film is beneficial for the bacterial adhesion which is a primary step leading to bacterial loss of viability to proceed favorably [111,2,5]. The electronic transfer between the TiO_2/Cu sample and the *E. coli* depends on the length of the charge diffusion in the composite film. This in turn is a function of the TiO_2 and Cu particle size and shape [124-125].

The interfacial distances between TiO_2 and Cu/CuO on the polyester surface range from below 5 nm and up. This allows the interfacial charge transfer (IFCT) to proceed with a high quantum efficiency [124,126]. Quantum size effects have been shown to occur in particles with sizes 10 nm having about 10^4 atoms as presented by the TiO_2 particles with sizes ~10 nm [126-127]. But in the CuO nanoparticles, the charge recombination increases takes place within shorter times due to the decrease in the space available for

charge separation. Also, the decrease of the space charge layer decreases further the potential depth.

Figure 4.2b presents in the left hand side TiO_2/Cu microscopy contrasted by high angular annular dark field (HAADF) showing the Cu-nanoparticles to be immiscible with Ti. Cu^{2+} does not substitute Ti^{4+} in the TiO_2 lattice because of the significant difference in the radii of Ti^{4+} (0.53 Angström) and Cu^{2+} (1.28 Angström). The right hand side inserts shows the mapping of the Cu, Ti and O.

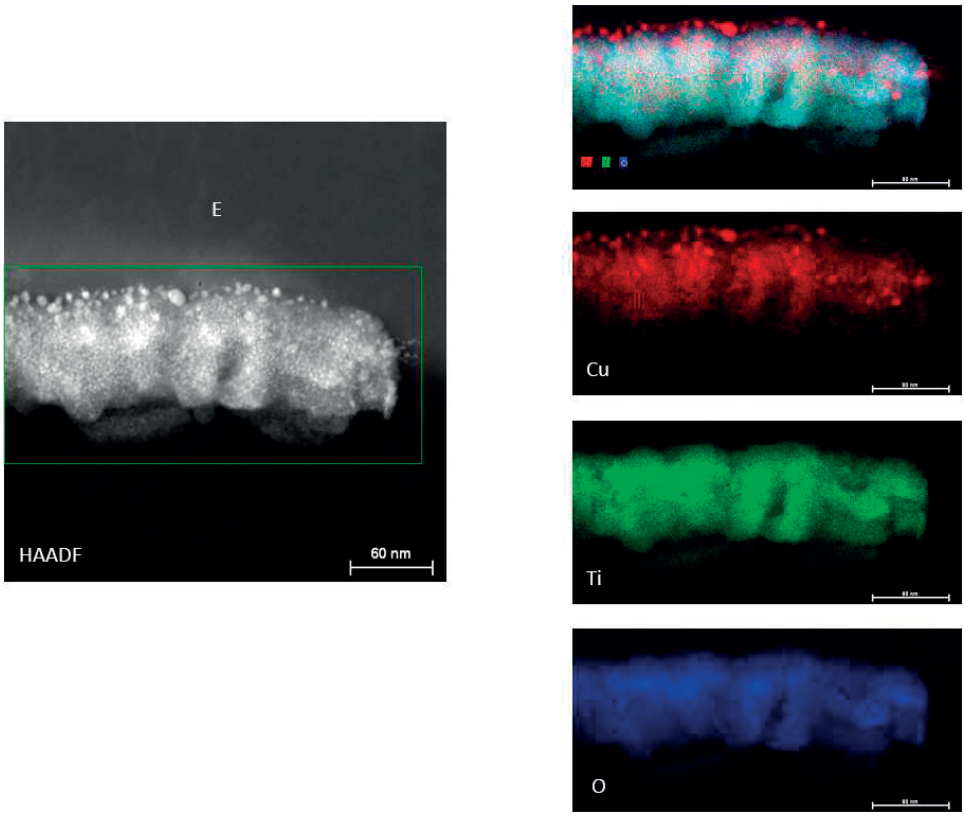

Figure 4.2b. High-Angle Annular Dark-Field imaging (HAADF) images of TiO_2/Cu HIPIMS sputtered for 150s showing the complete sample and the mapping of Cu, Ti and O by Z-contrast imaging in the TEM image.

Due to its size, the CuO/Cu nanoparticles with particle size > 8 nm are not able to penetrate into the bacteria core through the cell wall porins with diameters of 1-1.3 nm [128]. Only Cu-ions are able to diffuse through bacterial porins leading to DNA damage and finally to the total loss of bacterial viability.

XRD pattern for anatase and TiO_2/Cu were deposited on the HIPIMS samples sputtered for 30 s, 150 s and 300 s.The distinct pattern of the Cu peaks were not observed since the loading <0.1% was too low to be detected by XRD. The Cu/Cu_2O/CuO were deposited on the TiO_2 surface and did not lead to lattice doping. The TiO_2 sharp peak at 24.6° shows the highly crystallized TiO_2 sputtered on polyester (See Annex 4).

4.3.3. X-ray photoelectron spectroscopy and Ar-etching of TiO_2/Cu films

The surface atomic percentage composition of C, O, N, S, Ti and Cu is shown in Table 4.2 as a function of bacterial inactivation time for HIPIMS sputtered samples up to 15 min. Table 4.2 shows a constant atomic percentage concentration implying that a rapid catalytic decomposition of the bacterial residues on the sample surface. Within 15 min the bacterial residues are destroyed enabling the catalyst recycling as shown in Figure 4.1g.

Table 4.2. Percentage surface atomic concentration of TiO_2/Cu (150 s) HIPIMS film as a function of bacterial inactivation time under simulated solar irradiation

Samples	C	O	N	S	Ti	Cu
TiO_2/Cu (150 s) at time zero	52.63	30.00	0.00	0.00	4.75	9.61
TiO_2/Cu (150 s) contacted with bacteria at time zero	54.21	31.02	0.09	0.00	5.71	10.97
TiO_2/Cu (150 s) at 5 min of bacterial inactivation	55.19	31.88	0.10	0.03	5.55	9.99
TiO_2/Cu (150 s) at 10 min of bacterial inactivation	53.04	30.57	0.06	0.00	5.57	10.02
TiO_2/Cu (150 s) at 15 min of bacterial inactivation	53.07	30.98	0.04	0.00	5.55	10.00

Figure 4.3a presents the atomic percentage concentration of Cu, Ti, O_2 and C of TiO_2/Cu samples sputtered for 150s as a function of depth penetration of the Ar-ions. It is readily seen that Cu, Ti and O decrease up to 240 Angströms due to the Ar-bombardment. The etching depth induced by the Ar-ions was referenced by the known etching value for Ta of 15 atomic layers per minute equivalent to ~30 Angstroms/min.

The penetration of the Cu inside the sample protects the Cu-clusters inside the 130 microns thick polyester network during the *E. coli* inactivation process. The increase in the C-content in Figure 4.3a is due to the etching removing the TiO_2/Cu layers making available the C-content of the polyester. The insert in Figure 4.3a shows the significantly

lower percentage of Cu and Ti for TiO_2/Cu sputtered by DC/DCP [95]. The concentration of Ti followed a different pattern compared to the one observed when sputtering by HIPIMS and increases beyond 100 Angstroms because Ti deposition was hindered by the Cu-layers.

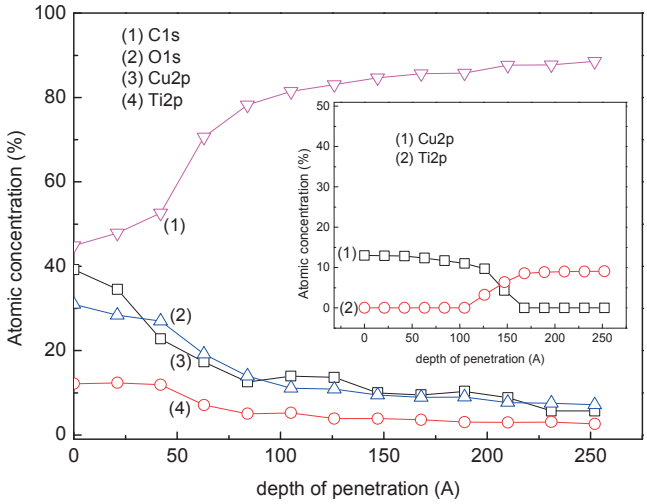

Figure 4.3a. XPS etching showing the microstructure of TiO_2/Cu film sputtered by HIPIMS up to 240 Angstroms (~120 atomic layers). Insert: depth profile of the TiO_2/Cu film sputtered by DC/DCP.

Figure 4.3b presents the 3-D view of the Cu 2p3/2 doublet and the Cu shake-up satellites at 933.4 eV and at 933.1 eV [97] for the TiO_2/Cu 150s HIPIMS sample. The Cu-enrichment within the 10 first layers is seen to decrease with sample depth and remain stable up to ~ 100 layers. Figure 4.3c shows the Ti 2p3/2 doublet peaks with a binding energies (BE) at 458.5 and 464.1 eV, increasing steadily as we go deeper into the TiO_2/Cu film up to ~125 layers.

XPS envelope for the Ti2p signals at zero, 5 min and 10 min showed a shift >0.2 eV. It is readily seen that redox Ti^{3+}/Ti^{4+} processes take place during bacterial inactivation shifting the peak from 457.8 to 458.3 eV. This is >0.2 eV accepted as a true change in the oxidation state of a specific specie [83,97].

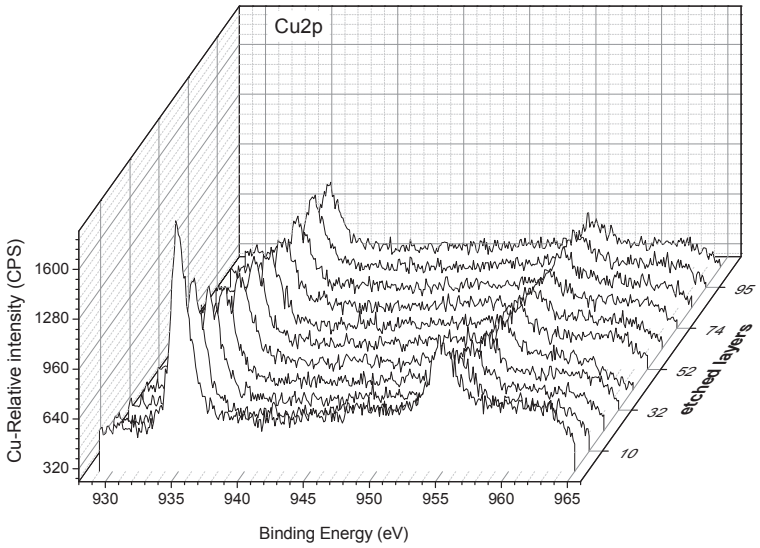

Figure 4.3b. Depth profile of an Ar-etched TiO_2/Cu HIPIMS sputtered sample showing the Cu penetration in the film.

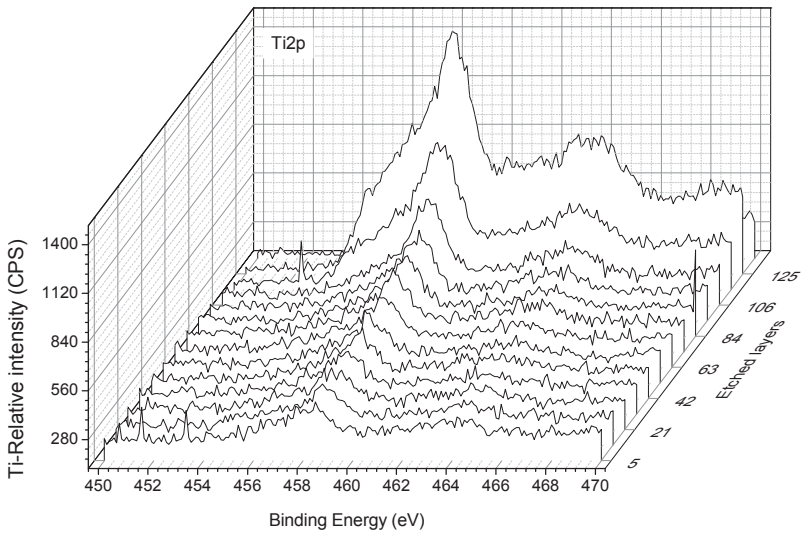

Figure 4.3c. Depth profile of an Ar-etched TiO_2/Cu HIPIMS sputtered sample showing the Ti penetration in the film.

Figures 4.3e present the deconvolution of the peaks for the Ti2p doublet before and after the bacterial inactivation process. Evidence is presented for the reduction from Ti(iV) to Ti(III) in Figures 4.3 by the shift of the deconvoluted peak from 457.9 eV at time zero to 458.3 eV after 10 min, at the end of the bacterial inactivation.

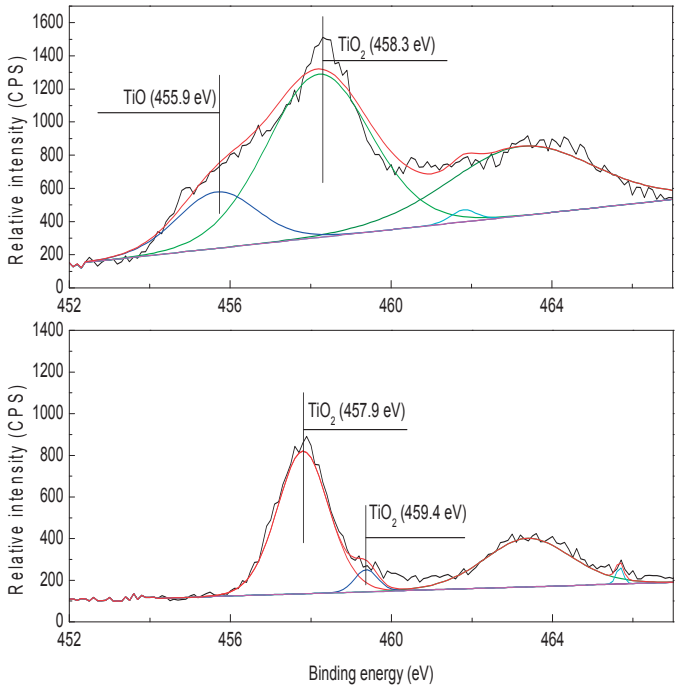

Figure 4.3e. XPS Ti2p deconvolution during bacterial inactivation with TiO_2/Cu HIPIMS sputtered for 150s and irradiated by solar simulated light before and after bacterial inactivation.

Evidence is presented in figures 4.3f and 4.3g by XPS for Cu-redox chemistry during the bacterial inactivation in addition to the redox chemistry described above in Figures 4.3d and 4.3e for Ti^{3+}/Ti^{4+} states. Figure 4.3f at time zero presents the experimental envelope for the XPS peaks at time zero at 934.3 eV for CuO and at 932.1 eV for Cu_2O. The Cu_2O peak in TiO_2/Cu in Figure 4.3f grows during the bacterial inactivation after 5 minutes and after 15 min when the bacterial inactivation is complete.

Table 4.3. Surface atomic concentration percentage of CuO and Cu_2O on TiO_2/Cu HIPIMS sputtered for 150 under light.

	% CuO	% Cu_2O
TiO_2/Cu at time zero	72	27
TiO_2/Cu at time 15 min	18	80

In agreement with Table 4.3a, a significant growth of the Cu_2O peak is detected in Figure 4.3g due to two reasons: a) the CuO initial decreases from 72% to 18% while concomitantly the Cu_2O grows from 27% to 80% in line with the redox catalysis taking place in TiO_2/Cu shifting the CuO peak in Figure 4.3g from CuO 934.3 eV to CuO 934.1 eV and b) the bacteria covering initially the TiO_2/Cu catalyst has been removed during the inactivation process.

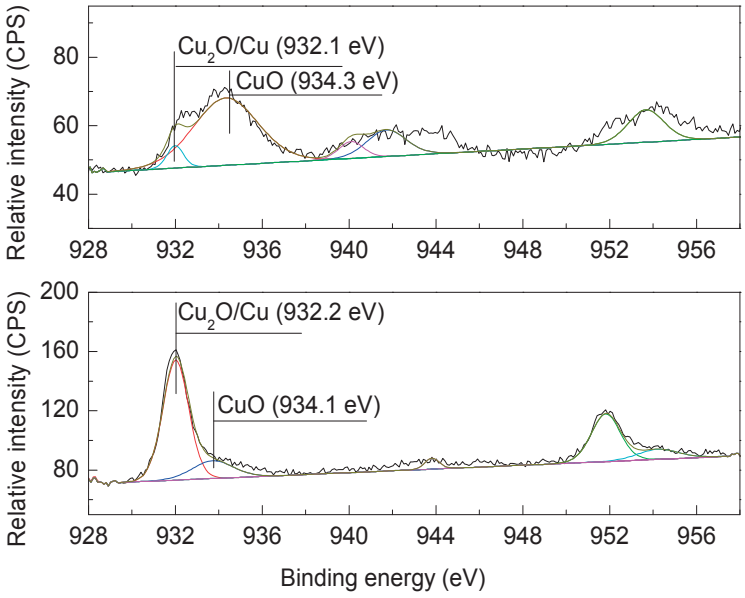

Figure 4.3g. Cu2p peak deconvolution at time zero and after 15 min after bacterial inactivation on a TiO_2 HIPIMS sputtered sample for 50s under solar simulated light.

It can be suggested that the interaction between Cu^+/Cu^{2+} and Ti^{3+}/Ti^{4+} in the TiO_2 /Cu samples play an active role accelerating the bacterial inactivation. The Ti^{3+}/Ti^{4+} surface electron trappers enhance the O_2 chemisorption at the surface more markedly in the TiO_2/Cu samples. This leads to a fast bacterial inactivation TiO_2/Cu compared to Cu in Figure 4.1d. The hole transition from TiO_2vb to the intra-gap states is followed by indirect electronic transitions from the intra-gap states reaching the TiO_2cb.

4.3.4. Mechanism of the bacteria inactivation under visible light.

Figure 4.4a shows the interfacial charge transfer between TiO_2 and Cu in the TiO_2/Cu photocatalyst TiO_2/Cu under light. In the TiO_2 semiconductor the light induces both the e^- transfer and h^+ transfer from TiO_2 to CuO since the potential energy levels of

the TiO_2cb and TiO_2vb lie at higher potential energy levels compared with the CuOcb and CuOvb levels.

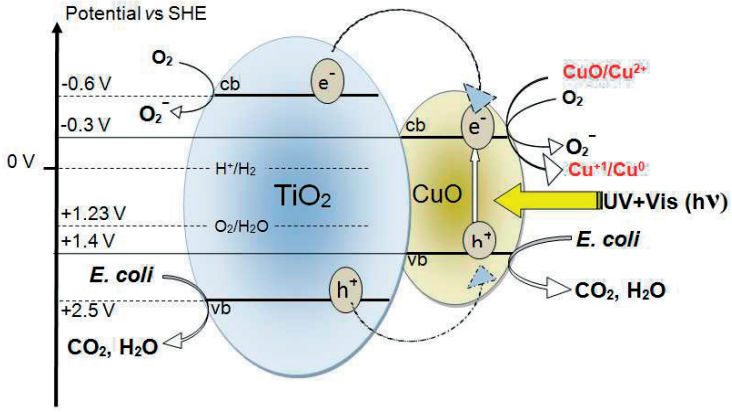

Figure 4.4a. Diagram suggested for of bacterial inactivation under solar simulated light photocatalyzed by TiO_2/Cu films on polyester.

The partial recombination of e-/h+ in the TiO_2 is hindered by the transfer of charges to the CuO facilitating the reactions occurring at the TiO_2cb and CuOcb as shown in Figure 4.4a. Under light, the CuO can be reduced to Cu_2O. The Cu_2O can reduce O_2 via a multi-electron process and re-oxidize to CuO. The charges generated by light in the TiO_2/Cu lead to the rapid loss of *E. coli* viability within 10 min (Figure 1b), along the O_2 and CuO reduction at the CuOcb as suggested in Figure 4.4a.

The interfacial charge transfer (IFCT) in the TiO_2/Cu sample seems to proceed with a high quantum efficiency since the bacterial inactivation proceeds within short times of about 10 min (Figure 4.1b). But the magnitude of the increase in the IFCT absorption of the TiO_2/Cu shown by the DRS spectra in Figure 4.1e is relatively small. The conduction band of CuO at -0.30 V vs SCE (pH 7) is at a more negative potential than the potential required for the one electron oxygen reduction $O_2 + H^+ + e^- \rightarrow HO_2^o$ -0.22 V [128-129]. Furthermore, the Cu^{2+} can react with e- (or O_2^-) $\rightarrow$ Cu^+ + (or O_2). The Cu^+ can reduce O_2 consuming electrons or be oxidized to Cu-ions by the photo-generated TiO_2 holes to Cu^{2+} [130]. The TiO_2vb holes react with the surface -OH of the TiO_2 releasing OH-radicals to inactivate bacteria [131].

Figure 4.4b presents the increase in fluorescence of the TiO_2/Cu HIPIMS sputtered samples irradiating up to 15 min in the solar simulator. The OH-radicals originate from the

reaction between the OH-radical and terephthalic acid leading to formation of a fluorescent hydroxy-product [123].

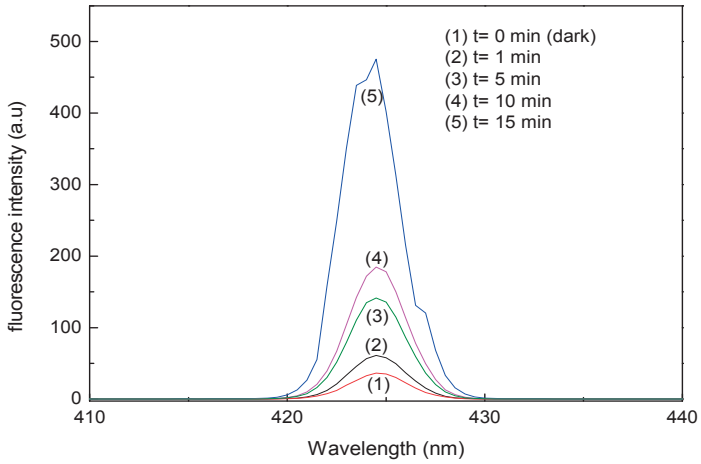

Figure 4.4b. Fluorescence intensity as a function of irradiation time for HIPIMS sputtered 150s samples on polyester irradiated under solar simulated light.

The TiO_2 vb holes in Figure 4.4a have the potential to degrade polyester during the bacterial inactivation cycles. But the stable repetitive *E. coli* loss of viability reported in Figure 4.1g shows that bacterial inactivation did not lead to the degradation of polyester up to the 8th reuse cycle.

4.3.5. DCP and HIPIMS sputtering of samples, applied power, charge density and bias voltage considerations

Figure 4.5a presents the loss of viability time vs thickness for DCP and HIPIMS TiO_2/Cu sputtered films. Figure 4.5a shows the much thinner TiO_2/Cu layer thickness necessary for complete bacterial inactivation sputtered by HIPIMS compared to DC/DCP. Fig 4.5a shows that the HIPIMS film with a thickness of 38 nm inactivated bacteria within ~10 min. Bacterial inactivation within similar time span was found to need more deposition time (more material) when using DC/DCP. Samples of 600 nm thick was needed to induce bacterial inactivation within the same time as HIPIMS samples.

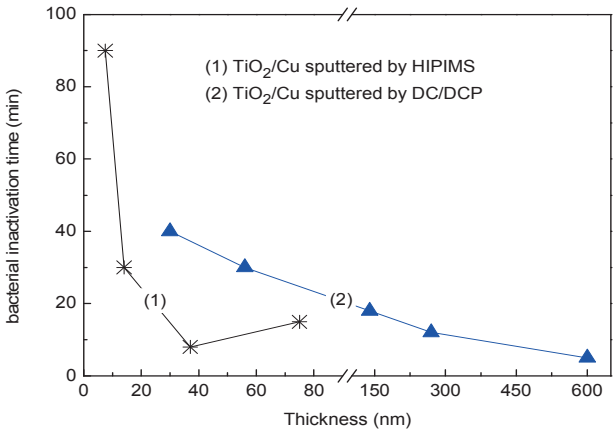

Figure 4.5a. Bacterial inactivation time *vs* nominal thicknesses for HIPIMS sputtered TiO_2/Cu films and by DC/DCP sputtered layers under solar simulated irradiation

In Figure 4.5b, left hand side presents a scheme for the DC sputtering proceeding with an ionization of the Cu-ions of 1% [132]. The DCP sputtering is schematically presented in Figure 4.5b (middle section) and proceeds with ionization of Cu-ions well above the values attained by DC [133]. Figure 4.5c, right-hand side involves HIPIMS sputtering leading to a Cu-ionization of ca. 70% and an electronic density of ~$10^{18\text{-}19}$ e-/m^3 [60]. The HIPIMS power per pulse was 1750 W/100 microseconds. This value is significantly higher than the power per pulse applied by DCP of 62.3 W/10 microseconds. The HIPIMS higher energy increased the ionization percentage $Cu^0 \rightarrow Cu^+/Cu^{2+}$ [134].

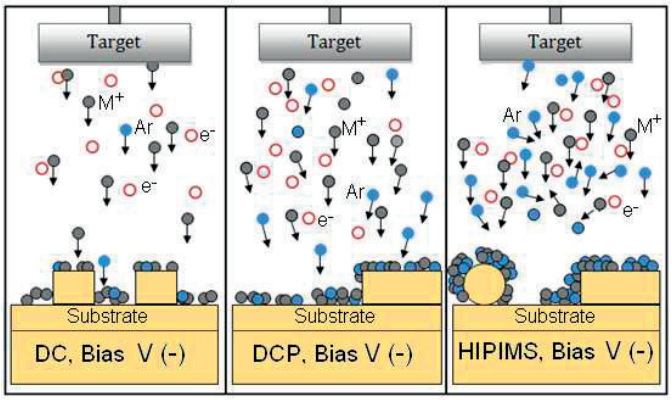

Figure 4.5b. Scheme for the magnetron chamber induced M^+ ionization by a) DC, b) DCP and c) HIPIMS sputtering of metal-ions (M^+) on 3-D substrates showing the higher density ionization induced by HIPIMS.

This increased arrival energy of the Cu-ions on the substrate allows the alignment of the Cu-ions on the polyester textiles showing high roughness surface leading to a uniform coverage of the 3-D polyester. The polyester 3-D presenting high roughness could not be quantified by atomic force microscopy (AFM) since it is beyond the AFM experimental range of 10 microns.

4.4. Conclusions

This study presents the first evidence for the surface functionalization of polyester by very thin HIPIMS layers of TiO_2/Cu able to inactivate bacteria in the minute range on 3-D surfaces like polyester fabrics. The TiO_2/Cu thin films were uniform, presented adhesive properties and led to repetitive loss of bacteria viability. A faster inactivation kinetics was observed by the TiO_2/Cu films compared to Cu or TiO_2 sputtered separately. HIPIMS sputtered sample for 10 min at 5 A led to a complete inactivation within 10 min under solar simulated light irradiation.

A considerable saving in metal and deposition time (energy) was found with HIPIMS compared to conventional DC/DCP-sputtering on 3-D surfaces. HIPIMS films of TiO_2/Cu and Cu on PES have been shown to preclude biofilm formation in the dark and more significantly under light irradiation.

The previous chapters showed bacterial inactivation kinetics on polyester textiles deposited with different energies applied to the sputtering targets. In addition to the textile surfaces, polyethylene bags can also harbour bacteria leading to HCAIs. This is why I choosed to prepare antibacterial, stable and adhesive polyethylene fabrics. The low surface energy of the polyethylene will be a challenge needing surface pretreatment/engineering as it will be shown in chapter 5.

Chapter 5

Innovative transparent non-scattering TiO_2 bactericide thin films inducing increased *E. coli* cell wall fluidity on PE

This chapter is based on the following publication: Sami Rtimi, Rosendo Sanjines, Mariusz Andrzejczuk, César Pulgarin, Andrzej Kulik, John Kiwi, Surface & Coatings Technology 254 (2014) 333–343 (Reproduced with permission of Elsevier, Copyright 2015).

5.1. Introduction

TiO_2 film preparation on glass, iron plates, textile fabrics and polymer films is a subject of timely research related to self-cleaning and antibacterial films [135-137,124]. Sol-gel commercial methods are used to prepare TiO_2 thin films on heat resistant substrates and they are generally adhered to heat resistant surfaces by calcination [138]. Colloid deposition on substrates requires temperature of few hundred °C for an adequate adherence to the selected substrate. The disadvantages of colloidal preparations to coat surfaces uniformly have been already discussed in chapter 3.

RF-plasma or UVC pretreatments induce surface sites able to bind TiO_2 nanoparticles [85,86,121,63]. RF-plasma pretreatment increases the polarity, roughness and hydrophilicity (C-OH) of polymeric films improving its bondability and interfacial adhesion [48,43]. The largest increase in surface polarity has been reported for the surfaces presenting the highest O/C atomic ratio [141-144]. The RF-plasma pretreatment induces negatively charged functional groups, e. g., carboxylic, percarboxylic, epoxide and peroxide groups by the atomic O, excited O, anionic and cationic O generated in the RF-plasma chamber. The functionalized negative sites bind the slightly positive sputtered $Ti^{4+}/(TiO_2)$ through electrostatic attraction involving chelation/complexation [85,141].

Kelly and Sarakinos have reported sputtering of TiO_2 films on substrates [56,53] and recently, Mills [90], Parkin [27], Foster [32], Dunlop [15] and Yates [31] have deposited antibacterial TiO_2 films on glass and polymers by chemical vapor deposition (CVD). The disadvantage of CVD is the high temperature required for the deposition, the high investment costs and the large amounts of heat used requiring costly cooling

systems. Radetic and Kostic [145,146] have reported polymer surfaces with antibacterial properties.

Polyethylene (PE) is a low cost and is widely available material. It is chemically inert, mechanically stable and flexible, UV-resistant and does not oxidize in air under sunlight. For this reason PE has been selected as the support for the TiO_2 film reported in this study. The PE-TiO_2 films are designed to increase the quantum yield for light induced processes due to their relatively high transparency [124,137,138,108]. This chapter describes the preparation of TiO_2 transparent, uniform, non-scattering films on PE (thermally stable up to 90°C). The low temperature preparation of TiO_2 on polymers at temperatures below the PE flowing point is investigated in this study.

This chapter addresses: a) design, preparation, evaluation and characterization of innovative pretreated PE-TiO_2 films inactivating *E. coli*, b) the bacterial inactivation kinetics under solar simulated light concomitant with the time of the PE-TiO_2 hydrophilic-hydrophobic conversion, c) the surface characterization addressing: the film thickness, optical absorption roughness, nanoparticle size, Ti-loading and surface atomic concentration and d) the ATR-FTIR spectroscopy description of the vibrational-rotational peak shifts due to the increase of the -CH inter-bond distance leading to cell wall lysis causing bacterial death.

The novelty of this work consists in the deposition of photoactive coatings on non thermoresistant substrate (PE) without loosing the mechanical stand. The PE is used for serum-bags and can be a source of contamination for the patient. Antibacterial coating on PE needs to respect the transparency of the PE allowing the visualization and the control of the serum/drug level inside the bag.

5.2. Experimental section

5.2.1. Pretreatment by RF-plasma and UVC; XRF determination of TiO_2

The low density polyethylene (LDPE) consists of highly branched low crystalline semi-transparent film with the formula $H(CH_2\text{-}CH_2)_nH$. The (LDPE) 0.1 mm thick was obtained from Goodfellow (ET311201), had a density of 0.92 g/cm^3, an upper working temperature of 90°C and a flowing point of 185°C. The single bond in PE makes it stable towards chemical/corrosive agents favoring its wide use as insulator.

The polyethylene fabrics were pretreated in two ways: a) in the cavity of the RF-plasma unit (Harrick Corp. 13.56 MHz, 100 W) at a pressure of 1 torr. Oxygen RF-plasma reacts with the PE surface inducing functional PE-surface groups by: a) etching

of the PE surface by the O-gas species, b) formation of surface O-hydrophilic surface groups and c) scission of intermolecular PE-bonds due to localized heat segmenting the fibers [148] and b) The PE was also functionalized by UVC irradiation using the 185/254 nm low-pressure mercury lamp obtained from Ebara Corp. Tokyo, Japan). The UVC lamp presented emission lines at 254 nm and 185 nm in a ratio 4:1 with a total power of 25W. The pretreatments were carried out at atmospheric pressure and at 1torr. The UVC activation, having a lower energy than the RF-plasma, does not lead to cationic or anionic oxygen species but only to atomic (O) and excited oxygen (O*). The radiant energy at 185 nm provides energies above 241 nm equivalent to 495 kJ/mole or 5.12 eV, the energy required for slitting $O_2 \rightarrow 2O^*$.

The Ti-content on the polyethylene was evaluated after the Ti sputtering in reactive O_2 gas by X-ray fluorescence (XRF) in a PANalytical PW2400 spectrometer.

5.2.2. Sputtering details of TiO_2 on PE and X-ray diffraction (XRD)

The TiO_2 was sputtered by direct current magnetron sputtering (DC) on PE as reported previously out of our laboratory [95]. Before sputtering the films, the residual pressure P_r in the sputtering chamber was set to $P_r \leq 10^{-4}$ Pa. The substrate to target distance was set at 10 cm. The TiO_2 thin films were deposited by reactive DC-magnetron sputtering (DC) in an O_2 gas flow from a 5 cm diameter Ti-target 99.99 % pure (Kurt J. Lesker, East Sussex, UK). The current on the Ti target was set at 280 mA, at a power of 128 Watt. The thickness of the sputtered layers was determined by means of a profilometer (Alphastep500, Tencor) by deposing TiO_2 films onto silica wafers.

The crystalline structure of the PE-TiO_2 film was investigated by X-ray diffraction (XRD) and recorded on an X'Pert MPD PRO from PANalytical equipped with a secondary graphite (002) monochromator and an X'Celerator detector operated in Bragg–Brentano geometry. A step size of 0.0081 was chosen and an acquisition time of 2 min per degree.

5.2.3. Diffuse Reflectance Spectroscopy (DRS)

Diffuse reflectance spectroscopy was carried out a Perkin Elmer Lambda 900 UV-VIS-NIR spectrometer provided for with a PELA-1000 accessory within the wavelength range of 200-800 nm and a resolution of one nm. The absorption of the samples was plotted in the Kubelka-Munk (KM) unit's *vs* wavelength.

5.2.4. Atomic force microscopy (AFM) and contact angle

The AFM images were acquired in contact mode using a PSIA Xe-100 AFM. Silicon nitride cantilevers were used with feedback set points around 1.0 nN. The images originate from the Z-scanner and are not influenced by the non-linearity and the hysteresis of the z-scanner. The roughness values involve an experimental error below 10%. The mean surface roughness (R_a) was calculated for the scanned area by applying eq (1)

$$R_a = \sqrt{\sum_{x,y}^{N} \frac{(Z_{x,y} - Z_{average})^2}{N^2}} \qquad \text{eq.(1)}$$

Where: R_a is the normalized standard deviation calculated from the local heights ($Z_{x,y}$) and the average height ($Z_{average}$) determined over the x,y coordinates (N) measured in the AFM image.

The hydrophilicity of the PE-TiO_2 films was determined by the water droplet contact angle by the sessile drop method on a DataPhysics OCA 35 unit.

5.2.5. Evaluation of *E. coli* inactivation on PE-TiO_2 and light sources

The samples of *E. coli* K12 were obtained from the Deutsche Sammlung von Mikroorganismen und Zellkulturen GmbH (DSMZ) ATCC23716, Braunschweig, Germany, to test the antibacterial activity of the PE-TiO_2 samples. The 2cm by 2cm samples were placed into a glass Petri dish to be inoculated with bacteria and irradiated in the cavity reactor. 100-µL of *E. coli* solution was contacted with the PE-TiO_2 uniform films. The 100 µL culture aliquots with an initial concentration of ~10^6 colony forming units per milliliter (CFU mL^{-1}) in NaCl/KCl (pH 7) were placed on coated and uncoated (control) PE fabrics. After preselected irradiation times, the fabric was transferred into a sterile 2 mL Eppendorf tube containing 1 mL autoclaved NaCl/KCl saline solution. This solution was subsequently mixed thoroughly using a Vortex for 3 min. Serial dilutions were made in NaCl/KCl solution. A 100-µL sample of each dilution was pipetted onto a nutrient agar plate and then spread over the surface of the plate

using standard plate method. Agar plates were incubated lid down, at 37°C for 24h before colonies were counted. The 100-µL of the *E. coli* solution was contacted with the PE-TiO_2 films. The PE samples were kept in a sterile oven at 60°C to avoid contamination prior to the photo-activated bacterial tests. The exposition of the PE-TiO_2 samples to the Suntest light was carried out on Petri dishes provided with a lid to prevent evaporation in the Suntest cavity. The agar was purchased from Merck GmbH, Microbiology division KGaA under the cat N° 1.05463.0500.

Three independent assays were carried for each PE-TiO_2 sample inactivating bacteria. The CFU statistical analysis was performed calculating the standard deviation values. The average values were compared by one-way analysis of variance and with the value of statistical significance. One way analysis of variance (one-way ANOVA) was used to compare the mean of the samples using the Fisher distribution. The response variable was approximated for the sample data obtained from the photocatalytic bacterial inactivation on tested samples presenting approximately the same distribution within similar sputtering times.

PE-TiO_2 samples were irradiated with the Xe-400W light in the Suntest solar simulator CPS (Atlas GmbH, Hanau, Germany). The integral light dose in the range of 310 to 800 nm was 52 mW/cm^2. The power density of 52 mW/cm^2 is equivalent to 52% of the maximum solar dose AM1 reaching perpendicularly at 12 AM the Equator latitude. A cut-off filter was added in the Suntest cavity to block the light between 290 and 310 nm amounting to about 3% of the total irradiation.

5.2.6. Fourier Transform Infrared Spectroscopy (FTIR-ATR) and malondialdehyde (MDA) formation during *E. coli* inactivation

FTIR spectra were measured in a Portmann Instruments AG spectrophotometer equipped with a Specac attachment (45° one pass diamond crystal). Spectra were taken by 256 scans with a resolution of 2 cm^{-1} in the range 900-4000 cm^{-1}. The position of the IR peaks was found by the second derivative of the spectra after Fourier deconvolution.

By ATR-IR spectroscopy the oxidative damage of lipids was detected by an increase in the bands a) at 1018 cm^{-1} assigned to O-O bonds of hydroperoxides, b) at 972 cm^{-1} assigned to trans C=C bonds and c) at 1720 cm^{-1} assigned to the formation of aldehydes during lipid peroxidation [108]. The lipid peroxidation leads to the formation of MDA. By high performance liquid chromatography (HPLC) the MDA was measured in an Agilent 1100 series HPLC equipped with a UV absorbance detector.

Filtered samples were injected via auto-sample and eluted at a flow rate of 0.9 ml/min through a Nucleosil C18 (Marcherey-Nagel) column. The mobile phase consisted of a solution 3 mM KH_2PO_4-MeOH (65-35v/v%). Chromatograms were monitored at 268 nm and the retention time of MDA was 3.9 min.

5.2.7. X-ray photoelectron spectroscopy (XPS) of PE-TiO_2 and transmission electron microscopy (TEM)

The X-ray photoelectron spectroscopy (XPS) of the PE-TiO_2 films was determined using an AXIS NOVA photoelectron spectrometer (Kratos Analytical, Manchester, UK) provided for with monochromatic AlK_α ($h\nu$=1486.6 eV) anode. The carbon C1s line with position at 284.6 eV was used as a reference to correct the charging effect. The surface atomic concentration was determined from peak areas using the known sensitivity factors for each element [97]. Spectrum background was subtracted according to Shirley [122]. The XPS spectral peaks of TiO_2 were deconvoluted with a CasaXPS-Vision 2, Kratos Analytical UK.

As the PE is soft, many tests with different embedding media were tried. Two pieces from the same sample were glued together without extra embedding and were cut using Cryo-ultramicrotomy sectioning at temperature –140°C (Ultramicrotome: Leica EM UC7). The section thicknesses were in the range 60-100 nm.

The microscope used during the course of this study was FEI Tecnai Osiris with accelerating voltage 200 kV. Imaging of PE-TiO_2 sputtered for 8 min was performed in Bright-field STEM and High Angle Annular Dark-field (HAADF) modes. Chemical analysis was performed on energy dispersive X-ray spectroscopy (EDX) system.

5.3. Results and discussion

5.3.1. PE pretreatment, TiO_2 surface sputtered PE, diffusion reflectance spectroscopy (DRS) and TiO_2 crystalline phases

Figure 5.1a shows the thickness of the TiO_2 sputtered on PE as a function of sputtering time. For the sample pretreated in air for 15 min by RF plasma and sputtered for 8 min, a TiO_2 thickness of ~58 nm was attained on PE equivalent to ~290 layers.

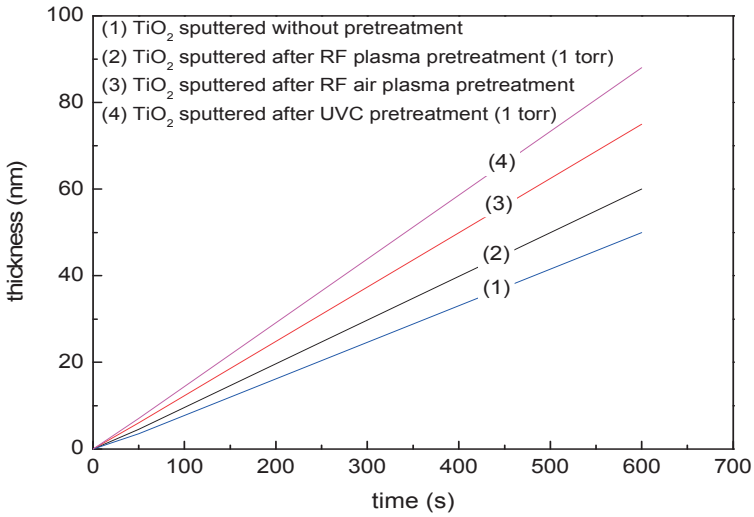

Figure 5.1a. Thickness calibration of TiO_2 sputtered on PE (1) PE without pretreatment, (2) PE pretreated with RF plasma for 15 min at 1 torr, (3) PE pretreated with RF-air plasma for 15 min and (4) PE pretreated with UVC for 20 min at 1 torr.

If one atomic layer contains 10^{15} atoms/cm^2 with a thickness of 0.2 nm, the rate of TiO_2 deposition was can be estimated as $6x10^{14}$ atoms/cm^{2}s. The TiO_2 sputtering for 8 min on PE pretreated by RF-plasma led to the highest TiO_2 loading on PE without affecting the PE transparency which is a sign of PE-degradation (See Table 5.1).

Table 5.1. X-ray fluorescence determination (XRF) analyses of PE-TiO_2 samples sputtered for different times with and without PE-pretreatment.

Sample	Surface TiO_2 wt % / wt PE
PE-TiO_2 (1 min), no pretreatment	0.009
PE-TiO_2 (3 min), no pretreatment	0.019
PE-TiO_2 (5 min), no pretreatment	0.031
PE-TiO_2 (8 min), no pretreatment	0.051
PE-TiO_2 (8 min), RF plasma pretreated under vacuum 15 min (1 torr)	0.081
PE-TiO_2 (8 min), RF air plasma pretreated for 15 min	0.096
PE-TiO_2 (8 min), UVC pretreated for 20 min (1 torr)	0.101

The surface atomic percentage concentration during bacterial inactivation reported in Table 5.2 remained stable, showing an invariant amount of TiO_2 on the topmost PE surface.

Table 5.2. Surface percentage atomic concentration of PE-TiO_2 sputtered for 8 min, before and after bacterial inactivation.

	Sample		C	O	Ti	N
Before bacterial inactivation	No pretreated PE		52.37	30	6.17	0.00
	Pretreatment	RF air plasma	55.14	33.27	8.82	0.07
		RF plasma	53.58	31.84	7.44	0.09
		UVC	54.01	33.11	7.62	0.11
After bacterial inactivation	No pretreated PE (irradiation for 270 min)		58.19	32.08	6.17	0.00
	Pretreatment	RF air plasma (60 min)	55.78	33.96	8.99	0.00
		RF plasma (90 min)	56.43	31.84	7.01	0.04
		UVC (60 min)	57.33	34.53	7.11	0.09

Tennakone reported back in 1991 [149] supported TiO_2 on PE by a single thermal treatment sprinkling anatase on PE and ironing at 74°C. The PE-TiO_2 was used to photomineralize phenol under UV and solar light. This study selected PE as the polymer substrate since it is stable against oxidation and UV-light, inexpensive and readily available. Ohtani et al., [150] reported in a separate study that PE undergoes a significant degradation when TiO_2 particles were embedded internally as compared when the TiO_2 was deposited only on the surface leading to a negligible PE degradation. In the present study RF-plasma pretreatment led to functional polar groups on the PE topmost layers since no color changes were observed indicative of PE-degradation as reported in references [149,150]. Until now sol-gel [151], dip-coating [152], CVD [153], plasma enhanced chemical vapor deposition [154], metal organic chemical vapor deposition (MOVCD) [149] and spray-methods have been used to bind TiO_2 to surfaces resisting high temperatures. But they are not convenient to deposit TiO_2 on PE since they involve calcination temperatures of few hundred degrees. The lack of binding sites of PE and its low surface energy lead to lower adhesion of TiO_2. To improve the deposition of TiO_2 relative to the former methods, the

PE has been pretreated to induce a higher amount of binding sites and subsequently sputtered TiO_2 nanoparticles. The amount of TiO_2 found on the pretreated PE was determined by XRF. Table 1 shows the TiO_2 amounts found on the pretreated surfaces.

For practical uses of PE-TiO_2 films an estimation of the electrical power required for the sputtering can be put forward for a sample when sputtering with a Ti-target at 500V and 0.3 A or 150W for 8 min. The electrical power needed is equivalent to ~0.2 KWh/4 cents taking the cost of 0.20 US per KWh. The sputtering cost is high, but the uniformity, stability and activity of the PE-TiO_2 may justify the expense for some special applications where a transparent photocatalyst are needed.

Figure 5.1b (i-iii) shows in Figure 1b (i) the photographic image of a non-scattering transparent PE-TiO_2 film obtained after 15 min RF-air plasma pretreatment and 8 min DC sputtering of TiO_2. Figures 5.1b (ii-iii) shows a drop of bacterial suspension on the PE-TiO_2 before and after the illumination on the PE-TiO_2 film.

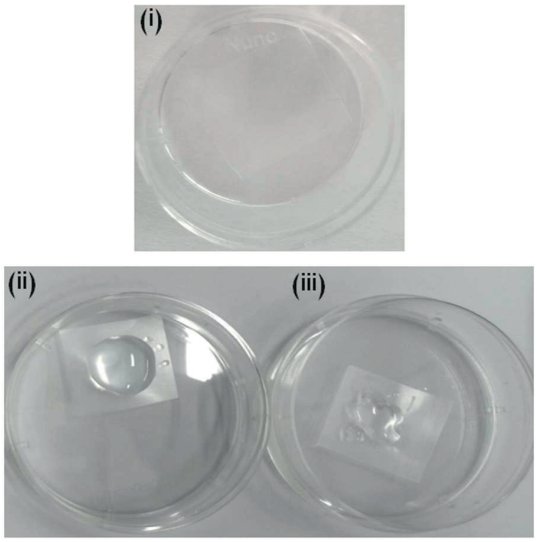

Figure 5.1b. (i) Photographic image of the transparent non-scattering PE-TiO_2 film obtained after 15 min RF-air plasma and sputtering for 8 min. (ii) and 1b (iii) show a bacterial suspension drop at time zero and after 60 min irradiation under solar simulated light (52 mW/cm^2).

The optical spectra of the samples (DRS) are routinely plotted in Kubelka-Munk (KM) unit's *vs* wavelength since the rough UV-Vis reflectance data cannot be used directly to account for the optical absorption due to the decrease in the transmittance introduced by the TiO_2 nanoparticles. KM/S units were used in Figure 5.1c.

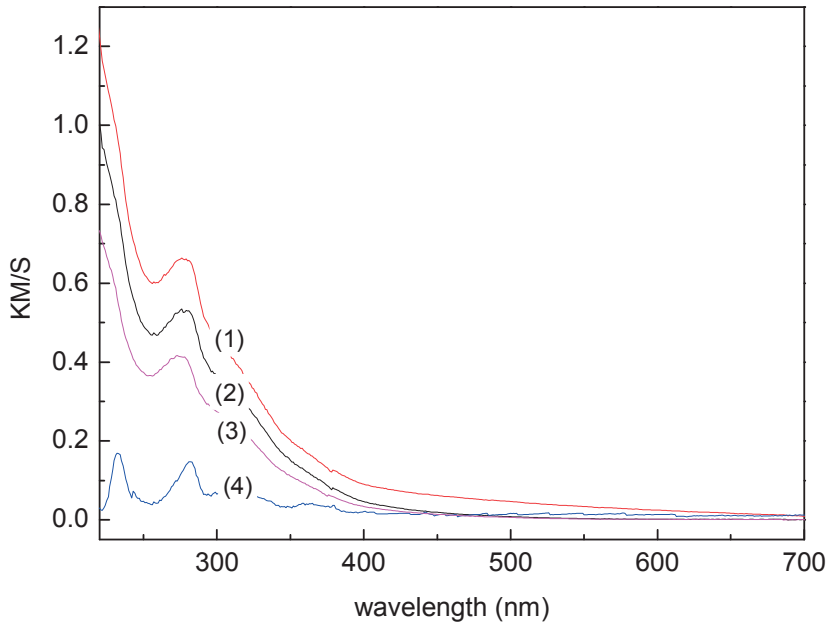

Figure 5.1c. DRS of TiO_2 sputtered (8 min) on PE: (1) pretreated with UVC 1torr (2) pretreated with RF air plasma (3) pretreated with RF plasma and (4) TiO_2 sputtered on PE for 1 min without pretreatment.

The DRS spectra of the PE-TiO_2 films confirm that the TiO_2 absorption is related to the type and pretreatment time preceding sputtering of TiO_2 (Figure 5.1c). Sputtering TiO_2 for 1 to 3 min on PE led to transparent TiO_2 films showing low absorbance and almost no antibacterial activity. A decrease of ~5% or more in optical transmittance has been reported for RF-plasma pretreated PE [155-156,125]. The decrease in transmittance observed for the PE-TiO_2 is due to the inherent high refractive index of TiO_2.

The XRD TiO_2 crystal phases on PE shows a high anatase (A) peak at θ=21.5° [149] for a PE-TiO_2 with and without RF-plasma pretreatment. But XRD peaks of rutile (R) at temperatures ≤ 130°C available in the DC-magnetron chamber were also observed (See Annex 5). The generation of rutile at low temperatures is due the structure forming function of the PE film on TiO_2 was previously reported for polyamide on TiO_2 textiles [85]. The XRD signals for both, the high anatase peak and the smaller rutile peaks became more intense as a function of the sputtering time.

5.3.2. Antibacterial kinetics evaluation and sample reuse cycles

Figure 5.2 shows the *E. coli* inactivation on PE-TiO_2 films under simulated solar light with an integrated light dose of 52 mW/cm^2. The fastest bacterial inactivation was found for pretreated PE samples TiO_2 sputtered for 8 min.

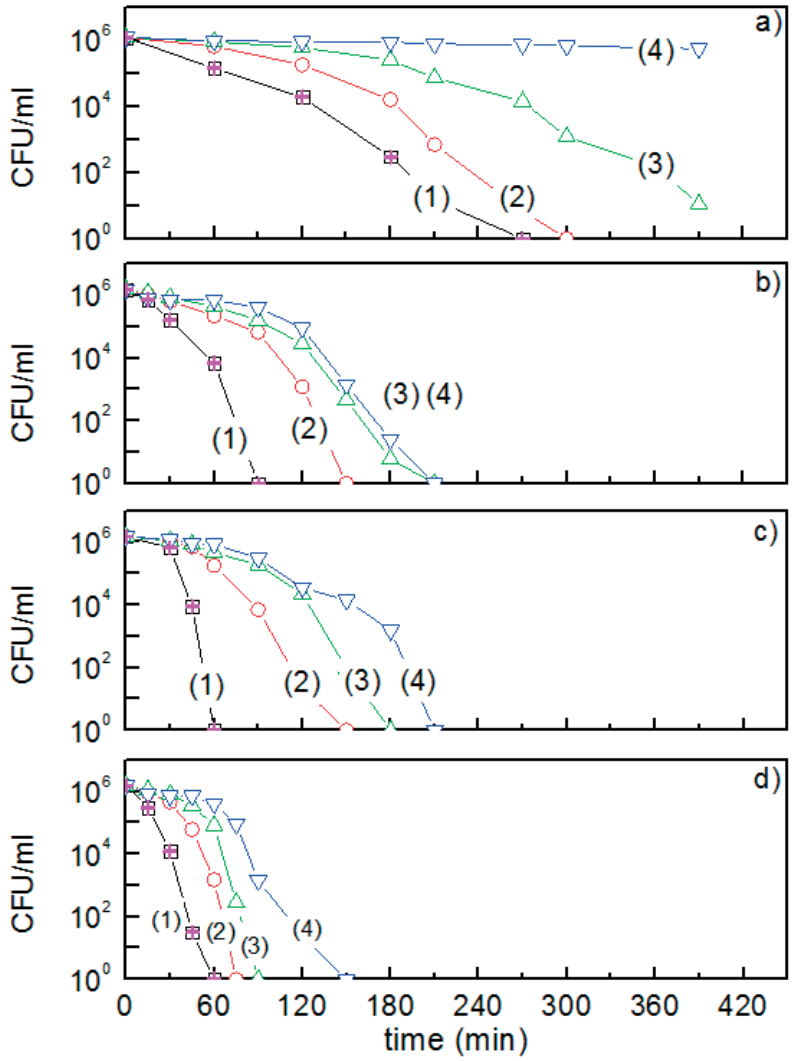

Figure 5.2. *E. coli* inactivation on TiO_2 sputtered on PE for 8 min irradiated with simulated solar light (52 mW/cm^2) **a)** TiO_2 sputtered for different times without RF-plasma pretreatment for: (1) 8 min, (2) 10 min, (3) 5 min and (4) PE alone. **b)** TiO_2 sputtered for 8 min with surface RF-plasma pretreatment at 1 torr for: (1) 15 min, (2) 20 min, (3) 30 min and (4) 5 min. **c)** TiO_2 sputtered 8 min RF air plasma pretreatment for: (1) 15 min, (2) 20 min, (3) 30 min and (4) 5 min. **d)** TiO_2 sputtered 8 min with UVC pretreatment for: (1) 20 min, (2) 15 min, (3) 10 min and (4) 5 min. Error bars: standard deviation (n=5%).

Figure 5.2a presents the bacterial inactivation on PE-TiO_2 samples sputtered for 8 min and RF-pretreated for different times. No significant bacterial inactivation was observed for bacteria on uncoated PE (Figure 5.2a, trace 4). Only trace 1) was subjected to statistical analyses since it showed the most favorable kinetics and presents the highest amount of TiO_2 sites in exposed positions interacting with bacteria [86,5]. PE-TiO_2 sputtered for 1 and up to 5 min did not contain sufficient TiO_2 to drive

a fast bacterial inactivation. The Ti-loading on PE was determined by XRF at times 1, 3, 5 min and the values found were 0.009, 0.019 and 0.031 TiO_2 wt% / wt PE respectively.

Samples sputtered for times longer than 8 min led to layer thickness >45 nm (Figure 5.2). Higher thicknesses lead to the bulk inward diffusion of charges decreasing the charge transfer between the PE-TiO_2 and bacteria [125]. Sputtering for 8 min led to a TiO_2 loading with the most suitable thickness for the charge diffusion able to reach bacteria in Figure 5.2c, trace (1). No bacterial inactivation was observed for bacteria on PE films in the dark.

To verify that no re-growth of *E. coli* occurs after the first bacterial inactivation cycle, the PE-TiO_2 film was incubated on an agar Petri dish for 24 hours at 37°C. No bacterial re-growth was observed meaning that there were no bacteria was present on the surface after the inactivation cycle.

The bacterial inactivation by PE-TiO_2 samples sputtered for 8 min and pretreated with RF-plasma in air for 15 min was investigated up to the 6^{th} cycle. The reuse cycles of the samples show stable inactivation kinetics up to the 5^{th}-cycle, then the reuse time became slower by ~20%. After each cycle, the samples were washed with distilled water and dried at 60°C to avoid bacterial contamination. After washing PE-TiO_2 the samples were left standing for 24 h to regain the sample initial hydrophobicity. This will be discussed below in section 5.3.4, when commenting on the hydrophilic-hydrophobic transformation induced by light irradiation PE-TiO_2 samples in Figure 5.5.

5.3.3. AFM topography of PE-TiO_2 sputtered surfaces

The roughness values for different PE samples were observed to be higher for pretreated samples compared to non-pretreated samples. Figure 5.3 presents PE-TiO_2 RF air plasma pretreated samples: a) R_g=7 nm was attained for PE-TiO_2 sputtered 8 min, without PE pretreatment. A larger R_g value of 16 nm was observed for PE-TiO_2 sputtered for 8 min and pretreated for 15 min at 1 torr.

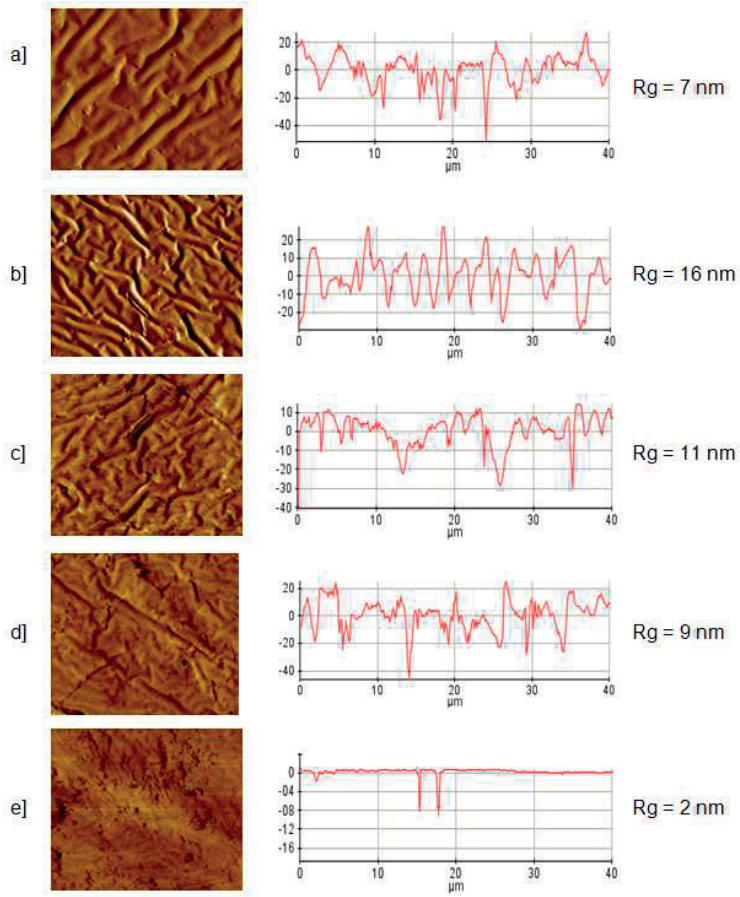

Figure 5.3. AFM topography of PE-TiO_2 a) PE-TiO_2 sputtered for 8 min without pretreatment, b) PE-TiO_2 sputtered for 8 min with RF plasma pretreated at 1 torr for 15 min, c) PE-TiO_2 sputtered for 8 min with RF air plasma pretreated for 15 min, d) PE-TiO_2 sputtered for 8 min with UVC pretreatment for 20 min in air, e) PE-TiO_2 sputtered for 1 min on a RF air plasma pretreated for 15 min.

The found roughness (Rg) for PE-TiO_2 pretreated by RF air plasma for 15 min and sputtered for 8 min was Rg=11 nm [48]. The trend in the Rg-values showed that a higher roughness lead to an accelerated bacterial inactivation involving thicker TiO_2 layers.

5.3.4. Contact angle and hydrophobic-hydrophilic photo-switching on PE-TiO_2

Figure 5.4a presents the hydrophobic to super-hydrophilic transformation occurring on the PE-TiO_2 sample induced by simulated solar light [157-158]. The decrease of the contact angle to less than 5° within 60 min is shown in Figure 5.4a, traces a-e. The recovery from the PE-TiO_2 hydrophilic surface to the initial hydrophobic surface proceeded within 24 hours in the dark (see Figure 5.4b).

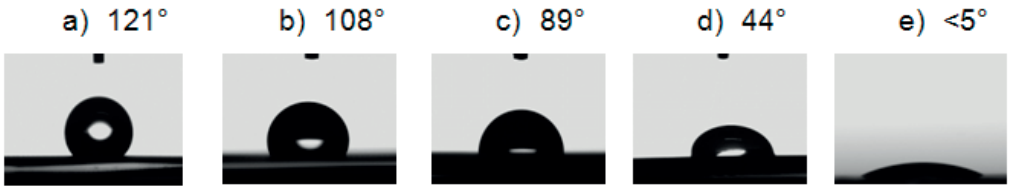

Figure 5.4a. Photo-induced induced hydrophilicity under Solar simulated light irradiation followed by water droplet contact angle of a PE-TiO_2 film pretreated by RF-air plasma for 15 min and sputtering for 8 min at times: a) t=0 min, b) 15 min, c) 30 min, d) 45 min and e) 60 min.

Figure 5.4b. Restoration of the initial hydrophilicity on the PE-TiO_2 as a function of times in the dark: a) 6 h, b) 12 h, c) 18 h and d) 24 h.

Figure 5.5 illustrates the rate of photo-induced hydrophilicity and of the back reaction to the initial hydrophobic PE-TiO_2 surface as a function of "cos Θ". The kinetics of the conversion to the super-hydrophilic state is shown in Figure 5.5, trace 1. The kinetics of the back-reaction is described in Figure 5.5, trace 2.

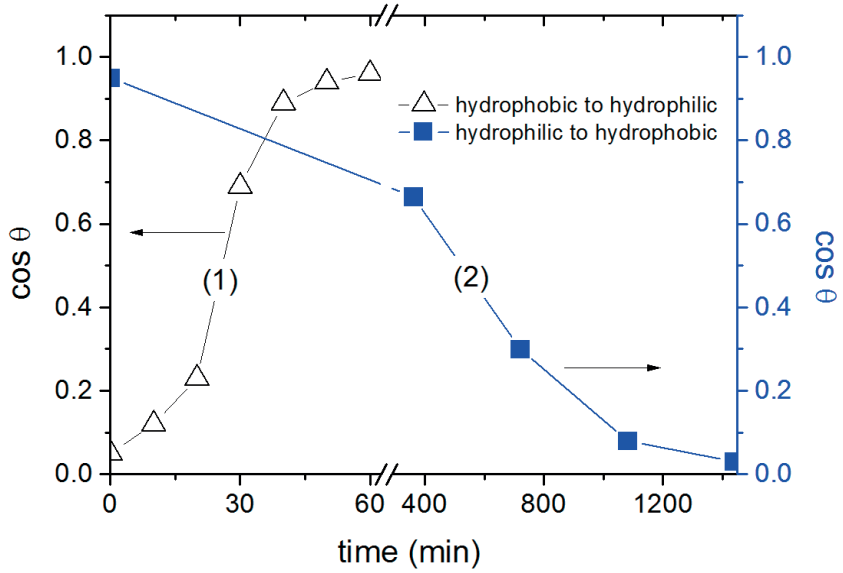

Figure 5.5. (1) Kinetics of the hydrophobic-hydrophilic transformation under solar simulated light of a film pretreated by RF-air plasma for 15 min and sputtering for 8 min at times up to one hour and (2) kinetics of the dark reverse reaction to the initial state for PE-TiO_2 film RF-air plasma pretreated for 15 min and sputtered for 8 min.

According to Young's theory the "cos Θ" of a liquid droplet on a solid surface is a function of the interfacial energy between the solid and the liquid. The contact angle conventionally measures the angle where the liquid meets the solid quantifying the wettability of a solid surface via the Young equation. The Young equation involves solid-vapor, liquid-vapor and solid-liquid interfacial energies. The solid-vapor interfacial energy is denoted by γ_{SG}, the solid-liquid interfacial energy by γ_{SL}, and the liquid-vapor interfacial energy (i.e. the surface tension by γ_{LG}, then the equilibrium contact angle θ_C is determined from these quantities by Young's equation:

$$0 = \gamma_{SG} - \gamma_{SL} - \gamma_{LG}\cos\theta_C \qquad \text{ep(2)}$$

In eq. (2), γ is the surface free energy and t=∞ corresponds to interfacial energy of the hydrophobic surface before irradiation. The rate of the hydrophobic to hydrophilic conversion and the reverse reaction were: 0.277 min^{-1} and $8.71x10^{-3}$ min^{-1} respectively. These rates were calculated according to the Young's equation in the following way [138,12]. During the irradiation the hydrophobic surface is converted to a hydrophilic surface reducing the interfacial energy between the solid and liquid surface. Seki and Tachiya [159] optimized this equation taking into account the difference in interfacial energy and the equation becomes:

$$\cos\theta = \left(\gamma_{SG} - \gamma_{SL}\right)/\gamma = \left(\gamma 1_C + \gamma 2\right)/\gamma = f1_C + f2 \qquad \text{eq(3)}$$

Where: f1 = $\gamma 1/\gamma$, f2 = $\gamma 2/\gamma$ and c is the surface fraction of hydrophilic region. Taking a single rate constant for the photo-assisted hydrophilic conversion and the back hydrophilic to hydrophobic conversion, Seki and Tachiya [159] obtained two equations. The first one applies for the hydrophilic to hydrophobic conversion in the dark and the second one for the photo-assisted hydrophilic conversion:

$$\cos\theta = f_{1cb}(0)\exp^{(-Kb)t} + f_2 \qquad \text{eq(4)}$$

$$\cos\theta = \left[\frac{f_1 c(0) - f_1 k_f}{(K_f + K_b)}\right]\exp^{-(kf+kb)t} + [f_1 k_f/(k_f + k_b) + f_2] \qquad \text{eq(5)}$$

The hydrophobic properties of the PE-TiO_2 surface before the photo-switching is important in antibacterial films (see Figures 5.4 and 5.5). *E. coli* and *S. aureus* present a preferential adhesion to hydrophilic surfaces [10,160,44]. Bacteria with hydrophobic surface properties like *S. epidermis* adhere preferentially to hydrophobic surfaces

[161]. Hydrophobic bacteria have been reported to adhere to a variety of surfaces forming biofilms to a greater extent than hydrophilic bacteria [162]. Recently, R. Amal et al., reported the reversible photo-switching behavior by TiO_2 and Ag-nanoparticles [163,109]. There has been a controversy for a long time if hydrophilic, hydrophobic or mixed hydrophilic-hydrophobic surfaces enhance bacterial adhesion, a step preceding bacterial inactivation. This study shows that the complete inactivation of *E. coli* occurs while PE-TiO_2 undergoes the transformation to the super-hydrophilic state within 60 min irradiation (Figures 5.2 and 5.5).

5.3.5. FTIR analysis and bacterial inactivation on PE-TiO_2

FTIR spectroscopy was used to monitor the changes in the structure/dynamics in the *E. coli* lipo-polysaccharide (LPS) bilayer induced by PE-TiO_2 under solar simulated light. LPS amphiphiles are localized in the outer *E. coli* bilayer cell wall consisting of LPS units covalently linked to lipid A, anchoring the LPS to the *E. coli* cell wall envelope. The LPS spectra did not vary within a wide hydration range since it is made up of fluid chains [164]. The (CH_2)- and (CH_3)- groups make up 70% of the *E. coli* bilayer envelope containing lipo-polysaccharide (LPS), phosphatidyl-ethanolcholine (PEC) and peptidoglycan (PGN).

The characteristic bands of the methylene ($-CH_2$) stretching vibrations in the 2800-2900 cm^{-1} spectral region are shown in Figure 5.6. Figure 6a shows the shift of the asymmetric methylene stretching vibrations at $n_a(CH_2)$ 2922.2 cm^{-1} and of the symmetric stretching vibrations of $n_s(CH_2)$ at 2849.2 cm^{-1} for RF-plasma pretreated samples for 15 min and sputtered for 8 min and then irradiated up to 60 min. The shifts in the peaks for RF-plasma pretreated PE-TiO_2 samples in Figure 5.6a,b are seen to be more important compared to the non-pretreated samples shown in Figures 5.6c,d. This is due to the lower amount of TiO_2 on the non-pretreated PE leading to longer bacteria inactivation times. The IR-assignment is possible due to the functional group related IR-parameters [15,108]. Shifts in the peak of the $-CH_2$ stretching vibrations reflect structural transformations that occurred in the LPS. These shifts are the precursors of the structural/conformation in LPS during lipid peroxidation leading to: peroxides; alcohols and carboxyl groups.

The decrease observed for the stretching vibrations in the IR-spectra in Figure 5.6a-d, was due to isolated double bonds in the LPS. The spectral changes reported

in Figures 5.6a-d are sensitive enough to monitor LPS conformation changes without introducing additional perturbations.

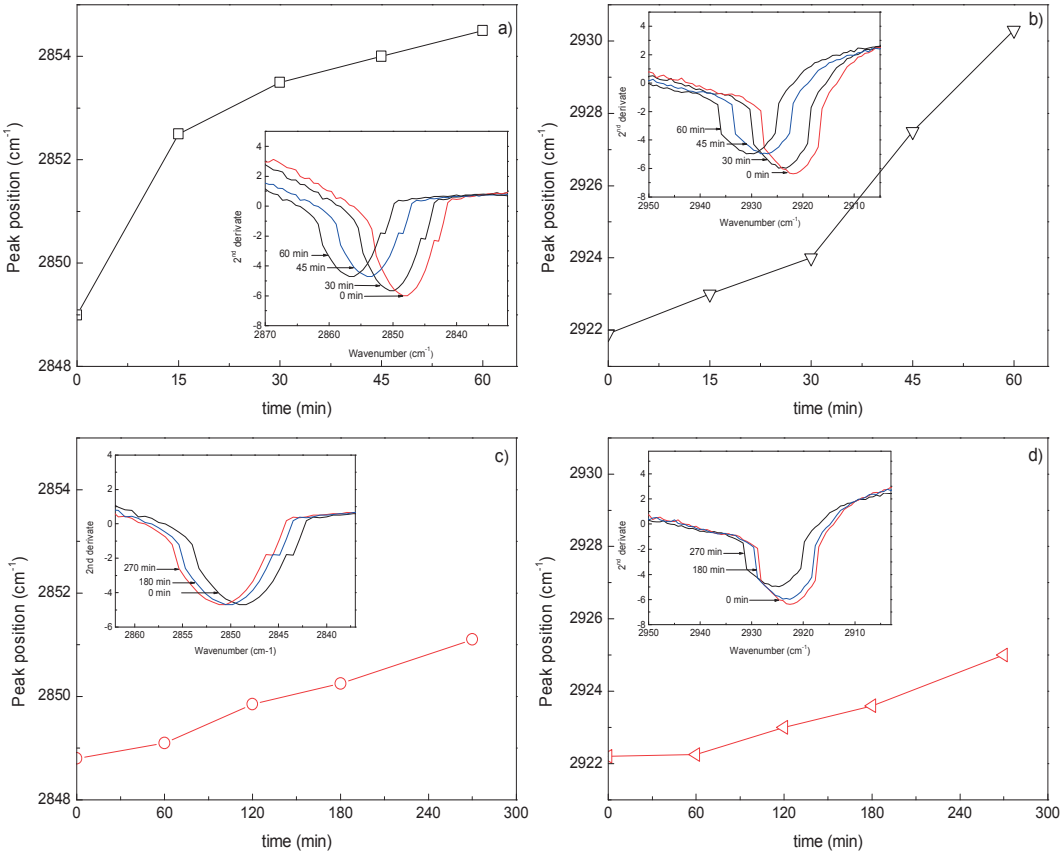

Figure 5.6. a and b show the shifts of νa(CH_2) vibrational bands on PE-TiO_2 samples pretreated with RF-air plasma for 15 min and then sputtered for 8 min. Shift of the stretching vibrations as a function of time detected by ATR-FTIR for the asymmetric νa(CH_2) vibrational bands and the symmetric νs(CH_2) vibrational bands for *E. coli* up to 60 min under solar simulated irradiation. Figure 5.6c and d show the IR shifts of νs(CH_2) vibrational bands for non-pretreated PE-TiO_2 sputtered for 8 min.

The discontinuous shifts in Figures 5.6a/b are suggested to occur due to an increased mobility of the LPS units in the LPS chain-packing [164]. The increased disorder modifies the frequencies of the -CH_2 symmetric and anti-symmetric bands, shifting the peak positions during the irradiation time. As the inactivation process, the shift of the asymmetric $V_a(CH_2)$ and the symmetric $V_s(CH_2)$ peaks reflect a variation in the density of the LPS polar head modifying the LPS packing-pattern [165]. This is associated to the enlarged intermolecular C-H bond distance in the LPS fatty chain [166] increasing the LPS fluidity [108].

Figure 5.2c, trace 1 showed that *E. coli* inactivation is complete within 60 min. This *E. coli* inactivation time corresponds to the time in which LPS stretching vibrations

attain the fluidity necessary for *E. coli* inactivation [167-168]. The discontinuous but constant increase in the LPS packing leads to longer -CH_2 interbond distances and ultimately to *E. coli* lysis and MDA formation as described in the section 5.3.6 below [169].

5.3.6. Evolution of MDA formation within the time of increase of hydrophilicity and IR-peak shifts-numerical correlation

Lipid peroxidation is a complex process whereby an unsaturated lipid reacts with molecular oxygen to yield lipid hydroperoxide and dialkyl-peroxides. The kinetics of MDA formation during photocatalytic oxidation of the cell wall bilayer is shown in Figure 5.7a.

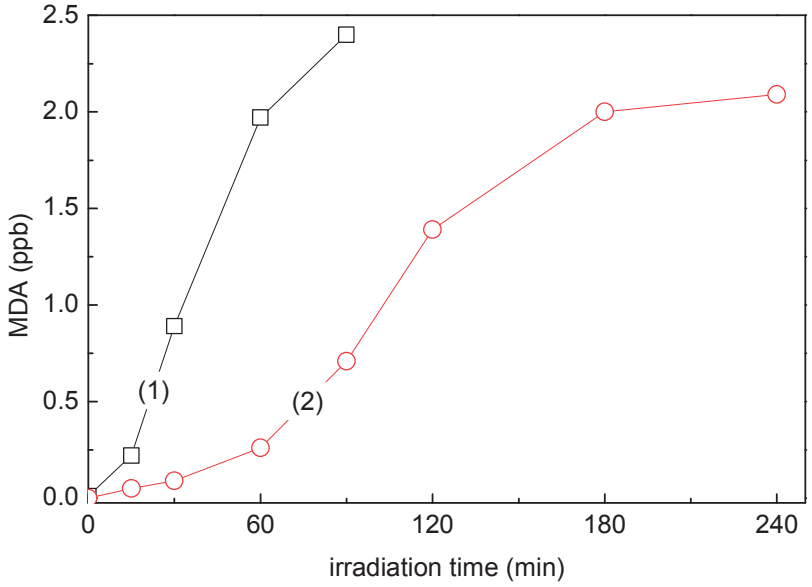

Figure 5.7a. Evolution of malondialdehyde (MDA) on Figure 6a,b on PE-TiO_2 samples pretreated with RF air plasma for 15 min and sputtered for 8 min : 1) *E. coli* irradiated under solar simulated light irradiation, 2) *E. coli* irradiated under solar simulated light irradiation as a function of time for non-pretreated PE-TiO_2 films sputtered for 8 min.

The breakdown of hydroperoxides and lipid endoperoxide radicals leads to the formation of various products including malondialdehyde (MDA) [170]. Figure 5.7a, trace 1 shows a steep increase within 60 min of the MDA production for RF-pretreated samples compared to the case of non-pretreated samples (Figure 5.7a, trace 2). The increase in MDA production occurs within similar times as: a) the increase in hydrophilicity shown in Figure 5.5a and 5.5b, b) the IR peak shifts seen in Figure 5.6. Quantitative evidence is shown for the increase in the hydrophilicity PE-TiO_2,

concomitant with the shift in amplitude of the IR-peaks and the evolution of MDA during bacterial cell wall peroxidation.

A significant increase in the hydrophilicity of PE-TiO_2 within 20-60 min was observed in Figure 5.5, trace 1. This increase in MDA shown in Figure 5.7a occurs within similar times observed for the shift of: a) the peak frequencies and b) the amplitudes reported in Figure 5.6.

Pearson's correlation coefficients were used to relate the cell wall fluidity to the increase of the photo-generated hydrophilicity. Figure 5.7b shows a relationship between the cell wall fluidity and hydrophilicity of 0.912. This negative correlation means that when contact angle decreases, the cell wall fluidity increases. The closer the value is to -1, the stronger the degree of linear dependence.

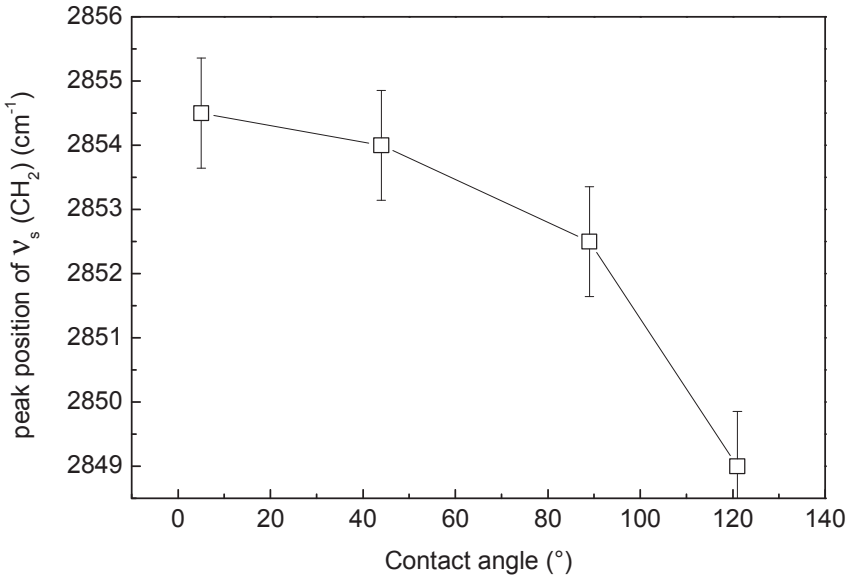

Figure 5.7b. Correlation between the peak shift of the symmetric -CH_2 stretching for *E. coli* irradiated samples (52 mW/cm^2) and the contact angle on PE-TiO_2 RF-air plasma pretreated for 15 min and sputtered for 8 min.

5.3.7. XPS analysis of PE-TiO_2 surfaces and EM images

Figures 5.8a-d show the deconvoluted signals of PE-TiO_2 films with no pretreatment and after pretreatment. The peaks of the Ti-O, Ti-OH and O-C signals for non-pretreated PE-TiO_2 are shown in Figure 5.8a. Figure 5.8b presents a PE-TiO_2 sample pretreated in air plasma for 15 min. A significant increase in the Ti-O peak is observed with respect to Figure 5.8a. The presence of Ti-O and Ti-OH species in the XPS spectrograms was evaluated by means of the peak area introducing the sensitivity factor for oxygen [146]. The Ti-OH on the PE-TiO_2 samples are noted by the peaks at

532.4 eV, 532.7 eV and 532.9 eV in Figures 5.8a-c. A redox process during RF-plasma pretreatment takes place during the sample pretreatment since a shift ≥ 0.2 eV was observed for samples pretreated with respect to the non-pretreated sample in Figure 5.8a [97]. Figure 5.8c shows the XPS signals for an RF-pretreated sample for 15 min and 1 torr. A redox reaction for the Ti-O takes place, since this peak differs in position respect to the peak for the PE-TiO_2 sample without pretreatment at 532.4 eV (Figure 5.8a).

Figure 5.8d shows that no Ti-OH signals could be detected for the UVC pretreated PE-TiO_2 sample for 20 min. The disappearance of the Ti-OH peak is due to a thermal effect since the UVC lamp increases the temperature in the cavity up to 95°C. This shows that the PE-TiO_2 does not involve chemisorbed water that would vaporize at lower temperatures [171]. The fraction of Ti-OH species with respect to total oxygen-species bonded to Ti is given in Table 5.3.

Table 5.3. Fraction of OH/(Ti-O+OH) on the PE-TiO_2 films

	OH/(Ti-O+OH) before irradiation	OH/(Ti-O+OH) after irradiation
PE-TiO_2 without pretreatment	0.11	0.15
PE-TiO_2 with RF air plasma pretreatment	0.23	0.39

Different pretreatment times of the PE gives rise to a different boundary Ti-O-C layer between PE and TiO_2 introducing a different accessibility of bacteria to the PE-TiO_2 [41]. Tables 5.2a and 5.2b show the PE-TiO_2 atomic surface concentration percentage for C, O, Ti and N before and after bacterial inactivation. The data reported shows only a marginal increase in C1s and O in Table 5.2b. This increase is due to adventitious hydrocarbons being absorbed from ambient air on the sample surface during the time of bacterial inactivation. The photocatalytic bacterial inactivation destroys rapidly the C, O and N-species on the catalyst surface, not allowing the accumulation of residues. Due to the rapid *E. coli* inactivation kinetics, the potential applications of the PE-TiO_2 films seems to be a valid proposition when optical transparency is required.

The differently pretreatment of the PE gives rise to boundary Ti-O-C layers between PE and TiO_2. The PE-TiO_2 films will react with their own specificity during bacterial inactivation. The decrease in the inactivation kinetics is possibly due to: a)

different accessibility of the bacteria to the Ti-O-C catalytic sites on the PE-TiO_2 and b) different distances between the interfacial layers and bacteria [170-171].

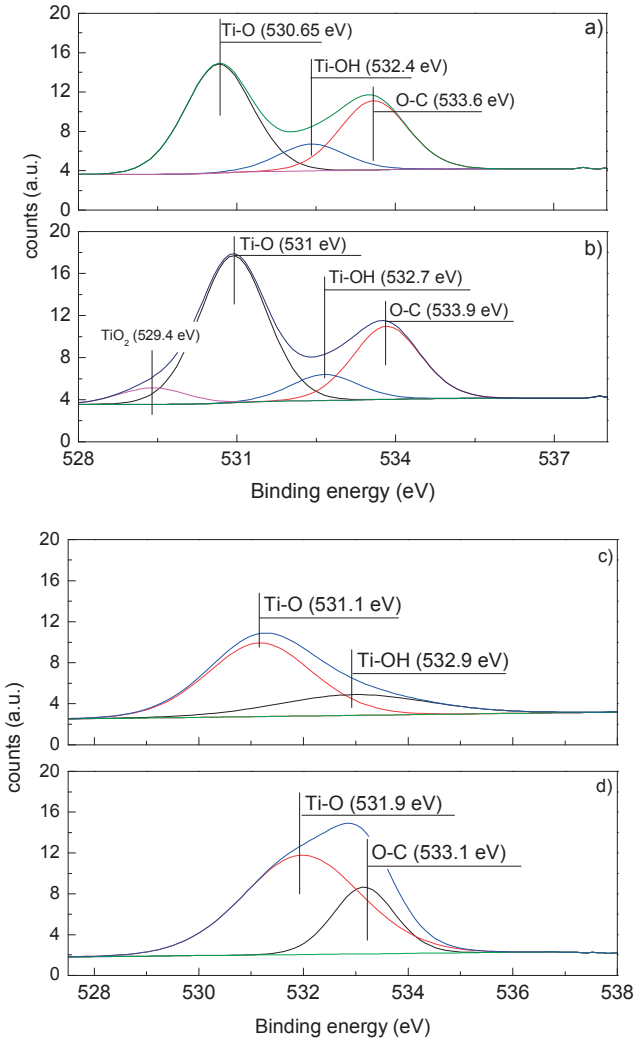

Figure 5.8. O1s deconvolution of PE-TiO_2 XPS spectral peaks: (a) without pretreatment, (b) after RF-air plasma pretreatment during 15 min and TiO_2 sputtered for 8 min, (c) RF-plasma pretreatment for 15 min (1 torr) and TiO_2 sputtered for 8 min and finally (d) UVC PE pretreatment for 20 min followed by TiO_2 sputtering for 8 min (1 torr).

Redox processes involving Ti^{4+}/Ti^{3+} occur on PE-TiO_2 during the photocatalytic bacterial inactivation. This is shown next in Figure 5.9. At time zero Figure 5.9 shows that a Ti^{4+} peak at 458.6 eV is slightly higher than the Ti^{3+} peak at 457.8eV, both oxidation states coexisting on the PE-TiO_2 sample. But after bacterial inactivation, the Ti^{3+} peak amounts to more than 90% of the XPS signal and the Ti^{4+} only amounts to

less than 10%. This redox reactions on the TiO_2 occurs concomitant to the increase of hydrophilicity within 60 min observed on the PE-TiO_2 samples (Figure 5.5a).

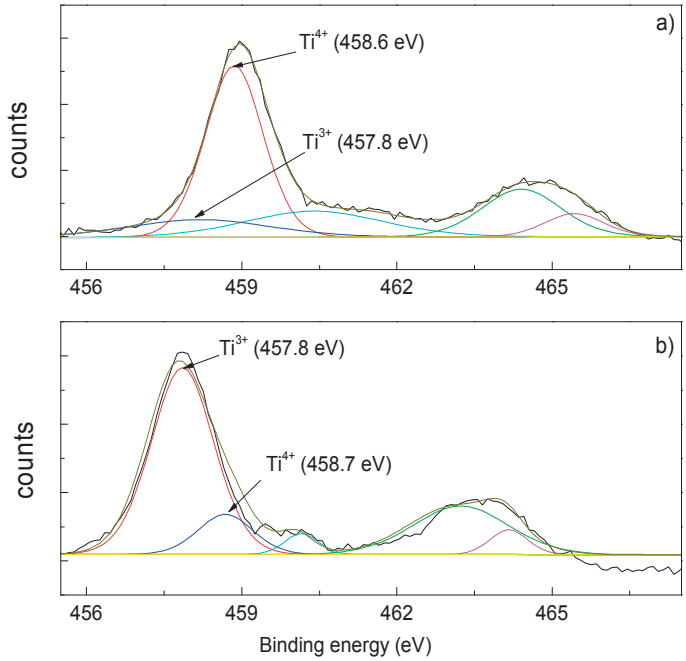

Figure 5.9. Ti2p peak deconvolution of PE-TiO_2 samples RF-air plasma pretreated during 15 min samples followed by TiO_2 sputtering for 8 min: a) before the bacterial inactivation process, time zero, and b) after bacterial inactivation under solar simulated radiation showing Ti^{3+}/Ti^{4+} oxidation states variation within the 60 min bacterial inactivation period.

Figure 5.10a-d show the SEM images for PE-TiO_2 RF air-plasma pretreated for 15 min and sputtered for 8 min, inducing the faster bacterial inactivation (Figure 5.6). Figure 5.10a show a continuous coating of TiO_2 on PE. TiO_2 thickness of ~60 nm is equivalent to 300 layers, taking an atomic layer thickness of 0.2 nm [125]. Figure 5.10b shows the High Angle Annular Dark Field (HAADF) used to map the scanning electron microscopy. The uniform distribution obtained by EDX of O and Ti on the coating is shown in Figures 5.10c and 5.10d.

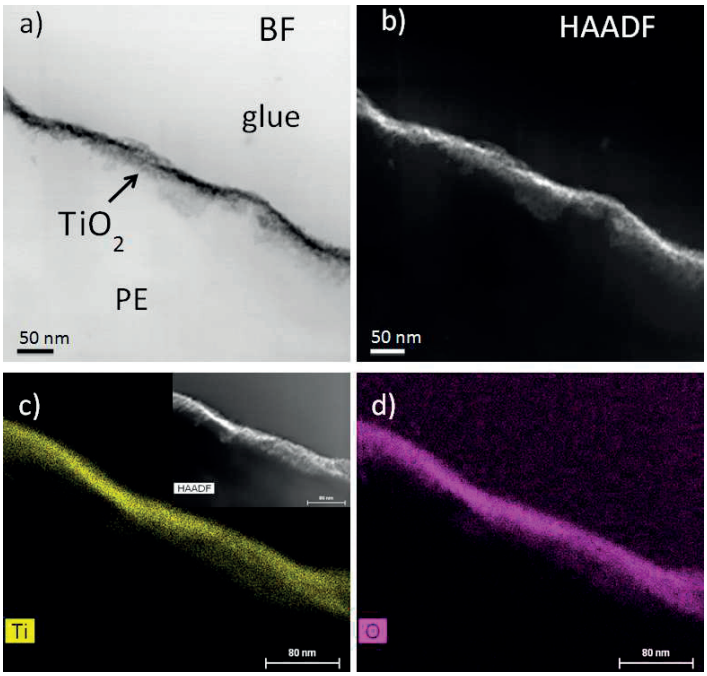

Figure 5.10. a) STEM Bright Field Image of PE-TiO_2 RF air-plasma pretreated for 15 min and TiO_2 sputtered for 8 min, b) STEM-HAADF image taken on the same sample area, c) EDX mapping of titanium and d) EDX mapping of oxygen.

Figure 5.10a shows the TiO_2 is dispersed uniformly over the PE-surface. By inspection of Table 5.1, it is readily seen that the TiO_2 content increases with longer sputtering times, accelerating the bacterial inactivation (see Figure 5.2). The conventional model bacterial inactivation of *E. coli* under light irradiation is shown next in Figure 5.11. This model has been generally cited widely for the overall disinfection mediated by TiO_2 photocatalysis [135-136,160,169].

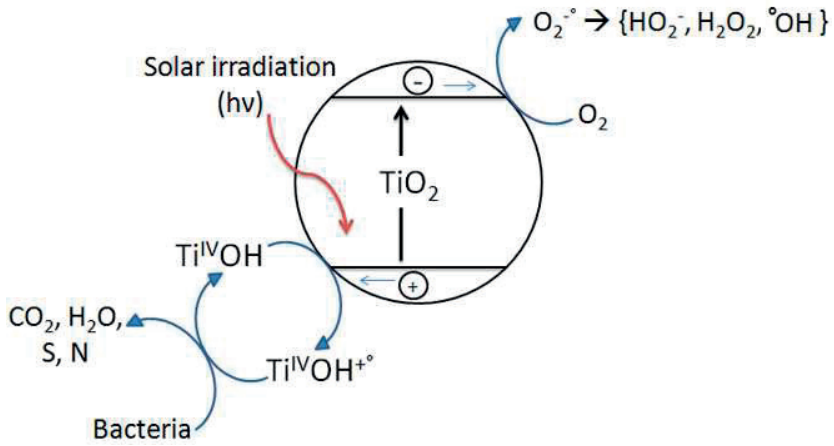

Figure 5.11. Bacterial inactivation scheme on PE-TiO_2 films under solar simulated light.

5.4. Conclusions

The findings reported in this study are; a) a uniform transparent non-scattering PE-TiO_2 film inactivating bacteria under low intensity solar simulated radiation and b) a quantitative correlation between the bacterial inactivation time and the hydrophilicity, roughness and IR peak shifts in the stretching vibration of the *E. coli* outer LPS layer due to the increase in the -CH_2 interbond length. Contact angle determination allowed the quantitative determination of the photo-switching rates related to bacterial inactivation.

In the previous 3 chapters, I studied bacterial inactivation on sputtered 2D surfaces. We had the idea to adapt the magnetron sputtering unit to depose 3D surfaces and to study the coating adhesion, its uniformity and its bacterial inactivation dynamics on complex shapes. Chapter 6 and 7 show the first account for the preparation of coated complex 3D-catheters able to bring the bacterial infection directly to the blood vessels.

Chapter 6

Quasi-instantaneous bacterial inactivation on Cu-Ag nano-particulate 3D-Catheters in the dark and under light: mechanism and dynamics

This chapter is based on the following publication: Sami Rtimi, Rosendo Sanjines, Cesar Pulgarin, John Kiwi, ACS-Appl. Mater. Interfaces 2016, 8, 47−55 (Reproduced with permission of ACS, Copyright 2016).

6.1. Introduction

Cu has been known for long time to have effective bactericide action [172-175]. More recently, Cu-ions have been reported to be biocidal by binding to specific sites in the DNA-phosphate destroying the DNA double helix or damaging the bacterial cell walls [176]. In the latter case, the Cu-ions enter into the cytoplasm causing membrane disruption [177]. Cu has also been shown to produce reactive oxygen species (highly oxidative radicals) and the Cu-ions stick to the negatively charged *E. coli* cell walls allowing Cu-ions penetration into the cells as reported by Borkow et al., [112,96]. Cu/Cu-oxides/Cu-ions in contact with microorganisms leading to cellular damage and bacterial death in the dark or under light has been reported by Hashimoto et al. [94,120,93]. Cu-toxicity to microorganisms has been suggested partly due to the displacement of bacteria essential metals [31,179-182]. Our group has worked during the last few years on the sputtering of uniform, adhesive kinetically fast Cu-surfaces to inactivate bacteria in the dark or under low intensity light [95,52,183]. This chapter focuses on Cu-Ag bimetal sputtered 3D-surfaces (catheters) in comparison to compare the inactivation performance with Cu or Ag sputtered surfaces.

Silver nano-particulates have been applied on cotton and artificial fibers like polyester, wound-pads, and thin polymer films like polyethylene. The silver ion-release kinetics [183-184] extends over long-operational times with a low concomitant cytotoxicity [185-190]. Ag is believed to react with microbial membranes, and once inside the cell Ag^+ attaches to DNA and RNA interrupting cell metabolism. Ag° shows a reduced bacterial inactivation performance compared with the Ag^+-ions when contacted with tissues [191-192]. Sol-gel commercial preparations are widely used at

the present time to prepare Ag-thin disinfecting films on heat resistant substrates. But the thickness of these sol-gel deposited films is not reproducible, they are not mechanically stable, and they exhibit low adhesion and can be wiped off by a cloth or thumb [12]. Colloid deposition on substrates require temperatures of few hundred degrees for an adequate adherence to the substrate and this will not work on low thermal resistant substrates like polyurethane (PU) [193], poly-methyl-methacrylate (PMMA) [194] and PE [47,144] used in hospital catheters. Electro-deposition of Cu and Ag has been used to coat catheters [195]. CVD has been used to heat metal/oxides in vacuum until they decompose and are mostly used to coat 2D-surfaces [14, 32,15,196]. The disadvantages of the CVD deposition approach are: a) the high temperatures needed precluding film deposition on textiles like polyester and b) the amount of heat used requiring costly cooling systems. Ag-films have been deposited by CVD leading to nano-particles films from 6 to 50 nm in size [14, 32,15,196]. To investigate on silver biocide surfaces is warranted since they are the strongest growth segment in the medical and health-care applications.

In this chapter we address: the design and the sputtering of Cu-Ag at relatively low temperatures of nano-composite films on catheters and their bacterial inactivation dynamics. Cu-Ag coated 3D-polyurethane catheter surfaces will be shown to inactivate bacteria within ≤5 minutes. The bacterial inactivation kinetics reported hereby is an improvement compared to two types of films reported recently by our laboratory: a) TiO_2/Cu films inactivating *E. coli* within ~10 min [95] and b) Ag-TaN films inactivating *E. coli* within ~20 min [197].

Until now, magnetron sputtering led to uniform and adhesive coatings on 2D-surfaces. The present chapter shows the first evidence of 3D-shapes coated with magnetron sputtering leading to fully covered 3D surfaces with highly adhesive antibacterial films.

6.2. Experimental section

6.2.1. Sputtering of Cu-Ag films and XRF determination of the film content

The coating of the 3D catheters was carried in the sputtering chamber with the geometry shown in section 2.5 (page 16-17). This sputtering set-up allows the deposition of uniform 3D-film coverage on the cylindrical catheter surfaces. Thin films were deposited by reactive DCMS in an Ar + O_2 gas flow from a 5 cm round target

(Kurt J. Lesker, East Sussex, UK). The sputtering current was set at 280 mA. The different Cu/Ag atomic ratios sputtered during the course of this study were: 25%-75%, 33%-67% and 50%-50% in %Cu-%Ag respectively. Single Ag and Cu surfaces were sputtered as control materials.

Sputtering Cu-Ag for 1 min leads to a thickness of about 50 nm with $2.5x10^{17}$ atoms/cm^2. This allows the estimation of a deposition rate $4.5x\ 10^{15}$ Cu-Ag atoms/cm^2s (height of each atomic layer as 0.2 nm). The error % in the coating between the periphery and the center of the sample was 5-8% on catheters 5 cm long. The film thickness was determined with a profilometer (Alphastep500, TENCOR). The thickness data was taken in triplicate. By X-ray fluorescence (XRF), the composition of the Cu-Ag coatings was evaluated in a PANalytical PW2400 spectrometer. The used catheters were Jelco Optiva W24G-Ref. No 1124 from Smiths Medical International Ltd. (Lancashire, UK).

6.2.2. CFU Evaluation, stereomicroscopy of Live/Dead cells, ICP-MS of samples and light source

PU-Catheters were sterilized by keeping them in an oven at 70 °C overnight since they cannot support autoclaving at 121 °C. 100 µL culture aliquots with an initial concentration of ~10^6 CFU mL^{-1} in NaCl/KCl (8/0.8 g L^{-1}, pH 7) were placed on coated and uncoated (control) catheters. Experiments were run at room temperature and the samples were placed on glass Petri dishes provided with a lid to prevent evaporation during the illumination. Then, the samples were transferred into a sterile 5 ml tube containing NaCl/KCl saline solution and subsequently mixed thoroughly using a Vortex for 2 min. Serial dilutions were made in NaCl/KCl solution. A 100 µL sample of each dilution was pipetted onto a nutrient agar plate and spread over the surface of the plate using the standard plate method. Agar plates were incubated lid down, at 37°C for 24h before colonies counting. Three independent assays were done for each sputtered sample. To verify that no re-growth of *E. coli* occurs after the first bacterial inactivation cycle, samples were incubated for 24 hours at 37°C. Then, 100 µL of the suspension was deposited on three Petri dishes to obtain the replica samples for the bacterial counting. These samples were incubated at 37°C for 24 h.

Fluorescence stereomicroscopy was carried out on samples inoculated with 10^8 CFU of *E. coli* and incubated in a humidification chamber. This method uses a fluorochrome-based staining procedure from Filmtracer™ LIVE⁄DEAD® Biofilm Viability

Kit (Molecular Probes, Invitrogen). The kit contains a combination of the SYTO® 9 green fluorescent nucleic acid stain and propidium iodide fluoro-chromes for the staining of live and dead cells, respectively. The samples fluorescence was monitored in a fluorescence stereomicroscope (Leica MZ16 FA, Leica Microsystems GmbH Wetzlar, Germany) and the images were processed using the LAS v.1.7.0 build 1240 software from Leica Microsystems CMS GmbH. Adhesion of bacteria to PU-catheters was allowed for 2 minutes before washing the sample with sterile Milli-Q water to remove non-adherent bacteria.

Determination of Cu and Ag-ions was carried out by inductively coupled-plasma mass-spectrometry (ICP-MS) in a FinniganTM ICPS unit equipped with a double focusing reverse geometry mass spectrometer with an extremely low background signal and a high ion-transmission coefficient. The samples washing solutions were digested with nitric acid 69% (1:1 HNO_3 + H_2O) to remove the organics in the solution and to guarantee that there were no remaining ions adhered to the flask wall. The samples droplets are introduced to the ICP-MS trough a peristaltic pump to the nebulizer chamber allowing the sample components evaporation and ionization.

The irradiation of the samples was carried out in a cavity provided with tubular actinic Osram Lumilux 18W/827 emitting in the range 360-700 nm with total output of 3 mW/cm^2. These lamps are used in hospitals and schools indoor illumination presenting an efficient compromise between the energy consumption and the intensity of the emitted light.

6.2.3. Contact angle determination, micro-oxidation analysis and FTIR of the LPS stretching vibration shift during bacterial inactivation

The film hydrophilicity was determined by dynamic water droplet contact angle (CA) by the sessile drop method on a DataPhysics OCA 35 unit. The interfacial potential and pH changes were followed on a Jenco 6230N (pH/mV/Temp meter) provided for with a microprocessor and a RS-232-C IBM interface. The peak shifts and displacements of the lipo-polysccharide (LPS) stretching peaks were followed in an ATR-IR Portmann Instrument equipped with a Specac attachment (45° one pass diamond crystal). Spectra signals comprised 256 scans with a resolution of 2 cm^{-1} in the range between 900 and 4000 cm^{-1}. The position of the IR peaks was found by the second derivative of the spectra after Fourier deconvolution.

6.3. Results and discussion

6.3.1. Cu, Ag, Cu-Ag coating thickness and determination of sample composition

Figure 6.1a shows the nominal thickness calibration of Cu-Ag sputtered films on non-porous Si-wafers by profilometry. Sputtering for 30s by direct current magnetic sputtering (DCMS) from a Cu-Ag (50%-50%) target, a nominal thickness of 22 nm was attained. In Figure 6.1a, the thicknesses of the coating with different Cu:Ag atomic ratios, increased with the percentage of silver in the Cu-Ag deposited films. A coating thickness of 22 nm corresponds to about 110 atomic layers [95,52,184].

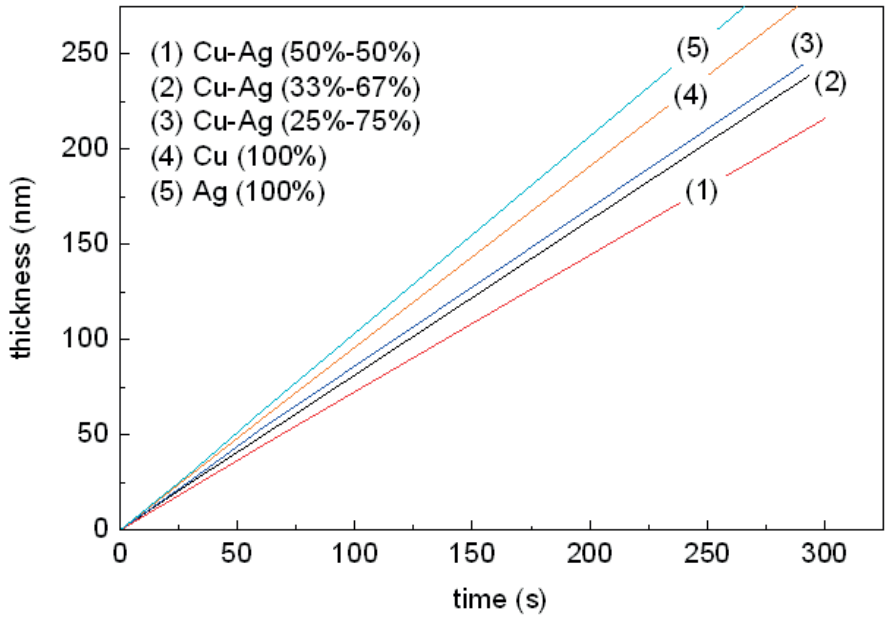

Figure 6.1a. Thickness calibration of the Cu, Ag and Cu-Ag layers sputtered on Si-wafers.

Figure 6.1b shows: (a) an uncoated catheter, (b) a Cu-Ag catheter sputtered for 60s, (c) the reverse side of the catheter (b) showing a uniform distribution of the coating on the 3-D shaped catheter. Finally, a sample sputtered only for 30s is shown in (d). Quantitative information about the microstructure by up-to-date surface techniques will be discussed below.

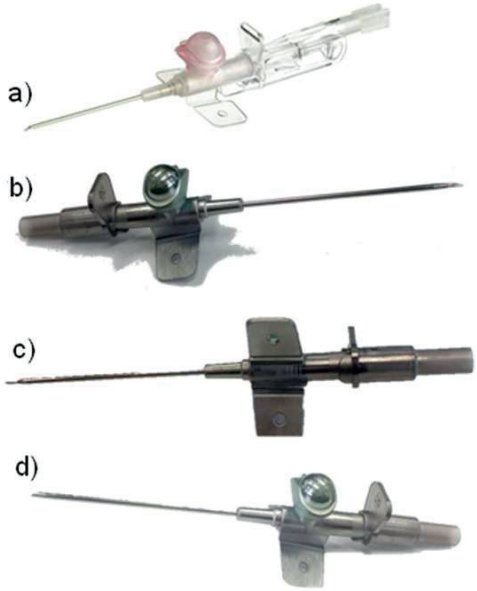

Figure 6.1b. Uniform sputtered coating on the catheters 3D-surfaces: a) uncoated catheter, b) 60 s sputtered Cu-Ag (50%-50%) catheter, c) 60 s sputtered Cu-Ag (50%-50%) back-side catheter and d) 30 s sputtered Ag catheter.

6.3.2. *E. coli* Inactivation as a Function of Cu, Ag and Cu-Ag Film Thickness

The *E. coli* inactivation time as a function of the thickness for Cu and Ag films is shown in Figure 6.2, traces 1-4 for Cu and Ag respectively. Figure 6.2 shows the complete *E. coli* inactivation by Cu-PU-catheter and Ag-PU-catheters within 30 min for Cu coatings with a nominal thickness of 60 nm (~300 atomic layers) and in the case of Ag with a nominal thickness of 105 nm (~525 atomic layers). Bulk inward diffusion of the photo-induced charge carriers in Cu- and Ag-films has been reported to be responsible for the charge transfer slowing the bacterial inactivation for a thickness layers ≥100 nm. [95,52,184].

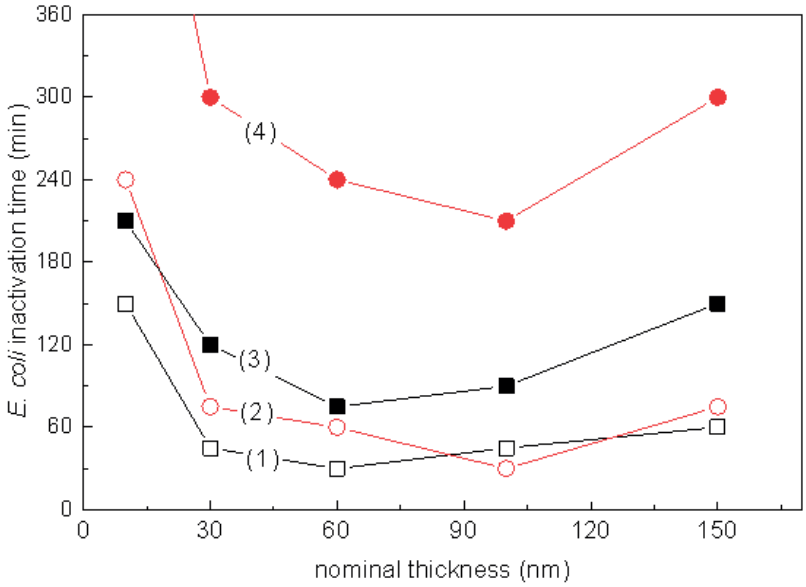

Figure 6.2. Effect of the coating thickness on the bacterial inactivation kinetics for: (1) Cu- PU-catheter under low intensity actinic light (3 mW/cm^2), (2) Ag-PU-catheter under low intensity actinic light (3 mW/cm^2), (3) Cu-PU-catheter in the dark, (4) Ag-PU-catheter tested in the dark.

Table 6.1 shows the Cu and Ag content on the sputtered catheters obtained by X-ray fluorescence (XRF). Table 6.1 shows the amount of Cu and Ag sputtered on the PU-catheters for 1 min from different targets. Sputtering Cu-Ag from mixed targets shows lower amounts of Cu and Ag compared to Cu and/or Ag sputtered from two single Cu and Ag targets.

Table 6.1. Cu and Ag content on the sputtered PU-catheters obtained by X-ray fluorescence (XRF).

Samples sputtered for 1 min		Wt%/wt PU
Cu-Ag (50%-50%)	Cu	0.05
	Ag	0.03
Cu-Ag (33%-67%)	Cu	0.02
	Ag	0.04
Cu-Ag (25%-75%)	Cu	0.01
	Ag	0.05
Cu (100%)		0.11
Ag (100%)		0.07

This may be due to the Cu and Ag ad-atoms competition when clustering on the PU-catheters. Table 6.2 shows the ICP-MS data of the Cu- and Ag-PU-catheters sputtered for 1 min.

Figure 6.2 showed that Cu-films due to their higher toxicity inactivate bacteria within shorter times compared to Ag-films under light and in the dark. The low ppb levels for Cu and Ag shown in Table 6.2 suggest an oligodynamic effect leading to bacterial inactivation by these films. No cytotoxicity on mammalian cells is induced by these sputtered thin films, since the Ag- and Cu release at the ppb level is below the sanitary regulations valid for mammalian cells as reported in the Table 6.2 below [96,93,95,52]. Ag-films do not provide the required level of efficacy to preclude biofilm formation, since the diffusion of Ag-ions from a metallic surface is short or negligible [180-184]. Therefore, this study addresses the investigation of the bacterial inactivation kinetics by Cu-Ag kinetics and efficiency of Cu-Ag films to overcome the drawbacks of Ag-films on catheters.

Table 6.2. Inductively coupled plasma mass spectrometry (ICP-MS) determination of the released Cu and Ag-ions from Cu-Ag PU-catheters sputtered for 1 min.

Sample (%Cu-%Ag)	Cu (ppb)		Ag (ppb)	
	The whole catheter	Needle only	The whole catheter	Needle only
50%-50%	20.78	3.46	9.29	1.54
33%-67%	22.92	3.82	1.20	0.2
25%-75%	24.23	4.03	0.80	0.13
100% Cu	26.64	4.44	--	--
100% Ag	--	--	19.10	3.18

6.3.3. Bacterial inactivation kinetics as a function of the Cu:Ag ratio

Figure 6.3a shows that the bacterial inactivation of *E. coli* was accelerated to 5 min on a 50%/50% Cu-Ag PU-catheter under actinic light irradiation or in the dark compared to Cu or Ag deposited independently. Sputtered Cu-Ag film presenting a 50%/50% Cu:Ag ratio led to the highest release of Ag-ions as shown in Table 6.2. Figure 6.3a show that in some cases the bacterial inactivation times become longer as the amount of Ag in the Cu-Ag film increases. The 50%/50% Cu-Ag involve Cu-Ag catalytic comprising the highest number of active catalytic centers held in exposed surface positions in contact with bacteria [174,93,95]. The bactericide action by the Cu-Ag film may also involve synergic effects between Cu and Ag, difficult to detect and quantify [173]. Films sputtered for one minute with less than 50% Cu-content led to longer bacterial inactivation times since not enough Cu was present to induce a high cytotoxic effect.

Figure 6.3a report bacterial inactivation kinetics being in some cases the same in the dark and under light. In this semiconductor character CuO/Cu_2O and Ag_2O is absent and the highly oxidative nanoparticle properties of Cu and Ag are the species leading to bacterial inactivation. Cu-Ag films inactivate bacteria within 5 min, 6 times faster compared to the 30 min inactivation period required for Cu (see Figure 6.2, trace 1).

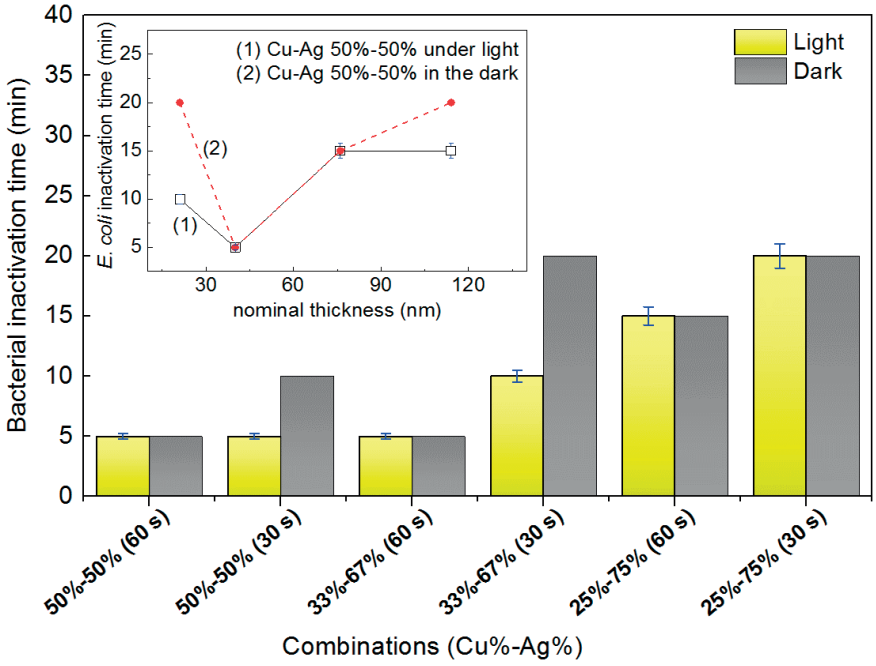

Figure 6.3a. *E. coli* inactivation on Cu-Ag PU-catheters sputtered for different times showing the effect of the atomic ratio of Cu:Ag on the bacterial inactivation time. The applied light is a low intensity actinic light (3 mW/cm^2). Error bars: standard deviation (n=5%).

Recent studies using Cu- and Ag-films report that the bacterial inactivation by CuO/Cu_2O and Ag_2O under light irradiation were faster compared to similar processes in the dark [172-174,93,52,12]. The insert in Figure 6.3a shows that thicker Cu-Ag coatings led to longer bacterial inactivation times in the dark and under light. Compaction of the coating at higher thicknesses may hinder the Cu and/or Ag ppb releases.

6.3.4. Stereomicroscopy of stained *E. coli* on Cu-Ag films on PU-catheters

To test the time at which *E. coli* cells suffer destabilization/damage leading to cell death (red dots indicate membrane damage), the cells were incubated on a Cu-Ag PU 50%/50% sample after light irradiation. Figure 6.3b shows the live/dead bacteria on the surface of a Cu-Ag PU-catheters. Figure 6.3b shows that after 2 min no living *E.*

coli bacteria could be identified. This lends further support for the short bacteria inactivation time ≤ 5 min reported in Figure 6.3a. Imaging under fluorescent light would facilitate the detection of the fluorescent species. But the applied light would be enough to inactivate *E. coli* on Cu-Ag films. Therefore, this experiment was not feasible. Figure 6.3b shows red stained/damaged membrane cells dead after 10 min. The Fluorochrome dye enters the cell and stains DNA due to the abnormal high permeability [109] of the damaged cell wall.

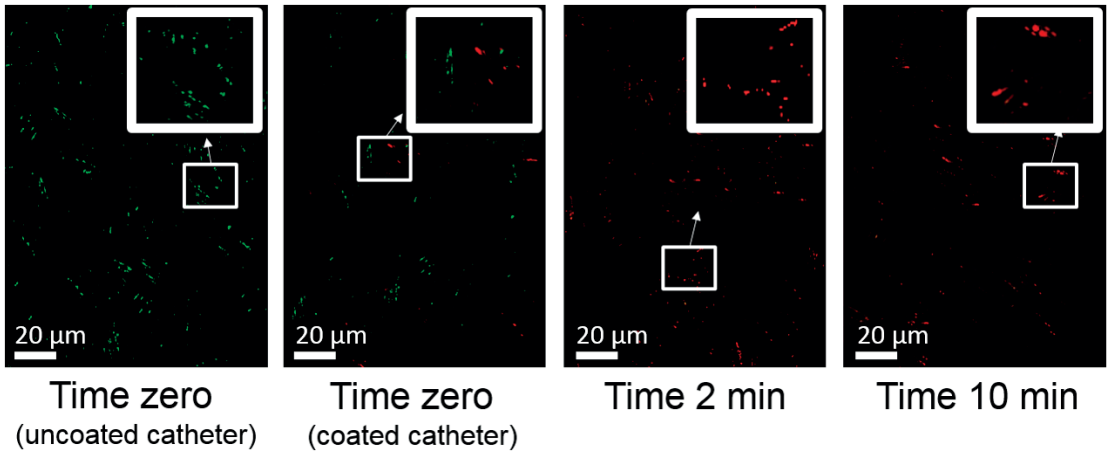

Figure 6.3b. Monitoring after 2 and 10 min, live/dead *E. coli* inactivation in the dark on Cu-Ag (50%-50%) PU-catheters sputtered for one min with respect to uncoated PU-catheter (left-hand side).

The faster inactivation kinetics of Cu-Ag films involves redox reactions between Cu and Ag as found in galvanic batteries. Ag acts as a cathode and Cu as the anode, releasing Cu^{+} on the Cu-Ag film.

$$Ag^{0} + Cu^{2+} \rightarrow Ag^{+} + Cu^{+} \qquad (1)$$

Ag introduces galvanic corrosion at the bimetal interface between the Cu and Ag and leads to the generation of Cu and Ag-ions during bacterial disinfection. The amount of these Cu/Ag-ions is shown in Table 6.2. This Galvanic effect is favored by the Ag-Cu nano-particle uniform distribution on PU. The Galvanic effect can be understood taking into account the potentials of Ag^{0}/Ag^{+} -0.80V SHE and Cu^{2+}/Cu^{+} 0.15V SHE driving reaction (1) with a potential of -0.65V SHE. This effect leads to atomic disorder [198,199] in the Cu-Ag film. This atomic disorder is higher for Cu-Ag films compared to Cu and Ag sputtered films. The biocidal effect of the Cu-Ag films can be accounted for by the positively charged Ag and Cu-ions as stated above in eq(1). These ions enter

subsequently the bacterial cell and interfere with the cellular electron transport chain [167,200].

6.3.5. Contact Angle (CA) and Interface Potential Shifts

Figure 6.4a shows the contact angle (CA) hydrophobic-hydrophilic transformation of Cu-Ag 50%/50% coated PU-catheters within 30 min under low intensity actinic light (3 mW/cm^2). The CA hydrophobic-hydrophilic transformation time does not coincide with the 5 time of min bacterial inactivation reported in Figure 6.3a. The reverse transformation to the initially hydrophobic state needed 24 hours and was completed either at 24°C or at 60°C in the dark.

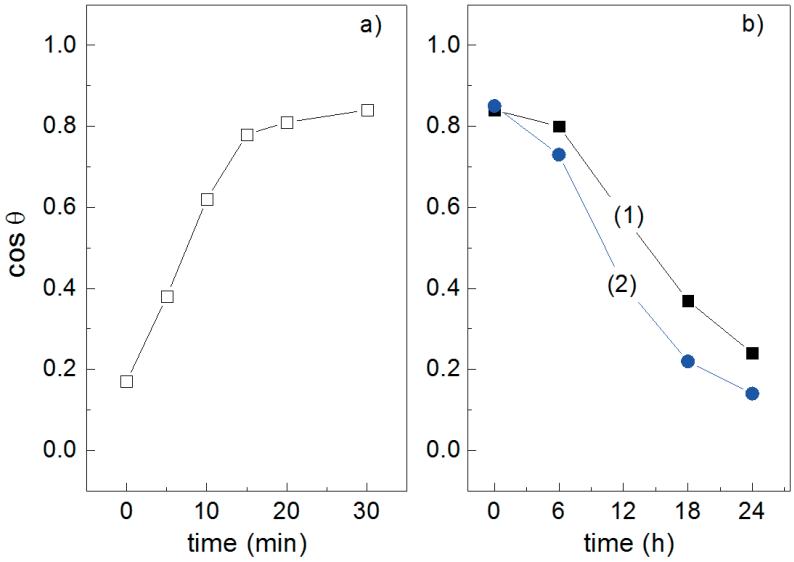

Figure 6.4a) Contact angle variation within the bacterial inactivation period showing the hydrophobic-hydrophilic transformation on the Cu-Ag (50%-50%) on one minute sputtered catheters irradiated under low intensity actinic light (3 mW/cm^2) and **b)** reverse hydrophilic-hydrophobic kinetics after bacterial inactivation in the dark re-establishing the initial hydrophobic state: (1) at room temperature (24°C) and (2) at 60°C.

Figure 6.4a shows the hydrophobic to hydrophilic transformation as a function of cos Θ took within ~30 minutes. The back transformation to the initial hydrophobic state occurs within 24 hours. The wettability is commonly evaluated in terms of the contact angle (CA) in Young's equation and Figure 6.4 was plotted by integrating "cos Θ" in the Young's equation [201,47,144].

$$0 = \gamma_{SG} - \gamma_{SL} - \gamma_{LG}\cos\theta_C \qquad \text{ep(2)}$$

The Young equation involves solid-vapor, liquid-vapor and solid-liquid interfacial energies. The solid-vapor interfacial energy is denoted by γSG, the solid-liquid

interfacial energy by γSL, and the liquid-vapor interfacial energy (i.e. the surface tension by γLG, then the equilibrium contact angle θ is determined from these quantities by Young's equation.

Interface potential shifts in the dark on Cu-Ag films are shown in Figure 6.5a (left hand side) as a function of the bacterial contact time. The interface potential shift is seen to be smaller with respect to the signals registered in Figure 6.5b for experiments carried out under actinic light. This is the evidence for the change in the permeability of the *E. coli* cell wall reflecting the increase in the bacterial K, Na, Mg-ions and other essential metabolic bacterial-ions, passing through the cell wall envelope [202-203] due to the increased permeability as the inactivation time became longer.

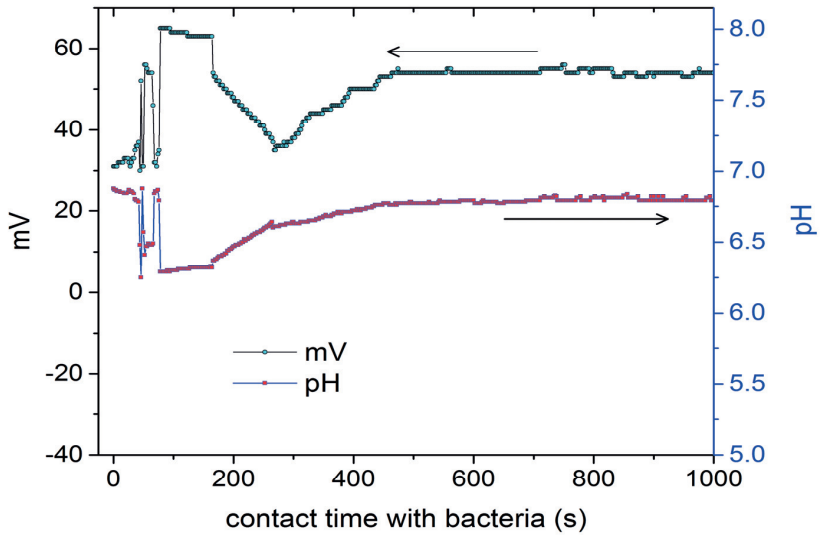

Figure 6.5a. Interfacial potential and local pH shifts of the bacterial culture contacted with Cu-Ag 50%/50% on PU-catheter in the dark.

The right hand side in Figure 6.5a shows the pH-shifts as a function of time when the bacterial culture was contacted with Cu-Ag 50%/50% films in the dark. The initial pH of 6.8 decreases to 6.4 within 5 min due to the production of long-lived carboxylic acids intermediates during bacterial degradation. Subsequently in Figure 6.5a, the pH recovers its original level when the carboxylic acids decompose generating CO_2. A pH-shift between 6.8 and pH 6.4 takes place within 150s. This is equivalent to a fourfold increase in the concentrations of H^+. The short changed carboxylic acids (branched or not) generated in solution during the bacterial inactivation period present a pK_a ~3. After 150 s, the pH increases again up to a pH ~6.7 due to short carboxylic acids being mineralized into CO_2 [167,108,164,166]. This is the final step in the bacterial

mineralization chain as reported for many organic compounds and dyes like methylene blue. Figure 6.5a shows that a small pH-recovery step in the dark involving acid de-carboxylation between pH 6.4 and 6.75 takes place due to the Kolbe CO_2 elimination reaction.

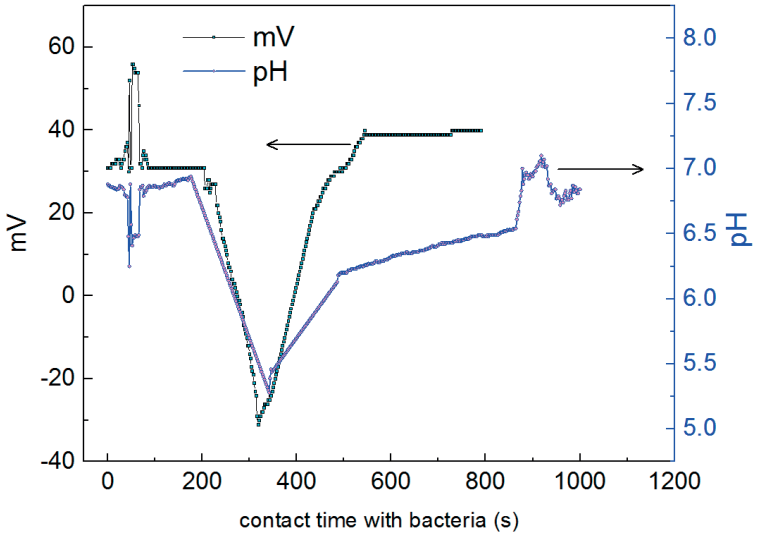

Figure 6.5b. Interfacial potential and local pH of the bacterial culture contacted with Cu-Ag 50%/50% on PU-catheter under a 3mW/cm^2 actinic light.

In Figure 6.5b the decomposition of the carboxylic acids lead to CO_2 through a photo-Kolbe reaction [204-205]. A steeper/decrease is observed in the pH-values compared to dark runs in Figure 6.5a. The solution pH recovers within 15 min to the initial value of 7.0 in Figure 6.6b. This is expected since the bacterial inactivation kinetics is faster for runs under light compared with dark runs in Figure 2.

$$RCOO^- + \text{actinic light} \rightarrow R^{\cdot} + CO_2 \qquad (3)$$

The interface potential on the Cu-Ag films decreases during dark bacterial oxidation as shown in Figure 6.5a, due to the increase permeability/destruction of the *E. coli* bilayer cell wall during bacterial inactivation. The increase in cell wall permeability leads to loss of the cell barrier integrity which is essential to control the exchange of ions. Figure 6.5b shows that the interface potential changes under low intensity actinic light are more significant compared to the same effect in the dark.

The fast bacterial inactivation by cytotoxic Cu-Ag films with the associated changes in pH would preclude pathogen biofilm formation/survival [206]. Biofilm formation has been reported in aqueous media occur within non-negligible time spans [207].

Therefore, the cytotoxic Cu-Ag films show a potential for applications in hospital settings as reported in this study.

6.3.6. Stretching Peak Shifts under Light and in the Dark during *E. coli* Inactivation

The ATR-FTIR spectroscopy was used to monitor the (-CH_2) LPS stretching vibration band shifts within the bacterial inactivation time and the results are shown in Figures 6.6a and 6.6b. The -(CH_2) and -(CH_3) groups make up 70% of the lipo-polysaccharides (LPS), phosphatidyl-ethanolcholine (PE) and peptidoglycan (PGN). These are the three main *E. coli* cell wall components. Figure 6.6a shows the peaks for runs under light showing the decrease in the methylene -$(CH_2)_s$ symmetric band concomitant with a stretching peak shift from 2832.6 cm^{-1} (time zero) up to 2841.6 cm^{-1} (10 min). The stepwise decrease in the -$(CH_2)_s$ band intensity occurs in parallel with the -$(CH_2)_s$ band position shift due to the perturbation of the outside lipid-polysaccharide layer (LPS) in contact with the Cu-Ag film [167,108]. The use of the second derivative of the FTIR spectral bands was used for the determination of the -$(CH_2)_s$ peak positions in Figure 6.6a. The decrease of the -$(CH_2)_s$ bands reflect the structural reorganization of the LPS outer layer [164] leading also to bacterial LPS lipid peroxidation [167]. Peroxides, alcohols and carboxyl type functionalities are formed during the peroxidation reactions as recently reported [199-203]. The FTIR of *E. coli*-$(CH_2)_s$ symmetric bands as a function of time in the dark are shown in Figure 6.6b. In this case the spectra are less defined, but a loss of amplitude between time zero and 10 min was observed, in a smaller scale compared with the amplitude decrease monitored in Figure 6.6a.

The -$(CH_2)_s$ symmetric band shifts are due to: a) an increase in the lipid bilayer fluidity and micro-viscosity of the outer LPS during photocatalysis [164] and b) an increase in the intermolecular C-H bond distance [166]. Figure 6.6c shows that the -$(CH_2)_s$ band shifts are directly related with the increase in the C-H intermolecular bonding distance. After 10 min the -(CH_2) functional groups attain the fluidity/mobility/intermolecular distance necessary for bond lysis [166,108].

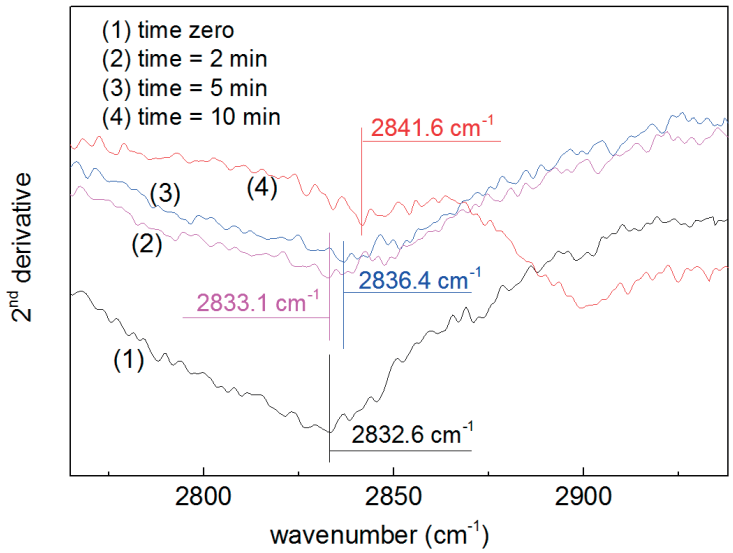

Figure 6.6a. FTIR-ATR spectroscopy of the symmetric -$(CH_2)_s$ *E. coli* on Cu-Ag (50%-50%) PU-catheter sputtered for 1 min under low intensity actinic light irradiation (3 mW/cm^2).

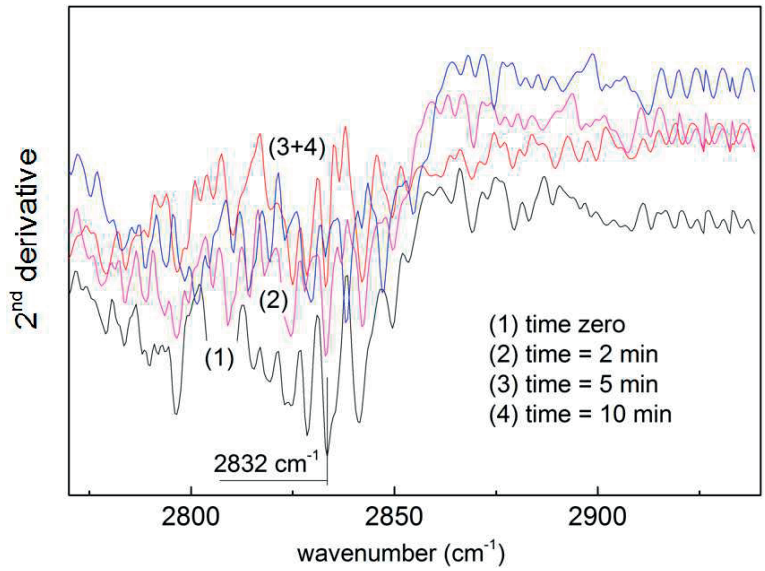

Figure 6.6b. FTIR-ATR spectroscopy of the -$(CH_2)_s$ symmetric *E. coli* on Cu-Ag (50%-50%) PU-catheter sputtered for 1 min in the dark.

The increase in the bond stretching within the time reported in Figure 6c was very short for *E. coli* on Cu-Ag films compared to the TiO_2-polyester recently reported for *E. coli* under light [108,167]. This explains the shorter *E. coli* bacterial inactivation times of *E. coli* on the Cu-Ag films compared to TiO_2 on polyester.

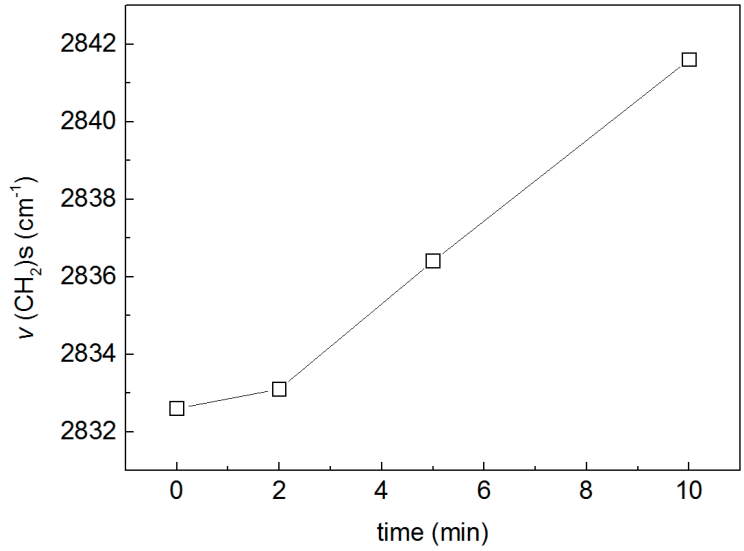

Figure 6.6c. FTIR-ATR -$(CH_2)_s$ symmetric vibration peak shift under low intensity actinic light (3 mW/cm^2) on Cu-Ag (50%-50%) PU-catheter sputtered for 1 min.

Figure 6.6d shows the FTIR 1653 cm^{-1} and 1625 cm^{-1} of the phosphatidyl-ethanolcholine PE-peptide group Amide I. The Amide I bands have been reported in the 1650-1592 cm^{-1} region [172-174,108]. Figure 6.6d shows the FTIR 1653 cm^{-1} stretching band vanishes completely within 2 min under actinic light irradiation. This is a proof for the rapid degradation of the peptide cell upper bilayers compared to the -$(CH_2)_s$ bands. This shows the higher stability of the -$(CH_2)_s$ functional groups on Cu-Ag films compared to Amide I. Next, Figure 6e shows the dark runs for the bands reported previously in Figure 6.6d. The step-wise reduction of the PE Amide I within 5 minutes occurs concomitant with the time of *E. coli* inactivation reported previously in Figure 6.3a.

Figure 6.6e shows the shift of the PE-band at 1653 cm^{-1}. This is due to the oxidation of the LPS polar heads, increasing the LPS fluidity [167] on the Cu-Ag PU (50%-50%) samples in the dark. Peptoglycan (PGN) -$(CH_2)_s$ lysis has been reported within times of 30-40 hours on supported TiO_2 polyester under light [108]. These times were much longer compared to the times reported for the photocatalytic degradation of *E. coli* phosphatidyl-ethanolamine (PE) and lipo-polysaccharide (LPS) on the same TiO_2-surfaces varying from one to two hours [108,167]. A synergistic mechanism is suggested to explain these short times for *E. coli* inactivation using for the PGN degradation the oxidative radicals produced during the degradation of PE and LPS. A synergic/collective/cooperative mechanism leads within short times to *E. coli*

inactivation as shown by CFU data and by the spectroscopic IR stretching shifts respectively in Figures 6.3a and 6.6a.

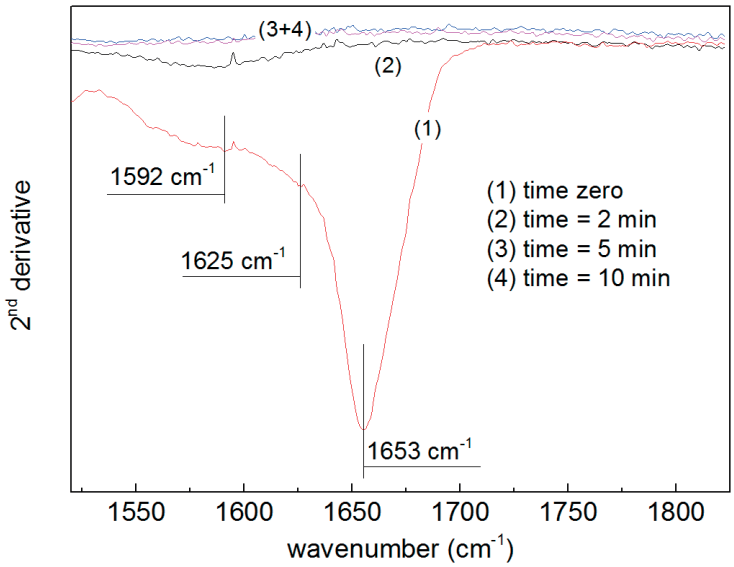

Figure 6.6d. FTIR-ATR spectra of *E. coli* Amide I bands on Cu-Ag (50%-50%) PU-catheter sputtered for 1 min under low intensity actinic light irradiation (3 mW/cm^2).

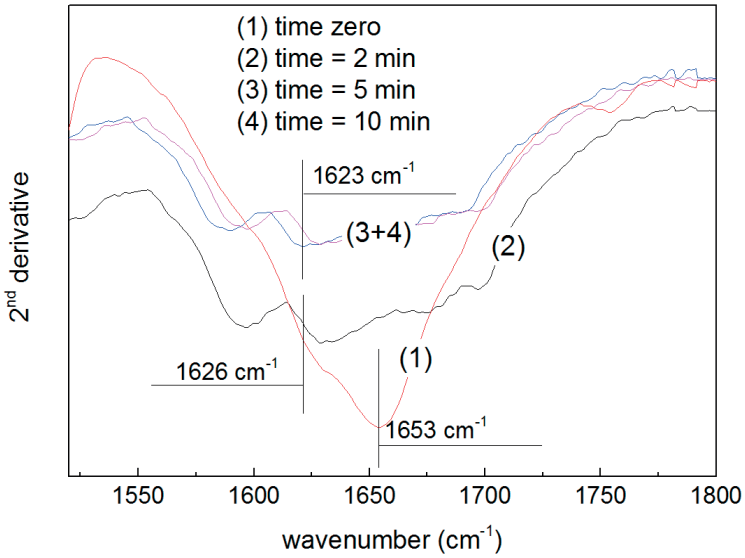

Figure 6.6e. FTIR-ATR spectra of *E. coli* Amide I bands on Cu-Ag (50%-50%) PU-catheter sputtered for 1 min in the dark.

6.4. Conclusions

This chapter reports the sputtering of uniform and adhesive bacterial Cu-Ag nano-composite film on 3D-catheter leading to similar inactivation times in the dark and under light. An ultrafast/quasi- instantaneous inactivation kinetics was obtained for *E.*

coli ≤ 5 min. The bacterial inactivation kinetics was seen to be a function of the Cu:Ag ratio in the film coating the PU-catheters. The effect Cu and Ag suggests that metal related effects predominate over the photo-induced effects by the oxide semiconductors CuO/Cu_2O and Ag_2O leading to bacterial inactivation. A mechanism of the Cu-Ag bacterial inactivation is suggested related to the pH and FTIR band shifts observed during the bacterial inactivation. The reversible hydrophobic/hydrophilic photo-switching on the Cu-Ag PU films is reported within the bacterial inactivation time. The Cu-Ag films present a potential for the application in medical devices, textiles, polymer thin films designed to preclude pathogenic biofilm formation.

Chapter 7

Microstructure of Cu-Ag uniform nanoparticulate films on polyurethane 3D-Catheters: surface properties

This chapter is based on the following publication: Sami Rtimi, Rosendo Sanjines, Cesar Pulgarin, John Kiwi, ACS-Appl. Mater. Interfaces 2016, 8, 56−63 (Reproduced with permission of ACS, Copyright 2016).

7.1. Introduction

Copper based antibacterial coatings have been widely investigated during the last decade. Bacterial cell walls damaging DNA double helix disruption caused by copper ions have been studied by Borkow [178,96], Parkin [172], Hashimoto [94] and Kiwi [81,52] among many others. Cu-ions electrostatic interaction with the negatively charged bacterial cell walls produce highly oxidative radicals ROS. This allows the Cu-ions to penetrate into the bacteria cytoplasm disturbing the cell metabolism and leading to cell death [183].

Silver nano-particulates have been widely applied on cotton and artificial fibers like polyester, wound-pads, and thin polymer films, all of them 2D-surfaces showing antibacterial activity [208]. Silver and copper antibacterial dynamics and mechanisms have been reported elsewhere and will not be discussed further in the study.

This chapter addresses the characterization of the surface properties and film microstructure of Cu and Ag films sputtered on PU 3D-catheters that were shown in chapter 6 to induce quasi- instantaneous bacterial inactivation. This is an important issue since some Cu and Ag-coatings have been reported not providing fast bacterial inactivation [180-182] which is essential to prevent in some cases the rapid formation of bacterial highly infectious biofilms. This is also important due to the direct contact of the catheter with blood since the catheter is a channel for the bacteria when contacting veins and arteries. Besides the extremely fast bacterial inactivation, the 3D catheters with Cu-Ag films presented in chapter 6 show a stable repetitive bacterial disinfection performance over many cycles. Different studies have reported the kinetics and mechanism of antibacterial metal/oxide films [10,209-211,176,177]. Cu-

coatings were shown to inactivate bacteria more efficiently compared to Ag-films, due to the higher cytotoxicity and diffusion length of the Cu/Cu-ions [178,93]. Additionally, Cu induces a significant anti-microbial effect at a very low concentration (ppb range) [52,183,212] without inducing cytotoxicity towards mammalian cells [212,213]. The Cu bactericide effect may proceed through an “oligodynamic effect”. This effect consists in the property of Cu atoms/ions released in the ppb range as Cu or as Cu-Ag when Ag is present, leading to bacterial inactivation [99].

Cu-Ag disrupt processes needed for the cell metabolism are influenced by the properties of the metal atoms and their interaction with the cell components [214]. Identifying the surface properties and microstructure of sputtered Cu-Ag will allow the design, of more performing films leading to even to shorter bacterial inactivation times. [10,209]. Hybrid films present, in some cases, a superior disinfection action compared to single metals films to kill pathogens [210]. Some laboratories have reported hybrid copper/silver prepared by sol-gel processes [215-216]. The principle of the sol-gel method is the homogenization of alcoxides, usually called sols followed by the gelling of the sol in a mould, drying (curing) and finally firing or sintering on heat resistant supports. But these Cu-Ag sols cannot be adhered to the 3D PU catheter by calcination since the PU takes only ~120°C. Therefore the Cu-Ag films present problems when adhered to the PU catheter walls at lower temperatures. By electro-deposition, devices have been coated with Cu-Ag leading to persistent bacterial disinfection. Their porosity, microstructure and specific surface area were measured and the activity of the hybrid metallic films against *E. coli* was also investigated [195].

Chapter 7 presents the characterization of sputtered Cu-Ag PU-catheters by the following techniques: DRS, XRD, AFM, STEM microanalysis and XPS. These complementary techniques provide a detailed description of the Cu-Ag film surface properties for the catheter mediated bacterial inactivation presented in chapter 6.

7.2. Experimental section

7.2.1. Sputtering of Cu-Ag on PU, thickness calibration and film composition

The sputtering set-up has been modified to allow the deposition of uniform 3D-film coverage on the cylindrical catheter surfaces. The modification of the sputtering unit will not be described in this chapter since they figure in section 6.2.1 (chapter 6). Before sputtering the films, the residual pressure P_r in the sputtering chamber was set

at $P_r \leq 10^{-4}$ Pa. The substrate target distance was 10 cm and during the sputtering the sample was rotated (20 rpm) to guarantee a homogeneous distribution of the coating on the 3D-catheter. The rotation rate was optimized to cover film homogeneity the 3D catheter surface. Thin films were deposited by reactive DCMS in an Ar + O_2 gas flow from a 5 cm round target (Kurt J. Lesker, East Sussex, UK). The sputtering current was set at 280 mA. The different Cu/Ag atomic ratios sputtered during the course of this study were: 25%-75%, 33%-67% and 50%-50% %Cu-%Ag respectively. In addition coatings were carried out sputtering 100% Ag and 100% Cu. The sputtering of the Cu-Ag on the PU films or catheters has been carried out for short times at ~120°C [52,212].

The film thickness was determined with a profilometer (Alphastep500, TENCOR). The thickness data were determined in triplicate by sputtering the corresponding film on Si-wafer. By X-ray fluorescence (XRF) the composition of the Cu-Ag coatings was determined in a PANalytical PW2400 spectrometer.

7.2.2. DRS and XRD of Cu-Ag on PU films

DRS was carried out in a Perkin Elmer Lambda 900 UV-VIS-NIR spectrometer provided for with a PELA-1000 accessory within the wavelength range of 200-800 nm and a resolution of 1 nm. The rough UV–Vis reflectance data cannot be used directly to assess the absorption of the Cu-Ag films because of the large scattering contribution of PU fabric to the DRS spectra. X-Ray Diffraction of the Cu-Ag films crystallographic phases was carried out by means of an X'Pert Philips diffractometer, Delft, NL. The Ka line of Cu (1.5409 Angstroms) radiation was used as reference.

7.2.3. Microanalysis of Cu-Ag PU by Scanning Transmission Electron Microscopy (STEM) and Atomic Force Microscopy (AFM)

The sputtered Cu-Ag PU films were prepared for analysis by embedding in epoxy resin 45359 Fluka and the fabrics were cross-sectioned with an ultramicrotome (Ultracut E) and at a knife angle at 35°. The Cu and Ag nano-particle distribution on the PU-film was investigated by EDX microanalysis in the scanning transmission electron microscopy mode (STEM) and the images were taken in a FEI Tecnai Osiris instrument at 200 kV.

The AFM image signals were acquired in contact mode using a PSIA Xe-100 AFM. Silicon nitride cantilevers were used with feedback set points around 1.0 nN. The AFM scanner and position sensors were calibrated using standard samples from

Mikromash. The experimental error in the roughness was below 10%. The mean surface roughness (Rg) was calculated for the scanned area.

7.2.4. XPS of Cu-Ag PU 3D-catheters

The X-ray photoelectron spectroscopy (XPS) of the Cu-Ag films was determined using an AXIS NOVA photoelectron spectrometer (Kratos Analytical, Manchester, UK) provided for with monochromatic AlK_a (h□=1486.6 eV) anode. The carbon C1s line with position at 284.6 eV was used as a reference to correct the charging effects. The surface atomic concentration was determined from peak areas using the known sensitivity factors for each element [97-98]. Spectrum background was subtracted according to Shirley [122]. The XPS spectral peaks were deconvoluted with a CasaXPS-Vision 2, Kratos Analytical UK.

7.2.5. Bacterial inactivation on sputtered PU 3Dcatheters

Bacterial inactivation procedure and irradiation source were described in chapter 6 and will not be repeated here (see section 6.2.2).

7.3. Results and discussion

7.3.1. DRS and X-ray Diffraction (XRD) of Cu-Ag PU-catheters

Figure 7.1 shows the diffuse reflectance spectroscopy (DRS) in Kubelka-Munk units of Cu-Ag on PU with the ratios: (1) 25%-75%, (2) 33%-67%, (3) 50%-50% and in the insert (4) CuO and (5) Ag_2O. The insert in Figure 7.1 shows the strong Ag_2O peak at 350 nm and CuO with a maximum absorption close to 430 nm shifting the light absorption by the sputtered PU-films into the visible range [102]. Polyurethane films have been deposited with Cu-Ag and investigated along the PU 3D-catheters to facilitate the analysis and data acquisition. The optical absorption range observed for the Cu-Ag nano-particulate on PU lies between 200 and 700 nm. The optical absorption between 500 and 600 nm is due to the inter-band transition of Cu_2O and the absorption between 600 to 700 nm has been attributed to the exciton band associated with the CuO (d-d) transition [94,120]. Figure 7.1, trace 3 shows the DRS spectra for the Cu-Ag 50%-50% on PU films showing a lower intensity compared to the bands Cu-Ag 25%-75% and Cu-Ag 33%-67% on PU films. An increase in the atomic disorder due to galvanic corrosion at the Cu/Ag interface within the Cu-Ag 50%/50% films, may be responsible for the decreased optical absorption intensity of

the Cu-Ag bands [198-199]. The later effect is favored by the Ag-Cu nano-particle uniform distribution on PU films.

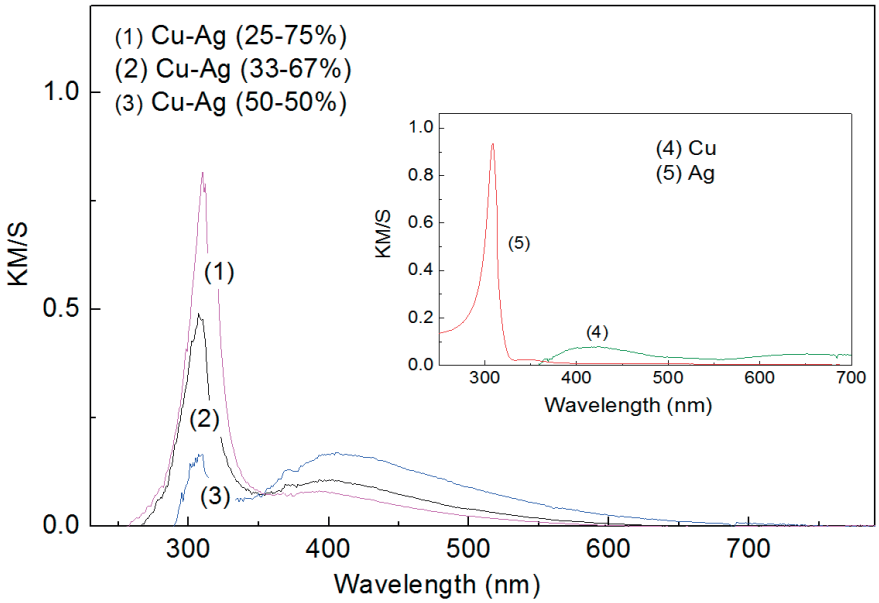

Figure 7.1. DRS of Cu-Ag with Cu-Ag atomic ratios p: (1) 25%-75%, (2) 33%-67%, (3) 50%-50%. The insert shows the data for: (4) Cu and (5) Ag.

Figure 7.2 presents the XRD spectrograms showing the presence of Cu_2O (111), Cu (200), Cu (020) and Ag (111). The Cu nano-particles present a more crystalline character compared to Ag nano-particles. The coordinated copper ions (Cu_2O (111)) have been suggested to be the catalytic active sites on Cu-based antibacterial surfaces [199,217]. The presence or absence of Cu-cations was reported to be important for the understanding of the surface reactivity of Cu_2O and other copper species [217-218,125,129]. In addition, metallic Cu and Ag were also present in the sputtered films with different Cu:Ag atomic ratios.

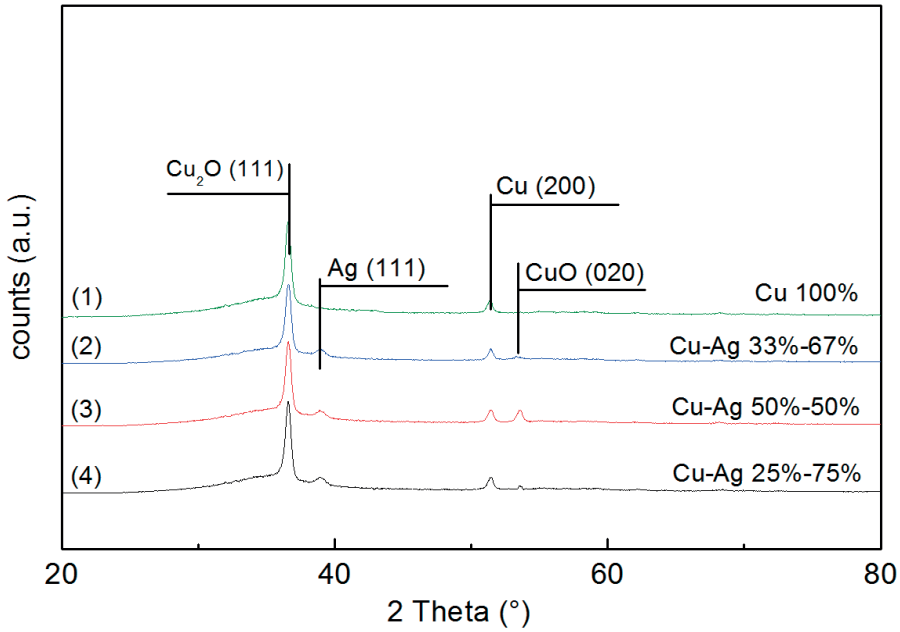

Figure 7.2. XRD spectrogram signals for sputtered PU-catheters: (1) Cu, (2) Cu-Ag 33%-67%, (3) Cu-Ag 50%-50% and (4) Cu-Ag 25%-75%.

7.3.2. Electron Microscopy (STEM) Observations: Distribution of Cu-Ag Sputtered Clusters on the Sputtered Films

Figure 7.3 presents the Cu and Ag nanoparticle distribution on the PU-film as investigated by the scanning transmission electron microscopy (STEM) mode. The mapping/distribution of Cu and Ag on Ag-Cu PU samples with different Cu:Ag atomic ratio is presented in Figure 7.3. The first row in Figure 7.3 shows a uniform Cu nano-particle distribution with particle sizes of 2-4 nm on the PU-film. The second row shows the images for a Cu-Ag PU film with a ratio 50%: 50% comprising a loading of 0.05 and 0.03 weight%/weight PU-catheter sample respectively as detected by X-ray fluorescence.

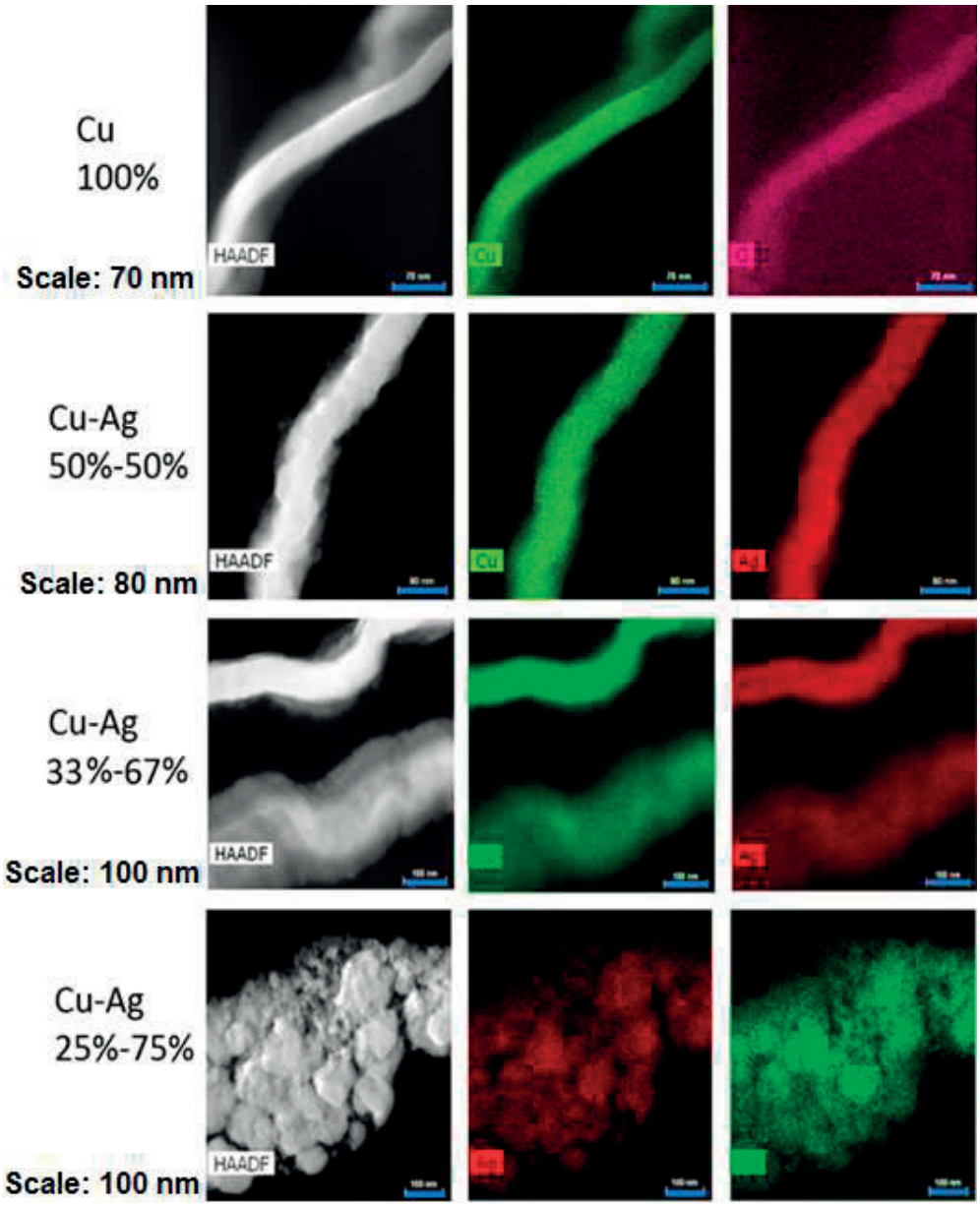

Figure 7.3. EDX microanalysis/distribution of the Cu and Ag nanoparticles on the PU-films with different Cu:Ag atomic ratios.

The third row shows the images for a Cu-Ag sample with a ratio 33%: 67%. Most of the Cu and Ag-metal clusters were < 5 nm in size. The small size of the nanoparticles favors the charge transfer and consequently the bacterial inactivation kinetics due to large surface area per unit mass [125,129]. Recently Snaith et al., [218] and Kopidakis et al., [219] reported that the thickness and grain sizes of the nanoparticles making up the film play a major role in the film charge transport/transfer. The Cu-Ag film leading to the fastest bacterial inactivation kinetics seems to present the optimal Cu and Ag ratio for the charge transfer and subsequent diffusion of the

ions towards the *E. coli* culture. The quantum size of the Cu-Ag clusters up to 10 nm consist of ~10^4 seem to effectively separate the induced charges inside the Cu-Ag bimetallic cluster in spite of their confinement in very reduced spaces [219,97, 201-211]. The last row in Figure 7.3 shows that an increase in the percentage of Ag in the Cu-Ag films leads to the formation of bigger agglomerates. The second and third columns in Figure 7.3 show images for the uniform distribution of the Cu and Ag nanoparticles according to their ratio in the bimetallic target from which they were sputtered. Scheme 7.1 shows the schematic charge transfer/transportation in a nano-particulate layer as reported by Snaith et al. [218]. The charge transfer/transport is limited by the size of the grains forming the thin layers without taking into account the variability of the interparticle contact area. This research details reported in the Snaith's study will not be further discussed in this chapter.

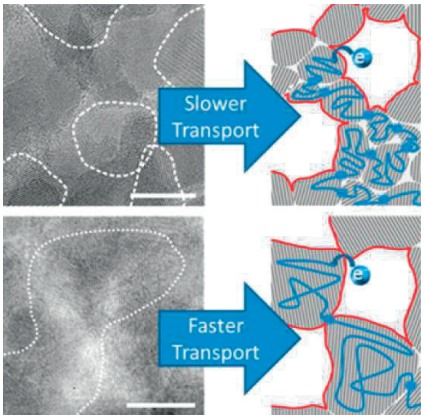

Scheme 1. Mobility of conduction band electrons influenced by grain boundaries (reproduced under license from ACS).

7.3.3. AFM roughness of Cu-Ag Films

Figure 7.4 shows the increasing Rg values from 13 nm up to 22 nm for Cu-Ag nano-particles. The concomitant Ag-film content increased from 50% and up to 75%. The AFM field scanned in Figure 7.4 was 0.3 x 0.3 micron. The Cu-Ag clusters with Cu:Ag atomic ratios of 50%/50%; 33%/67% and 25%/75% led to particles with increasing sizes and roughness as shown in the first row in Figure 7.4. The increase in silver content in the Ag-Cu films led an increase in the Cu-Ag cluster size and roughness (Rg). The second row in Figure 7.4, shows Rg-values of 5 nm and 10 nm for Cu and Ag clusters respectively on PU films. The sizes for the Cu clusters were found between 5-10 nm and for the Ag-clusters between 28-48 nm, following the same trend as the respective Rg-values. These observations coincide with the STEM

microanalysis (Figure 7.3) showing that increasing the Ag content led to big clusters/agglomerates.

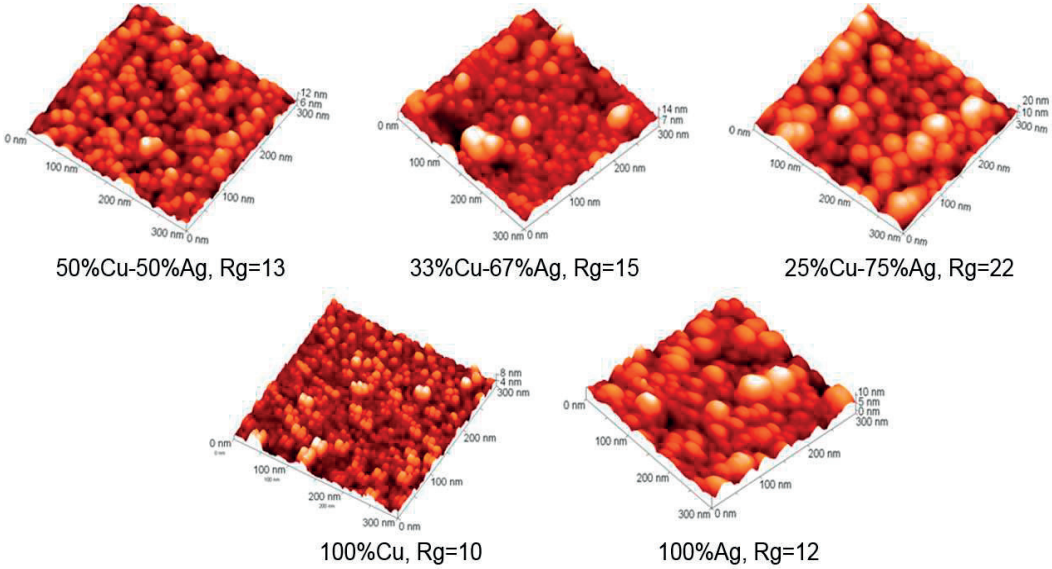

Figure 7.4. Atomic force microscopy (AFM) of Cu-Ag sputtered films with different atomic ratios of Cu and Ag.

7.3.4. XPS of the Cu-Ag PU 3D catheters

Figure 7.5a shows the deconvoluted doublet of the $Cu2p_{1/2}$ band at time zero for a Cu-Ag film 50%/50% not contacted with bacteria. The assignment of the Cu_2O (BE at 932.1 eV) and for the CuO (BE 933.7 eV) was carried out according to Wagner et al., [97] and Nogier et al., [38] and the charging effects on the samples were corrected according to Shirley [122]. Besides the peaks of Cu_2O and CuO an additional peak of $Ag_2Cu_2O_4$ was identified at 932.9 eV. Evidence was found for the $Ag_2Cu_2O_4$ inner charge re-distribution of Cu and Ag favoring the disorder in Cu-Ag structures as recently reported [220-221]. Cu would share a delocalized valence charge distribution leading to $Ag_2Cu_2O_4$ due to the structural disorder introduced when Cu contacts Ag at the Cu-Ag interface. The valence band of $Ag_2Cu_2O_4$ was estimated between 2.11-2.15 eV [223].

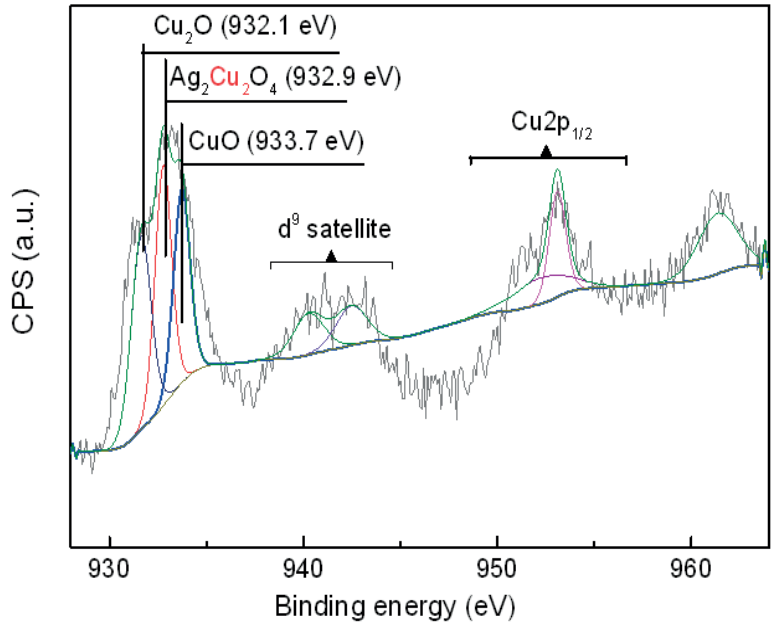

Figure 7.5a. Deconvoluted doublet of the $Cu2p_{1/2}$ bands at time zero for a Cu-Ag film 50%/50% showing the Cu-oxides and $Ag_2Cu_2O_4$ for a sample not contacted with bacteria.

The deconvoluted $Ag3d_{1/2}$ doublet in the Cu-Ag 50%/50% PU film at time zero is shown in Figure 7.5b. The Ag and AgO are detected along $Ag_2Cu_2O_4$ for a sample not contacted with bacteria. The Ag-oxide peaks are present but in a smaller amount compared to Cu-oxides peaks as shown in Figures 7.5a and 7.5b. It is difficult to discern in Figure 7.5b about the presence of Ag_2O since the AgO/Ag_2O peaks are very close [97, 221]. Figure 7.5c shows the deconvoluted O1s doublet for a sample of Cu-Ag film 50%/50% at zero time not contacted with bacteria. Some peaks are found similar to the peaks reported in Figure 7.5a, with the exception of CuO and Ag_2O, suggesting that the CuO and Ag_2O exists only in small amounts.

Table 7.1 present the Cu-oxides and Ag-oxides present on Ag-Cu films presenting different ratios of Cu:Ag.

Table 7.1. Cu and Ag species present of Cu-Ag films with different atomic ratios of Cu:Ag.

	Cu-Ag (50%-50%)	Cu-Ag (33%-67%)	Cu-Ag (25%-75%)
Cu species	CuO, Cu_2O, Cu	CuO, Cu_2O	CuO, Cu_2O
Ag species	AgO, Ag	AgO, Ag_2O, Ag	AgO, Ag_2O, Ag
Mixed phase	$Ag_2Cu_2O_4$	$Ag_2Cu_2O_4$	--

In Table 7.1: a) XPS signals suggest that Cu exists as a metal only in the Cu-Ag 50%/50% sample. Therefore, metallic Cu seems necessary for an efficient charge transfer since this sample lead to the faster bacterial inactivation, b) Ag_2O is absent in the Cu-Ag 50%/50% sample. AgO was detected being the most active Ag-oxide in *E. coli* inactivation in agreement with results reported in a recent study [48], c) the Ag^0 metal seems to be a necessary component for an accelerated bacterial inactivation in the three PU films with different Cu:Ag ratios investigated in this study, and finally d) the $Ag_2Cu_2O_4$ detected in the most active sample Cu-Ag 50%/50% seems to play an important role in any catalyst/photocatalyst [224] leading to bacterial inactivation

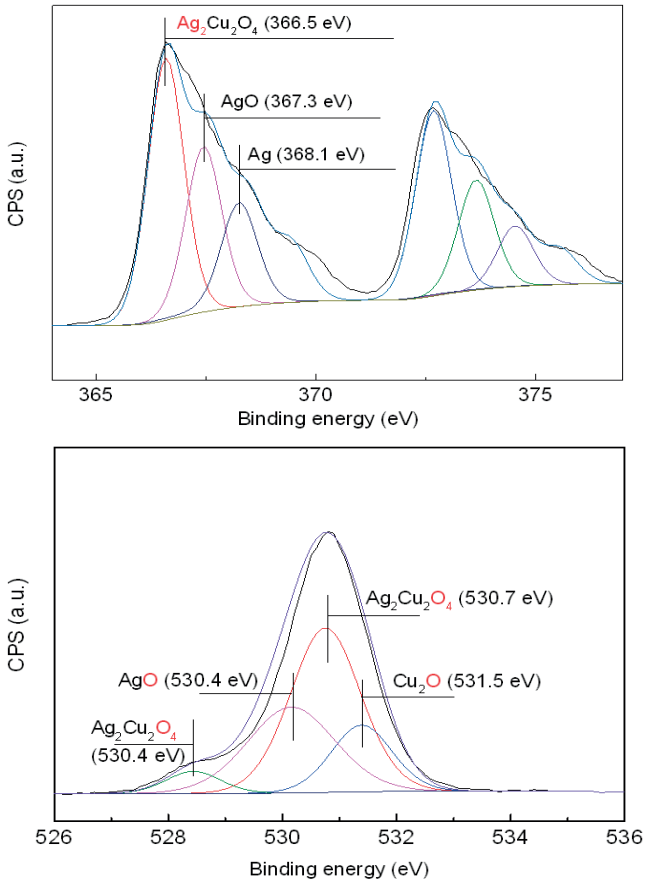

Figure 7.5b. Deconvoluted doublet of the $Ag3d_{1/2}$bands at time zero for a Cu-Ag film 50%/50% not contacted with bacteria showing the Cu-oxides and $Ag_2Cu_2O_4$.
Figure 7.5c. Deconvoluted doublet of the O1s bands at time zero contacted with bacteria by a Cu-Ag film 50%/50% showing the Cu-oxides/Ag-oxides and $Ag_2Cu_2O_4$

The O1s band for the O-doublet and the respective Cu-, Ag oxides and $Ag_2Cu_2O_4$ peaks are show in Figure 7.5c. The etching of Cu-Ag 50%/50% films under 5 KeV Argon-ion bombardment in the XPS unit is shown next in Figure 7.5d. The signal

intensity (counts) increases up to 48 nm (or 240 layers) for the $Ag3d_{1/2}$ doublet and becomes more spiked at deeper levels due to the higher crystal symmetry of the Ag-oxide nano-particles in the film. A similar trend was observed for the $Cu2p_{1/2}$ bands.

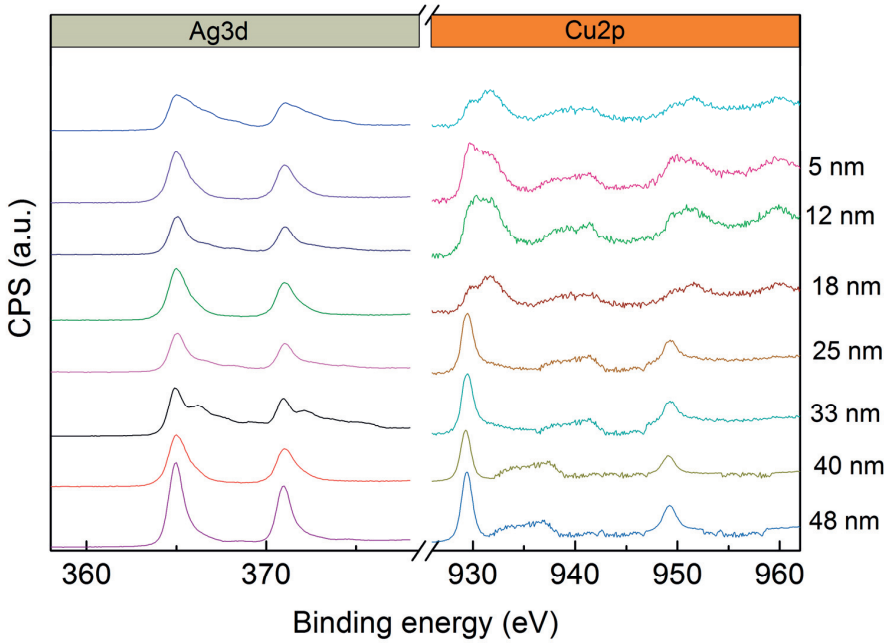

Figure 7.5d. XPS etching of Cu-Ag (50%-50%) sputtered for 60 s.

Table 7.2 presents the atomic surface concentration percentage of several elements before and after bacterial inactivation. The C1s content increases slightly due to: a) the C-adsorbed in the catalyst during the bacteria inactivation and b) the C contained in the residual gas atmosphere when handling the sample during the XPS experiments.

Table 7.2. Atomic surface % XPS of different elements on Cu-Ag PU-catheters contacted with bacteria before and after bacterial inactivation.

	Before bacterial inactivation	After bacterial inactivation
C1s	71.40	72.24
O1s	14.35	15.82
Ag3d	4.92	4.4
Cu2p	9.34	7.54

The small increase observed in the O1s content is due to the oxidized species formed during bacterial degradation in air atmosphere. The decrease of the Ag3d and the Cu2p signals after bacterial inactivation is assigned to the removal of the bacterial culture containing carbonaceous species allowing the original surface to re-appear

after bacterial degradation. Table 7.3 shows in the dark and under light the reduction of C-reduced species like C-C; C-H; C=C (B.E. 284.6-285 eV) after 10 min with the concomitant increase in oxidized species after bacterial inactivation like C-O; C=O; COOH (B.E. 287.2-287.6 eV) and O=C-OH (B.E. 289.1 eV) [97-98]. The amount of reduced species during the dark inactivation was lower compared to the ones observed under light as expected.

Table 7.3. XPS analysis of the C-species on the surface of a Cu-Ag PU-catheters 50%/50% as a function of bacterial contact time in the dark, and under low intensity actinic light.

		C-C, C=H, C-H	C-O, C=O, COOH	O=C-OH
Dark condition	Time zero	0.31	0.32	0.36
	10 min	0.22	0.37	0.41
Under light (3 mW/cm^2)	Time zero	0.31	0.33	0.35
	10 min	0.15	0.41	0.44

7.3.5. Bacterial Inactivation Dynamics on Cu-Ag PU 3Dcatheters

Figure 7.6 shows that the bacterial inactivation time of *E. coli* was accelerated to 5 min on a 50%/50% Cu-Ag PU 3D-catheter compared to Cu or Ag deposited independently on PU-catheters. Bacterial inactivation times become longer as the loading of Ag in the Cu-Ag film increases (see Figure 7.6c and 7.6d). The 50%/50% Cu-Ag atomic ratio involves Cu-Ag catalytic sites comprising the highest number of active centers held in exposed surface positions in contact with bacteria. Films sputtered for one minute with less than 50% Cu-content led to longer bacterial inactivation times as shown in Figures 7.6c and 7.6d.

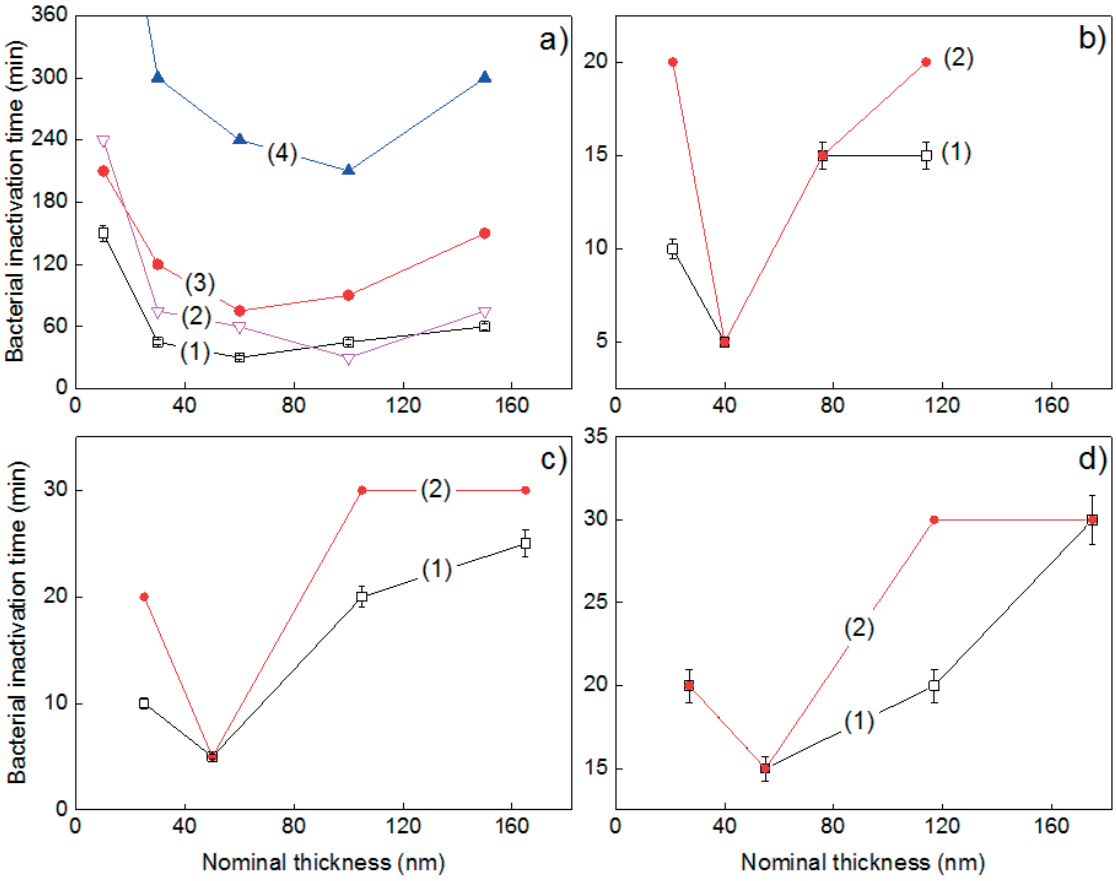

Figure 7.6. Effect of the coating thickness on the bacterial inactivation kinetics for: **a)** (1) Cu- PU-catheter under low intensity actinic light (3 mW/cm^2), (2) Ag-PU-catheter under low intensity actinic light (3 mW/cm^2), (3) Cu-PU-catheter in the dark, (4) Ag-PU-catheter tested in the dark. **b)** Cu-Ag (50%-50%) sputtered on PU-catheters: (1) under low intensity light (3 mW/cm^2) and (2) in dark conditions. **c)** Cu-Ag (33%-67%) sputtered on PU-catheters: (1) under low intensity light (3 mW/cm^2) and (2) in dark conditions. **d)** Cu-Ag (25%-75%) sputtered on PU-catheters: (1) under low intensity light (3 mW/cm^2) and (2) in dark conditions. Error bars: standard deviation (n=5%).

The low Cu-content in the film was not enough to lead to a fast bacterial inactivation. This means that Cu and Ag nano-particles with their high oxidation potentials predominate over the semiconductor CuO/Cu_2O and Ag_2O behavior that would accelerate bacterial inactivation under light compared to dark runs. Light irradiation leads to charge separation in semiconductor devices like CuO and Ag_2O. Cu-Ag films inactivate bacteria within 5 min, 6 times faster compared to the 30 min inactivation period required for Cu. By ICP-MS, films with a 50%/50% Cu:Ag atomic ratio led to the highest kinetics ions release [183,79]. In-depth bacterial inactivation dynamics and cytotoxicity tests are underway to clear further this issue.

7.4. Conclusion

In chapter 7, we report for the first time the characterization of surface properties and detailed microstructure of sputtered bimetal Cu-Ag antibacterial coating on 3D-objects, in this case PU-catheters. The details of hybrid nano-composites Cu-Ag films with different atomic ratios were investigated using STEM and AFM imaging. The bacterial inactivation kinetics were shown to be a function of the Cu:Ag ratio sputtered on the catheter. Optical and crystalline properties were reported by way of DRS and XRD. By XPS, different oxidation states have been identified before and after bacterial inactivation showing that redox catalysis takes place within the period of bacterial inactivation. The Cu-Ag coated 3D-catheters showed stable performance during repetitive recycling leading to bacterial disinfection.

Chapter 8: Conclusions and perspectives

In this thesis we have addressed the deposition of thin uniform, adhesive films able to reduce bacterial infections in the dark and under light within acceptable times and stable enough to work in a repetitive fashion. These films consisted of TiO_2, TiO_2/Cu and bimetallic Cu-Ag. This thesis presents the design, sputtering (synthesis), bacterial evaluation and surface characterization of the antibacterial films on polyester (PES), polyethylene (PE) and 3D polyurethane (PU)-catheters. The most suitable inactivation kinetics of *E. coli* taken as a standard probe was optimized on these films, which is important in the potential application of these films on textiles, thin polymer films, and catheters/implants. A systematic, detailed and comprehensive investigation is presented for the several novel coatings explored during the thesis work. Resuse cycles show sufficient life-time for application in hospital facilities.

Despite the recent progress made in this area during the last decade, improvements will be necessary in the coming years in order to synthesize high-quality functionalized coatings using more sophisticated approaches. Moreover, synthesis and surface engineering of NP's will be developed involving a more complex chemical, physical and surface functionalization addressing inorganic-organic composite coatings. The higher stability of these films and how to translate the laboratory findings into large-scale industrial synthesis is a short range objective of the possible work in this area.

Surface pretreatments have a high potential to improve coated implants such as the acceleration of osseointegration even in poor quality bone and the protection from chemical corrosion by body fluids. Future work in this area must be focused on the research of the toxicity induced by the bactericide films in meta-materials applied to 2D and 3D objects. Biofilms are nowadays the most dangerous way of spreading highly infectious pathogens into the environment, in public places and healthcare facilities. Films showing quasi-instantaneous antibacterial kinetics will preclude biofilm formation. The technology presented herein has the potential to open new industrial segments in the rapidely developing health sector. Further research is required to translate the present findings into performing industrial products e.g. Cu-Ag catheters as prepared and evaluated in this thesis and tested in the CHUV showing instantaneous bactericide action in vitro and in vivo as recently reported from our EPFL laboratory.

Nowadays, a plethora of coating techniques is being investigated to get a desired biological response (high bactericidal long-range stable effect) at the interface between an implant and the surrounding living tissue. For this end, the make up of the sputtered films has to be chosen to fulfil an antibacterial activity concomitant with mammalian cells biocompatibility. In addition to the application of DCMS for metallic surgical/cutting tools coating, some industries recently started using this technology to develop tools used in the dental surgery and also in spine and orthopedic implants showing the high potential of this approach. The substrates are in the majority thermo-resistant and the coating can easily be applied and heated-up to better bind the substrate. The novel 3D devices developed in this thesis need to be transferred to an industrial scale to fully benefit from these innovative coatings.

References

[1] A. Kramer, I. Schwebke, G. Kampf, How long do nosocomial pathogens persist on inanimate surfaces? A systematic review, BMC Infect. Dis. 6 (2006) 130-138.

[2] S. Dance, S. The role of environmental cleaning in the control of hospital acquired infections J. Hosp. Infect. 73 (2007) 378-389.

[3] A. G. Rincon and C. Pulgarin, Photocatalytical inactivation of *E. coli*: effect of (continuous–intermittent) light intensity and of (suspended–fixed) TiO_2 concentration, Appl. Catal. B. 44 (2003) 263-284.

[4] R. Plowman, N. Graves, A. Griffin, L. A. Roberts, V. Swan, B. Cookson, Taylor, The rate and cost of hospital-acquired infections occurring in patients admitted to selected specialties of a district general hospital in England and the national burden imposed, J. Hosp. Infect. 47 (2001) 198-204.

[5] K. Page, M. Wilson, P.I. Parkin, Antimicrobial surfaces and their potential in reducing the role of the inanimate environment in the incidence of hospital-acquired infections, J. Mater. Chem. 19 (2009) 3819-3831.

[6] J. Kiwi, C. Pulgarin, Innovative self-clening and bactericidal textiles, Catal. Today 151 (2010) 2-7.

[7] S. Silver, L.T. Phung, G. Silver, Silver as biocides in burn and wound dressings and bacterial resistance to silver compounds, J. Ind. Microbiol. Biotechnol. 33 (2006) 627.

[8] J. L. Clement, P. S. Jarret, Metal-Based Drugs, Encyclopedia of Inorganic and Bioinorganic Chemistry 1 (1994) 467.

[9] Y.A. Krutyakov, A.A. Kudrinskiy, A.Y. Olenin, G.V. Lisichkin, Russ. Chem. Revs. 77 (2008) 233.

[10] A. H. Foster, B. I. Ditta, S. Varghese, S. Steele, Photocatalytic disinfection using TiO_2: Spectrum and mechanism of antimicrobial acivity', Appl. Microb & Biotechnol. 90 (2012) 1847-1868.

[11] M. Paschoalino, N. C Guedes, W. Jardim, E. Mielczarski, J. Mielczarski, P. Bowen and J. Kiwi, Inactivation of *E. coli* mediated by high surface area CuO accelerated by light irradiation >360 nm, J. Photochem. Photobiol. A 199 (2008) 105-111.

[12] L. Zhang, R. Dillert, D. Bahnemann, M. Vormoor, Photo-induced hydrophilicity and self-cleaning: models and reality, En. & Environ. Sci. 5 (2012) 7491-7507.

[13] C. Page, M. Wilson, N. Mordan, W. Chrzanowski, P. Knowles, P.I. Parkin, Study of the adhesion of Staphylococcus aureus to coated glass substrates, J. Mater. Sci, 46 (2010) 6355-6363.

[14] K. Page, R. Palgrave, P.I. Parkin, M. Wilson, Sh. Savin, A. Chadwick, Titania and Silver-Titania composite films on glass-potent antimicrobial coatings, J. Mater. Chem. 17 (2007) 95-104.

[15] M. S. P. Dunlop, P. C. Sheeran, A. J. M. Byrne, S. A. McMahon, M. A. Boyle, G. K. McGuigan, Inactivation of clinically relevant pathogens by photocatalytic coatings, J. Photochem. Photobiol. A. 216 (2010) 303-3010.

[16] S. Wang, W. Zhu, P. Yu, X. Wang, T. He, G. Tan, C. Ning, Antibacterial nanostructured copper coatings deposited on tantalum by magnetron sputtering, Materials Technology, 30 (2015) B120-B125.

[17] O Baghriche, A. Ehiasarian, E. Kusiak-Nejman, A. Morawski, C. Pulgarin, R. Sanjines, J. Kiwi, Advantages of high power impulse magnetron sputtering (HIPIMS) of silver for improved *E. coli* inactivation, Thin Solid Films, 520 (2012) 3567-3573.

[18] Thüringer Surface and Biomaterial Kolloquium, 13/15 September Zeulenroda, Germany.

[19] M. Schnabelrauch, Surface and Biomaterial Kolloquium, 13/15 September, p13-14, Zeulenroda, Germany.

[20] S. Nahzi, Biomedical Materials, Springer, New York, 43 (2009) 35-43.

[21] M. J. Domek, M. W. Chevalier, S. C. Cameron, G. A. McFeters, Evidence for the role of copper in the injury process of coliform bacteria in drinking water, Appl. Env. Microb. 48 (1984) 289-293.

[22] J. O. Noyce, H. Michels, C. W. Keevil, Potential use of copper surfaces to reduce survival of epidemic meticillin-resistant *Staphylococcus aureus* in the healthcare environment, J. Hosp. Infect. 63 (2006) 289-297.

[23] S. A. Wilks, H. Michels, C. W. Keevil, The survival of *Escherichia coli* O157 on a range of metal surfaces, Int. J. Food Microb.105 (2005) 445-454.

[24] S. Noimak, Ch. Dunnill, M. Wilson, I. P. Parkin, The role of surfaces in catheter-associated infections, Chem. Sc. Revs. 38 (2009) 3435-3448.

[25] G. Borkow, J. Gabbay, Copper as abiocidal tool, Curr. Med. Chem, 12-13 (2005) 2163-2170.

[26] R. B. Thurman, C. P. German, The molecular mechanisms of copper and silver ion disinfection of bacteria and viruses, Crit. Rev. Environ.Comntrol 18 (1989) 259-315.

[27] K. Page, M. Wilson, I. Parkin, Antimicrobial surfaces and their potential in reducing the role of the inanimate environment in the incidence of hospital-acquired infections, J. Mater. Chem. 19 (2009) 3818-3831.

[28] D. Monroe, Looking for chinks in the armor of bacterial biofilms, Plos Biol., 5 (2007) e307.

[29] M. Haenle, M. Fritshe, C. Zietz, R. Bader, F. Heidenau, An extended spectrum bactericidal titanium dioxide (TiO_2) coating for metallic implants: in vitro effectiveness against MRSA and mechanical properties, J. Mater Sci: Mater. Med. 22 (2011) 381-387.

[30] F. Heidenau, W. Mittelmeier, R. Detsch, M. Haenle, F. Stenzel, G. Ziegler, H. Gollwitzer, A novel antibacterial titania coating: Metal ion toxicity and *in vitro* surface colonization, J. Mater. Sci. Mat. Med. 16 (2005) 883-889.

[31] H. M.Yates, L. A. Brook, I. B. Ditta, P. Evans, H. A. Foster, D. W. Sheel, A. Steele, Photo-induced self–cleaning and biocidal behviour of titania and copper oxide multilayers, J. Photochem. Photobiol A, 197 (2008)187-205.

[32] H. A. Foster, P. Sheel, W.D. Sheel, P. Evans, S. Varghese, N. Rutschke, M.H. Yates, Antimicrobial activity of titatnia/silver and titania/copper films prepared by CVD, J. Photochem. Photobiol. A. 216 (2010) 283-289.

[33] A.P. Frise, Choosing disinfectants, J. Hosp.Inf. 43 (1999) 255-264.

[34] A.N. Neely, M.P. Maley. Survival of Enterococci and Staphylococci on Hospital Fabrics and Plastic, J. Clin. Microb. 38 (2000) 724-726.

[35] H.A. Cohen, J. Amir, A. Matalon, R. Mayan, S. Beni, A. Barzilai, Stethoscopes and otoscopes--a potential vector of infection? Family Practice, 14 (1997) 446-449.

[36] J. Boyce, G. Potter-Bynoe, C. Chevenert, T. King, Environmental Contamination Due to Methicillin-Resistant *Staphylococcus aureus* Possible Infection Control Implications, Inf. Control Hosp. Epid. 18 (1997) 622-627.

[37] A. Bhalla, N. Pultz, D. Gries, A. Ray, E. Eckstein, D. Aron, C. Donskey, Acquisition of Nosocomial Pathogens on Hands after Contact With Environmental Surfaces Near Hospitalized Patients, Inf. Control Hosp. Epid. 25 (2004)164-167.

[38] X. Ding, Z. Liu, J. Su, D. Yan, Human serum inhibits adhesion and biofilm formation in Candida albicans, BMC Microbiology 14 (2014) 80.

[39] S. Vogt, K.-D. Kühn, W. Ege, K. Pawlik, M. Schnabelrauch, Novel Polylactide-Based Release Systems for Local Antibiotic Therapies, Materialwissenschaft und Werkstofftechnik (Mater. Sci. Eng. Technol.) 34 (2003) 1041-1047.

[40] G. Ginalska, M. Osinska, A. Uryniak, T. Urbanik-Sypniewska, A. Belcarz, W. Rzeski, A. Wolski, Antibacterial activity of gentamicin-bonded gelatin-sealed polyethylene terephthalate vascular prostheses, Eur. J. Vasc. Endovasc. Surg. 29 (2005) 419-424.

[41] L. Weaver, J. O. Noyce, H. T. Michels, C. W. Keevil, Potential action of copper surfaces on meticillin-resistant *Staphylococcus aureus*, J. Appl. Microb.,109 (2010) 2200-2205.

[42] D. Quaranta, T. Krans, C. Espirito-santo, C. Elowsky, G. Grass. Appl. Environ Microb. 77 (2011) 416-417.

[43] A. Torres, C. Ruales, C. Pulgarin, A. Aimable, P. Bowen, J. Kiwi, Enhanced Inactivation of E coli by RF-plasma Pretreated Cotton/CuO (65 m2/g) under Visible Light, Appl. Mater, Interf, 2 (2010) 2547- 2552.

[44] L. Rio, E. Kusiak, J. Kiwi, C. Pulgarin, A. Trampuz, A. Bizzini, Comparative methods to evaluate the bactericidal activity of copper-sputtered surfaces against methicillin-resistant Staphylococcus aureus, J. Appl. Microb. 78 (2012) 8176-8182.

[45] S. Rtimi, R. Sanjines, C. Pulgarin, J. Kiwi. Quasi-Instantaneous Bacterial Inactivation on Cu-Ag Nano-particulate 3D-Catheters in the Dark and Under Light: Mechanism and Dynamics. ACS Appl. Mater. Interfaces, DOI: 10.1021/acsami.5b09730.

[46] S. Rtimi, R. Sanjines, C. Pulgarin, J. Kiwi. Microstructure of Cu-Ag Uniform Nanoparticulate Films on Polyurethane 3D-catheters: Surface Properties. ACS Appl. Mater. Interfaces, DOI: 10.1021/acsami.5b09738.

[47] S. Rtimi, R. Sanjines, M. Andrzejczuk, C. Pulgarin, A. Kulik, J. Kiwi, Innovative transparent non-scattering TiO_2 bactericide thin films inducing increased E. coli cell wall fluidity, Surface and Coatings Technology 254 (2014) 333-343.

[48] M. I. Mejia, G. Restrepo, J. M. Marin, R. Sanjines, C. Pulgarin, E. Mielczarski, J. Mielczarski, J. Kiwi, Magnetron-Sputtered Ag-Modified Cotton Textiles Active in the Inactivation of Airborne Bacteria, ACS Appl. Mater. & Interf. 2 (2010) 230-235.

[49] O. Baghriche, J. Kiwi, C. Pulgarin, R. Sanjinés, J. Photochem. Photobiol. A, 229 (2012) 39-45.

[50] M. Polak, A. Ohl, M. Quaas, G. Lugoski, K. Schröder, Adv. Engin. Mater., 12 (2010) B511-B518.

[51] B. Finke, M. Polak, F. Hempel, H. Rebl, C. Zietz, R. Bader, J. Nebe, K. Weltman, K. Schröder, Materials Science Forum 706-709 (2011) 478-483

[52] S. Ritmi, O. Baghriche, R. Sanjines, C. Pulgarin, M. Bensimon, J-C. Lavanchy, J. Kiwi, Growth of TiO_2/Cu Films by HIPIMS for Accelerated Bacterial Loss of Viability. Surface and Coatings Technology 232 (2013) 804-813.

[53] P. Kelly and R. Arnell, Vacuum 156 (2000) 159-172.

[54] J. Sicha, J. Musil, M. Meissner, R. Cerstvy, Appl. Surf. Sci., 254 (2008) 3793-3800.

[55] J. Lin, J. Moore, W. Sproul, B. Mishra, Z. Wu, L. Wang, The structure and properties of chromium nitride coatings deposited using dc, pulsed dc and modulated pulse power magnetron sputtering, Surf & Coat. Technol. 204 (2010) 2230-2239.

[56] K. Sarakinos, J. Alami, D. Konstantinidis, High power pulsed magnetron sputtering : A review on scientific and engineering state of the art, Surf & Coat. Technol. 204 (2010) 1661-1684.

[57] P.J. Kelly, J. Hisek, Y. Zhou, R.D. Pilkington, R.D. Arnell, Advanced coatings through pulsed magnetron sputtering, Surface Engineering 20 (2004) 157-162.

[58] U.Helmersson, M. Lattemann, J. Bohlmark, A.P. Ehiasarian, J.T. Gudmundsson, Ionized physical vapor deposition (IPVD): A review of technology and applications (Review), Thin Solid Films, 513 (2006) 1-24.

[59] J.T. Gudmundsson, N. Brenning, D. Lundin, U. Helmersson, High power impulse magnetron sputtering discharge (Review), Journal of Vacuum Science and Technology A: Vacuum, Surfaces and Films, 30 (2012) 030801.

[60] V. Kousznetsov, K. Macak, J. Schneider, U. Helmersson, I. Petrov, Surf. Coat. Technol. 122 (1999) 290-295.

[61] J. R. Morones, J. L. Elechiguerra, A. Camacho, K. Holt, J. B. Kouri, J. T. Ramirez, M.J. Yacaman, Nanotechnology 16 (2005) 2346.

[62] T. Yuranova, G. Rincon, A. Bozzi, S. Parra, C. Pulgarin, P. Albers and J. Kiwi, Antibacterial textiles prepared by RF-plasma and Vacuum-UV mediated deposition of silver, J. Photochem. Phobiol. A, 161 (2003)185-192.

[63] T. Yuranova, A.G. Rincon, C. Pulgarin, D. Laub, N. Xanthopoulos, H-J. Mathieu and J. Kiwi, J. Photochem. Photobiol. A., 2006, 181, 363-369.

[64] L. Macomber, J.A. Imlay, The iron-sulfur clusters of dehydratases are primary intracellular targets of copper toxicity, Proc. Natl. Acad. Sci. USA, 106 (2009) 8344-8349

[65] C. Cervantes, F. Gutierrez-Corona, FEMS Microbiol. Rev 14 (1994) 121.

[66] C. Trapalis, M. Kokoris, G. Perdikakis, G. Kordas, J. Sol-Gel Sci. Technol. 26 (2003) 1213.

[67] A. M. Mulligan, M. Wilson, J. C. Knowless, Biomaterials 24 (2003) 1797.

[68] M. Paschoalino, N. C Guedes, W. Jardim, E. Mielczarski, J. Mielczarski, P. Bowen and J. Kiwi, J. Photochem. Photobiol. A 199 (2008) 105-111.

[69] K. Sunada, Y. Kikuchi, K. Hashimoto, A. Fujishima, Environ. Sci. Technol.; 32 (1998) 726

[70] S. Rtimi, C. Pulgarin, R. Sanjines, V. Nadtochenko, J.-C. Lavanchy, J. Kiwi, Preparation and Mechanism of Cu-Decorated TiO_2-ZrO_2 Films Showing Accelerated Bacterial Inactivation, ACS Applied Materials and Interfaces 7 (2015) 12832-12839

[71] A.Y. Peleg and D.C. Hooper, Hospital-Acquired Infections Due to Gram-Negative Bacteria, The New England Journal of Medicine 362 (2010) 1804-1813

[72] L. Geranio, M. Heuberger, E. Nowack, The behavior of Silver nano-textiles during washing, Environ. Sci Technol. 43 (2009) 8113-8118.

[73] Daoud, W. Self-cleaning Materials and Surface, Woodhead Pub. Co, UK, 2013.

[74] G. Ginalska, D. Kawalczuk, M.Osinska, Int. J. Pharmacy, 339 (2007) 39-46.

[75] P. A. Trambyah, Int. J. Microb. Agents, 24 sup.1 (2004) S44-S48.

[76] L. Corral, M. Nolla-Sallas, R. Iglesia, R. Catalan, J. Hospital Infect. 55 (2003) 212-219.

[77] R. E. Gilbert, M. Harden, Curr Opin. Infect. Dis., 21 (2008) 235-245.

[78] I. Banerjee, R. Pangule, R. Kane, Adv. Mater., 23 (2011) 690-718.

[79] S. Rtimi, M. Pascu, R. Sanjines, C. Pulgarin, M. Ben-Simon, A. Houas, J.-C. Lavanchy, J. Kiwi, ZrNO–Ag co-sputtered surfaces leading to E. coli inactivation under actinic light: Evidence for the oligodynamic effect, Applied Catalysis B: Environmental, 138–139 (2013) 113-121

[80] C. Castro, R. Sanjines, C. Pulgarin, P. Osorio, S. A. Giraldo, J. Kiwi, J. Photochem. Photobiol. A, 216 (2010) 295-302.

[81] P. Osorio, R. Sanjines, C. Ruales, C. Castro, C. Pulgarin, J-A Rengifo, J-C Lavanchy, J. Kiwi, Antimicrobial Cu-functionalized surfaces prepared by bipolar asymmetric DC-pulsed magnetron sputtering (PMS), J. Photochem. Photobiol. A., 220 (2011) 70-76.

[82] A. Ehiasarian, C. Pulgarin, J. Kiwi, Inactivation of bacteria under visible light and in the dark by Cu films. Advantages of Cu-HIPIMS-sputtered films, Env. Sci. Pollut. Res. 19 (2012) 3791-3797.

[83] E. Kusiak-Nejman, A. Morawski, A. Ehiasarian, O. Baghriche, C. Pulgarin, E. Mielczarski, J. Mielczarski, A. Kulik, J. Kiwi, *E. coli* Inactivation by High Power Impulse Magnetron Sputtered (HIPIMS) Cu-Surfaces, J. Phys. Chem. C. 115 (2011) 21113-21119.

[84] P. A. Tamiyah, Int. J. Antimicrob. Agents, 24 (2004) S44-S48.

[85] A. Bozzi, T. Yuranova, J. Kiwi, Self-cleaning of wool-polyamide and polyester textiles by TiO_2-rutile modification under daylight irradiation at ambient temperature, Journal of Photochemistry and Photobiology A: Chemistry 172 (2005) 27-34.

[86] O. Baghriche, S. Rtimi, C. Pulgarin, C. Roussel, J. Kiwi, RF-plasma pretreatment of surfaces leading to TiO_2 coatings with improved optical absorption and OH-radical production, Applied Catalysis B: Environmental, 130–131 (2013) 65-72.

[87] W. H. Boucher, G. H. Talbot, J.S. Bradley, J.S. Edwards, D. Gilbert, L.B. Rice, M. Scheld, B. Spellberg, J. Bartlett, Clin. Infect. Diseases, 48 (2009) 1-12.

[88] D. Pittet, D. Tarara, P.R. Wenzel, JAMA, 271 (1994) 1598-1601.

[89] B. Allegranzi, S. Bagheri-Nejad, C. Combescure, W. Graafmans, H. Attar, L. Donaldson, D. Pittet, Lancet, 377 (2011) 228-241.

[90] A. Mills, P. Hill, P. Robertson, J. Photochem. Photobiol. A, 237 (2012) 7-23.

[91] H. Ishiguro, Y. Yao, Y. Nakano, M. Hara. K. Sunada, K. Hashimoto, J. Kajioka, S. Fujishima, Y. Kubota, Appl. Cat. B, 129 (2013) 56-61.

[92] M. Pelaez, N. Nolan, S. Pillai, M. Seery, P. Falaras A. Kontos, M. S. P. Dunlop, J. Hamilton, J-A Byrne, K, O'Shea, M. Enterazi, D. Dionysiou, Appl. Cat. B. 25 (2012) 331-349.

[93] X. Qiu, M. Miyaguchi, K. Sunada, M. Minoshima, M. Liu, Y. Lu, D. Li, Y. Shimodaira, Y. Hosogi, Y. Kuroda, K. Hashimoto, Hybrid $CuxO/TiO_2$ Nanocomposites as Risk-Reduction Materaials in Indoors Environments, ACS Nano 6 (2012) 1609-1618.

[94] K. Sunada, S. Watanabe, K. Hashimoto, Bactericidal Activity of Copper-Deposited TiO_2 Film under weak UV Light Illumination, Environ & Environ. Sci Technol. 37 (2003) 4785-4789.

[95] O. Baghriche, S. Rtimi, C. Pulgarin, R. Sanjines, J. Kiwi, Innovative TiO_2/Cu surfaces inactivating bacteria < 5 min under low intensity visible/actinic light ACS Appl. Mater. & Interf. 4 (2012) 5234-5240

[96] G. Borkow, J. Gabbay, Copper, An Ancient Remedy Returning to Fight Microbial, Fungal and Viral Infections, Current. Chem. Biol. 3 (2009) 272-278.

[97] C. Wagner, W. Riggs, L. Davis, G. Mullenberg, (Eds) Handbook of X-ray Photoelectron spectroscopy, Perkin-Elmer Corporation Physical Electronics Division, Minnesota, USA, 1979.

[98] J. Nogier, M. Delamar, P. Ruiz, M. Gratzel, R. Thampi, J. Kiwi, X-Ray. Catal. Today, 20 (1994) 109-123.

[99] O. Bondarenko, J. Jugason, A. Ivask, K. Kasemets, M. Mortimer, A. Kahru, Toxicity of Ag, CuO and ZnO Nano-particles to Selected Envirinmental Test Organism an Mammalian Cells In-vitro: a Critical Review, Arch. Toxic 87 (2013) 1181-1200.

[100] http://www.opsi.gov.uk/si/si2000/20003184.htm#30

[101] J. Brewer, J. Clinic. Neurophys, 121 (2010) 459-60.

[102] K. Hardee, A. Bard, Electrodes, X. Photochemical Behavior of Several Polycrystalline Metal Oxides Electrodes in Aqueous Solutions, J. Electrochem. Soc. 124 (1977) 215-224.

[103] W. K Nägeli (English archive) Denkschr. Allgemein. Naturfors Ges, 33 (1983) 174-182.

[104] E. Rentz, Viral J. of Nutritional and Environ. Medicine, 13 (2003) 109-118.

[105] M. Pourbaix. Atlas of Electrochemical Equilibria in Aqueous Solutions, Nace International Pub. Co, Cebelcor, Brussels, 1974.

[106] K. Kühn, I. Chaberny, K. Massholder, M. Sticker, V. Benz, V. H-G. Sonntag,I. Erdinger, Chemosphere 53 (2003) 71-77.

[107] A. Thill, O. Zeyons, O. Spalal, F Chauvat, J. Rose, M. Auffan, A-M Flank, Environ. Sci. Technol. 40 (2006) 6151-6156.

[108] V. Nadtochenko, A. Rincon, S. Stanka. J. Kiwi, Dynamics of *E. coli* Photokilling due to Cell Wall Lysis during TiO_2 Photocatalysis, J. Photochem. Photobiol. A., 169 (2005) 131-137.

[109] C. Gunawan, W. Teoh, P. Marquis, J. Lifla, R. Amal, Induced Antimicrobial Resistance to Nano-silver, Small 5 (2009) 341-344.

[110] I. Vizcarra, Ph. Emge, Ph. Miermeister, M. Chabria, R. Konradi, V. Vogel, J. Möller, Biointerphases, 8 (2013) 22-30.

[111] K. Taylor. R. Roberts, J. Roberts, J. The challenge of hospital acquired infections (HAI), Nat. Audit Office, 2002.

[112] G. Borkow, and J. Gabbay, Puttting copper into action. Copper impregnated products with potental biocidal activities. J. FASEB, 188 (2008) 1728-1730.

[113] O. Akhavan, R. Azimiriad, S. Safa, E. Hasani, $CuO/Cu(OH)_2$ hierarchical nano-structures as bactericidal photocatalysts, J. Chem. Mater. 21 (2011) 9634-9640.

[114] O. Akhavan, E. Ghaderi Copper-oxide nanoflakes as highly sensitive and fast response self-sterilizing biosensors, J. Chem. Mater. 21 (2011)12935-12940.

[115] O. Akhavan, E. Ghaderi, Cu and CuO nanoparticles immobilized by silica thin films as antibacterial materials and catalysts, Surf. & Coatings Technol. 205 (2010) 219-223.

[116] M. Heinlaan, I. Blinova, H-C. Dubourguier, A. Kahru, Toxicity of nanosized and bulk ZnO, CuO and TiO_2 to bacteria Vibrio fischeri and crustaceans Daphnia magna and Thamnocephalusplatyuru, Chemosphere, 71 (2008) 1308-1316.

[117] I Perelshtein, G. Applerot, N. Perkas, E. Wehrschuetz-Sigl, A. Hasmann G. Guebitz, A. Gedanken CuO cotton nanocomposites: Formation, morphology, and antibacterial activity, Surf. Coat Technol. 204 (2009) 54-57.

[118] L Esteban-Tejeda, F. Malpartida, A. Esteban-Cubillo, C. Pecharroman and J. S Moya, Antibacterial and antifungal activity of a soda-lime glass containing copper nanoparticles, Nanotechnology 20 (2009) 505701.

[119] F. Gao, P. Huan, X Shuoping, L. Qingyi, Copper-based nanostructures: promising antibacterial agents and photocatalysts, Chem. Com. (2009) 3571-3573

[120] H. Irie, S. Miura, K. Kamiya K. Hashimoto, Efficient visible light-sensitive photocatalysis: Grafting Cu(II) ions onto TiO_2 and WO_3 photocatalysts, Chem. Phys. Letts. 457 (2008) 201-205.

[121] O. Baghriche, S. Rtimi, C. Pulgarin, R. Sanjines, J. Kiwi, Effect of the spectral properties of TiO_2, Cu, TiO_2/Cu sputtered films on the bacterial inactivation under low intensity actinic light J. Photochem. Photobiol. A, 251 (2013) 50-56

[122] D. Shirley, Corrections of electrostatic charged species in XPS-spectroscopy, Phys. Rev. B5 (1972) 4709-4716.

[123] K. Ishibashi, A. Fujishima T. Watanabe, K. Hashimoto, Detection of active oxidative species in TiO_2 photocatalysis using the fluorescence technique, Electrochem. Comm. 2 (2000) 207-2010.

[124] W. Tung, W. Daoud, Selfcleaning fibers via nanotechnology: a virtual reality J. Mat. Chem. 21 (2011) 7858-7869.

[125] J. Mathews, Epitaxial Growth, Part B, IBM Thomas Watson Res. Center, Academic Press, New York (1975) 382-436.

[126] V. Nadtochenko, V. Denisov, O. Savinov, J. Kiwi. Laser kinetic spectroscopy in the interfacial charge transfer between membranes cell wall, J. Photochem. Photobiol. A, 181 (2006) 401-407.

[127] J. Kiwi, C. Morrison, Dynamics of Charge Transfer on Li-doped Anatase based Catalyst powders with Enhanced Water Photo-cleavage under UV–irradiation, J. Phys. Chem. 88 (1984) 6146-6172.

[128] J. H. Nikaido, Prevention of Drug Access to Bacterial Targets. Permeability Barriers and Active Flux, Biol. Chem. 269 (1994) 3905-3909.

[129] A. Nozik, Photo-electrochemistry: Applications to Solar Energy Conversion, Annual Rev. Phys. Chem. 2 (1978)189-222.

[130] J. Bandara, I. Guasaquillo, P. Bowen L. Soare, W-F Jardim J. Kiwi, Photocatalytic Storing of O_2 as H_2O_2 Mediated by High Surface Area CuO. Evidence for the Reductive-Oxidative Interfacial Mechanism of Reaction, Langmuir, 21 (2005) 8554-8559.

[131] D. Ward, A. Bard, Photocurrent enhancement via trapping of photo-generated electrons of titanium dioxide particles, J. Phys. Chem. 86 (2004) 3599- 3604.

[132] I. Petrov, A. Myers, J. E. Greene and J. R. Abelson, Mass and energy resolved detection of ions and neutral sputtered species incident at the substrate during reactive magnetron sputtering of Ti and mixed Ar + N_2 mixtures, J. Vac. Sci. Technol. A 12(1994) 2846-2851.

[133] J. Alami, P. Persson, J. Gudmunsoon, J. Bohlmark, J. Helmersson J., Ion-assisted physical vapor deposition for enhanced film properties on nonflat surfaces J. Vac. Technol. A, 23 (2005) 278-280.

[134] S. Rossnagel, & J. Hopwood, Magnetron sputter deposition with high levels of metal ionization J., Appl. Phys. Letts, 63 (1993) 32-34.

[135] A. Fujishima, K. Hashimoto, T. Watanabe, TiO_2 Photocatalysis, Bkc Inc. Pub. Co., Tokyo, 2000.

[136] A. Mills, S. Lee, J. of Photochem. Photobiol. A 152 (2002) 233-247.

[137] M. Lazar, W. Daoud, RSC Advances 3 (2013) 4130-4140.

[138] A. Fujishima, T. Rao, D. Tryk, J. Photochem Photobiol. C. 1 (2000) 1-21.

[139] W. Doaud, J. Xin, J. Am. Ceram. Soc. 87 (2004) 953-955.

[140] W. Daoud, J. Xin, J. Sol-Gel Sci. Technol. 29 (2004) 25-29.

[141] C. Chan, T. Ko, H. Hiroaka, Surf. Sci. Reports 24 (1996) 1-54.

[142] J. Kassanen, M. Suvanto, T. Pakkanen, J. Appl. Polym. Sci. 119 (2007) 2235-2245.

[143] A. Bozzi, T. Yuranova, I. Guasaquillo, D. Laub, J. Kiwi, J. Photochem. Photobiol. A. 174 (2005) 156-164.

[144] S. Rtimi, C. Pulgarin, R. Sanjines and J. Kiwi, RSC-Adv. 3 (2013) 16345-16348.

[145] M. Radetic, V. Vodnik, S. Dimitrijevic, P. Jovancic, Z. Saponjic, J. Nedeljikocic, J. Polym. Adv. Technol. 19 (2008) 1816-1821.

[146] M. Kostic, N. Radic, M. Obradovic, S. Dimitrijevic, M. Kuraica, Plasma Process. Polym. 6 (2009) 58-67.

[147] R. Bacsa, J. Kiwi, T. Ohno, P. Albers, V. Nadtochenko, J. Phys. Chem. B. 109 (2005) 5994-6003.

[148] M. Dhananjeyan, E. Mielczarski, K. Thampi, Ph. Buffat, M. Bensimon, A. Kulik, J. Mielczarski, J. Kiwi, J. Phys. Chem. B 105 (2001) 12046-12055.

[149] K. Tennakone, C. Tilikaratne, I. Kottegoda, J. Photochem. Photobiol. A. 87 (1995) 177-179.

[150] B. Ohtani, S. Adzuma, S. Nishimoto, T. Kayiga, Polym. Degrad. Stab. 235 (1992) 53-60.

[151] Y. Chen, E. Stathatos. D. D. Dyonisiou, Surf. Coat. Technol. 202 (2008) 1944-1950.

[152] G. Balasubramiam, D. D. Dyonisiou, M. T. Suidan, I. Baduin, J-M Laine, Appl. Cat. B 47 (2004) 973-84.

[153] C. Kuo, Y. Tseng, C. Huang, Y. Li, J. Molec. Catal. 270 (2007) 93-100.

[154] H. Nizard, M. L. Kopsovina, Y. V. Shubin, Surf. Coat. Technol. 202 (2008) 4076-4085.

[155] J. Houska, S. Mraz, J. M. Schneider, J. Appl. Phys. 112 (2012) 073527

[156] J.S. Cho, Y. Han Cuomo, J. Solid State Sci. 10 (2008) 941-949.

[157] R. Wang, K. Hashimoto, A. Fujishima,; A. Chikuni, M. Kojima, E. Kitamura, A. Shimohigishi, M. Watanabe, Nature 388 (1997) 431-432.

[158] N. Sakai, R. Wang, A. Fujishima, T. Watanabe, K. Hashimoto, Langmuir 14 (1998) 5918-5920.

[159] K. Seki, N. Tachiya, J. Physical Chemistry B, 108 (2004) 4806-4810.

[160] S. Pigeot-Rémy, F. Simonet, E. Errazuriz-Cerda, J. C. Lazzaroni, D. Atlan, C. Guillard, Appl Cat. B 104 (2011) 390-398.

[161] R. Poole, C. Kumar, I. Salmon, B. Chance, J. Gen. Microb. 129 (1983) 1335-1344

[162] M. Van Loosdrecht, J. Lyklema, W. Norde, G. Schraa, A. Zender, Appl. Environ. Microb. 53 (1987) 1893-1897.

[163] C. Xu, D. Wellia, R. Amal, W. Liao, J. Loo, T. Tan, Langmuir 2 (2010) 11226-11232.

[164] D. Naumann, C. Schultz, A. Sabich, M. Kasrowsky, H. Labishinsi, New Insights into the Phase Behavior of a Complex Anionic Amphiphile: Architecture and Dynamics of Bacterial Deep Rough Lipo-polysaccharide Membranes as seen by FTIR, X-ray, and Molecular Modeling Techniques, J. Molec. Struct. 214 (1989) 213-246.

[165] J. Pitha, N. Jones, Can. J. Chem. 44 (1966) 3031-3050.

[166] C. Selle, W. Pohle, H.J. Fritzshe, Molecular Structuctural FTIR Spectroscopic Features of Lyotropically Induced Phase Transitions in Phospholipid Model Membranes. J. Molec. Struct. 481 (1999) 402-405.

[167] J. Kiwi, V. Nadtochenko, New Evidence for TiO_2 Photocatalysis during Bilayer Lipid Oxidation, J. Phys. Chem. B 108 (2004) 17675-17684

[168] W. Levin, N. Lewis, Anal. Chem. 62 (1990) 1101-1111.

[169] D. Blake, P. Maness, Z. Huang, E. Wolfrum, J. Huang, W. Jacoby, Sep. Purif. Methods 28 (1999) 1-50.

[170] A. Harmer, E. Farneth, Q. Sun, J. Am. Chem. Soc. 118 (1996) 7708-7716.

[171] M. Dhananjeyan, J. Kiwi, P. Albers, O. Enea, Helv. Chim. Acta 84 (2001) 3433-3445.

[172] I. A. Hassan, I.P. Parkin, S.P. Nair, C.J. Carmalt, Antimicrobial Activity of Copper and Copper(I) Oxide Thin Films Deposited via Aerosol-Assisted CVD. J. of Mater. Chem. B. 2 (2014) 2855-2860.

[173] Y-H. Chan, Ch.-F. Huang, K-L. Ou, P-W. Peng, Mechanical Properties and Antibacterial Activity of Copper Doped Diamond-Like Carbon Films. Surf. Coat. Technol. 2011, 206, 1037-1040.

[174] M. Ben-Sasson, K.R. Zodrow, Q. Genggeng, Y. Kang, E.P. Giannelis, and M. Elimelech Surface Functionalization of Thin-Film Composite Membranes with Copper Nanoparticles for Antimicrobial Surface Properties. Environ. Sci. Technol. 48 (2014) 384–393.

[175] L.A. Tamayo, P.A. Zapata, F.M. Rabagliati, M.I. Azocar, L.A. Munoz, X. Zhou, G.E. Thompson, M.A. Paez Antibacterial and Non-Cytotoxic Effect of Nanocomposites based in Polyethylene and Copper Nanoparticles. J. Mater. Sci. 26 (2015) 129.

[176] Y. Ohsumi, K. Kitamoto, Y. Anraku, Changes Induced in the Permeability of the Yeast Plasma Membrane by Cupric-Ion, J. Bacteriol. 170 (1988) 2676-2682.

[177] S. Robin, T. Soulimane, S. Lavelle, Interactions of Biofilm-forming Bacteria with Abiotic Surfaces, Ch 9 in RSC Nanoscience an Nanotechnology No 21, p131-135, Edited by S. Tofail, RSC 2012.

[178] G. Borkow, J. Gabbay, Biocidal Textiles can help Fight Nosocomial Infections, Med. Hypothesis 70 (2008) 990-994.

[179] S. Gould, A. Fielder, M. Morgan, J. Kenny, D. Naughton, The Antimicrobial Properties of Copper Surfaces against a Range of Important Nosocomial Pathogens, Anals Microb. 59 (2009) 151-156.

[180] J. Lemire, J. Harrison, R. Turnner, Antimicrobial Activity of Metals: Mechanisms, Molecular Targets and Applications, Nature Rev. Microbiol. 11 (2013) 371-384.

[181] N. Cioffi, L. Torsi, N. Dilaranto, G. Tantillo, L. Ghibelli, L. Sabbatini, T. Bleve-zecheo, G. Zambonin, E. Traversa, Copper Nanoparticle/Polymer Composites with Antifungal and Bacteriostatic Properties, Chem. Mater. 17 (2005) 5255–5262

[182] A. Deitch, A. Marino, T. Gillepsie, M. Albright, Silver-Nylon: a New Antimicrobial Agent, Antimicrob. Agents Chemother 23 (1983) 356-359.

[183] S. Rtimi, R. Sanjines, C. Pulgarin, J. Kiwi, Accelerated *Esherichia coli* inactivation in the Dark on Uniform Copper Flexible Surfaces, Biointerphases 9 (2014) 029012.

[184] J. Liu, D. Sonshine, S. Shervani, D. Hurt, Controlled Release of Biologically Active Ag from Ag-Surfaces, ACS Nano 4 (2010) 6903-6913.

[185] C. Fox, M. Modak, Antibacterial Silver-sulfadiazine, Antimicrob. Agents Chemother 5 (1974) 582-588.

[186] J.H. Klasen, A Historical Review of the Use of Silver in the Treatment of Burns. Renewed interest for silver, Burns 26 (2000) 131-138.

[187] P.V. Ashrani, G.L. Mun, P.M. Hande, S. Valyaveettil, Cytotoxycity and Genotoxicity of Ag-Nanoparticles in Human Cells, ACS Nano 3 (2009) 279-290.

[189] K. Holt, J. A. Bard, Interaction of Ag^+ Ions with the Respiratory Chain of *E. coli*: An Electrochemical and Scanning Elctrochemical Microscopy Study of the Antimicrobial Mechanism of Micromolar Ag-ions, Biochemistry 44 (2000) 13214-13223.

[190] L. Sondi, S. Sondi, Silver Nanoparticles as Antimicrobial Agents: a Case Study on E. coli as a Model Gram Negative Bacteria, J. Coll. Interf. Sci. 275 (2002) 177-182.

[191] H. Nikaido, Porins and Specific Diffusion Channels in Bacterial Outer Membranes, J. Biol. Chem. 269 (1994) 3905-3909.

[192] X-Z. Li, H. Nikaido, K. Williams, Silver Resistant Mutants of *E. coli* Display Active Efflux of Ag-ions and are Deficient in Porins. J. Bacteriol 179 (1997) 6127-6132.

[193] J. McLean, A. Hussain, M. Sayer, P.J. Vincent, D.J. Hughes, T.J. Smith, Antibacterial Activity of Multilayer Silver-Copper Surface Films on Catheters, Can. J. Microbiol. 39 (1993) 895-899.

[194] I. Slamborova, V. Zajicova, J. Karpiscova, P. Exnar, I. Stobor, A New Type of Protective Hybrid Coating Containing Ag and Cu and Showing Excellent Antibacterial Effects against MRSA, Mater. Sci. Eng C 33 (2013) 265-273.

[195] H. Jing, Y. Zhiming, L. Li, Antibacterial Properties and Corrosion Resistance of Cu and Ag/Cu Porous Materials, J. Biomater. Res. A 87 (2008) 33-37.

[196] S. Noimark, C. Dunnill, M. Wilson, P.I. Parkin, The Role of Surfaces in Catheter-Associated Infections, Chem. Soc. Rev. 38 (2009) 3435-3448.

[197] O. Baghriche, S. Rtimi, A. Zertal, R. Sanjines, C. Pulgarin, J. Kiwi, Accelerated Bacterial Reduction on Ag–TaN Compared with Ag–ZrNand Ag–TiN Surfaces, Appl Cat. B 174 (2015) 376-382.

[198] A.J. Thornton, Structure and Topography of Sputtered Coatings, J. Vac. Sci. Technol. 11 (1974) 666-670.

[199] E. Belin-Ferré, Surface Properties and Engineering of Complex Intermetallic, Singapore, Hackensack, N.J. USA, World Scientific, v3, 2010.

[200] J. Kiwi, V. Nadtochenko, Evidence for the Mechanism of Photocatalytic Degradation of the Bacterial Wall Membrane at the TiO_2 Interface by ATR-FTIR and Laser Spectroscopy, Langmuir 21 (2005) 4631-4641.

[201] S. Rtimi, J. Nesic, C. Pulgarin, R. Sanjines, M. Bensimon, J. Kiwi, Effect of Surface Pre-treatments on the Interfacial Processes at the Solid-Air Interface TiO_2 Films Leading to Fast Bacterial Inactivation in the Dark and Under Light, Interface Focus 5 (2015) rsfs. 2014.0046.

[202] Z. Lu, L. Zhou, Z. Zhang, W. Shi, Z. Xie, H. Xie, D. Pang, P. Shen, Cell Damage Induced by Photocatalysis in TiO_2 Thin Films, Langmuir 19 (2003) 8765-8768.

[203] S. Maheshwari, K. Singh, U. Minchita, R. Balakrishna, Elucidation of Cell Killing Mechanism by Comparative Analysis of Photoreactions on Different Types of Bacteria, Photochem. Photobiol. 88 (2012) 414-422.

[204] A. Kraeutler, A. Bard, Heterogeneous Photocatalytic Synthesis of Methane from Acetic Acid: new Photo-Kolbe Reaction Pathway, J. Am. Chem. Soc. 100 (1978) 239-2244.

[205] S. Sato, Photo-Kolbe Reaction at the Gas-Solid Interface. J. Phys. Chem, 87 (1983) 3531-3537

[206] C. Espirito Santo, E. Lam, C. Elowsky, D. Quaranta, S. Domaille, C. Chang, G. Grass, Bacterial Killing by Dry Metallic Copper Surfaces, Appl. Env. Microb. 77 (2011) 794-802.

[207] D. Quaranta, T. Krans, S. Espirito, C. Elowsky, D. Domaille, C. Chang, G. Grass, Mechanisms of Contact Mediated Killing of Yeast Cells on Dry Metallic Copper Surfaces, Appl. Env. Microb. 77 (2011) 416-426.

[208] O. Baghriche, C. Ruales, R. Sanjines, C. Pulgarin, A. Zertal, I. Stolitchnov, J. Kiwi, Ag-Surfaces Sputtered by DC and Pulsed DC-Magnetron Sputtering Effective in Bacterial Inactivation: Testing and Characterization, Surf. .Coat. Technol. 206 (2012) 2410-2416

[209] A. Fujishima, X. Zhang, D. Tryck, TiO_2 Photocatalysis and Related Surface Phenomena, Surf. Sci. Repts. 63 (2008) 515-582.

[210] J. Schneider, M. Matsuoka, M. Takeuchi, J. Zhang, Y. Horiuchi, M. Anpo, D. Bahnemann, Chemical Reviews 114 (2014) 9919-9986.

[211] G. Walters, P.I. Parkin, The Incorporation of Noble Metal Nanoparticles into Host Matrix Thin Films: Synthesis, Characterization and Applications J. Mater. Chem. 19 (2009) 574-590.

[212] S. Rtimi, M. Ballo, C. Pulgarin, J. Entenza, A. Bizzini, J. Kiwi, Duality in the *Escherichia coli* and Methicillin Resistant *Staphylococcus aureus* Reduction Mechanism under Actinic Light on Innovative Co-sputtered Surfaces. Critical Issues, Appl. Cat. A 498 (2015) 4185-4191.

[213] C. Gunawan, W. Teoh, C. Marquis, R. Amal, Cytotoxic Origin of Copper (II) Oxide Nanoparticles: Comparative Studies with Micron-Sized Particles, Leachate and Metal Sulfate Salts, ACS Nano 9 (2011) 7214-7225.

[214] C. Greulich, D. Braun, A. Peetsch, J. Diendorf, B. Siebers, M. Epple, M. Koller, The Toxic Effcts of Ag-ions and Ag Nano-Particles Towards Bacteria and Human Cells Occurs in the Same Concentration Range, RSC Advances 2 (2012) 6981-6987.

[215] A. Villegas, M. Garcia, J. Llopis, J. Fernandez-Navarro, Optical Spectroscopy of Hybrid Sol-Gel Coatings Doped with Noble Metals, J. Sol-Gel Sci.Technol. 11 (1998) 251-265.

[216] L. Merhari, Hybrid Nanocomposites for Nanotechnology, 2nd Ed. Springer Science, New York, 2009.

[217] A. Onsten, M. Gothelid, U.O. Karlsson, Atomic structure of Cu_2O (111), Surf. Sc. 603 (2009) 257–264

[218] P. Docampo, S. Guldin, U. Steiner, H.J. Snaith, Charge Transport Limitations in Self-Assembled TiO_2 Photo-anodes for Dye-Sensitized Solar Cells, J. Phys. Chem. Lett. 4 (2013) 698−703

[219] N. Kopidakis, N. R. Neale, K. Zhu, J. van de Lagemaat, A.J. Frank, Spatial Location of Transport-Limiting Traps in TiO_2 Nanoparticle Films in Dye-Sensitized Solar Cells. Appl. Phys. Lett. 2005, 87.

[220] D. Munoz-Rojas, J. Fraxedas, P. Gomez-Romero, P. Casano, Room temperature Solid-State Transformation from $Ag_2Cu_2O_3$ to $Ag_2Cu_2O_4$ by Ozone Oxidation, Journal of Solid State Chemistry 178 (2005) 295–305.

[221] D. Munoz-Rojas, G. Subias, J. Fraxedas, P. Gomez-Romero, N. Casano-Pastor, Electronic Structure of $Ag_2Cu_2O_4$. Evidence of Oxidized Silver and Copper and Internal Charge Delocalization, J. Phys. Chem. B 109 (2005) 6193-6203

[223] J. Pierson, D. Horwat, Influence of the Current Applied to the Silver Target of Ag-C-O Films Deposited by Reactive Sputtering, Appl. Surf. Sci. 53 (2007) 7522-7526.

[224] D. Adams, L. Brus, C. Chidsey, S. Creager, C. Creutz, Ch. Kagan, V.P. Kamat M. Lieberman, S. Lindsay, M. Marcus, R. Metzger, M. Beyerle, J. Miller, M. Newton, D. Rolison, O. Sankey, K. Schance, J. Yardley, X. Zhu, Charge Transfer on the Nanoscale: Current Status, J Phys. Chem. B 107 (2003) 6668–6697.

Annexe 1. Stereomicroscopy images of live and dead *E. coli* on TiO_2/Cu-PES showing the loss of bacterial viability within 120 min.

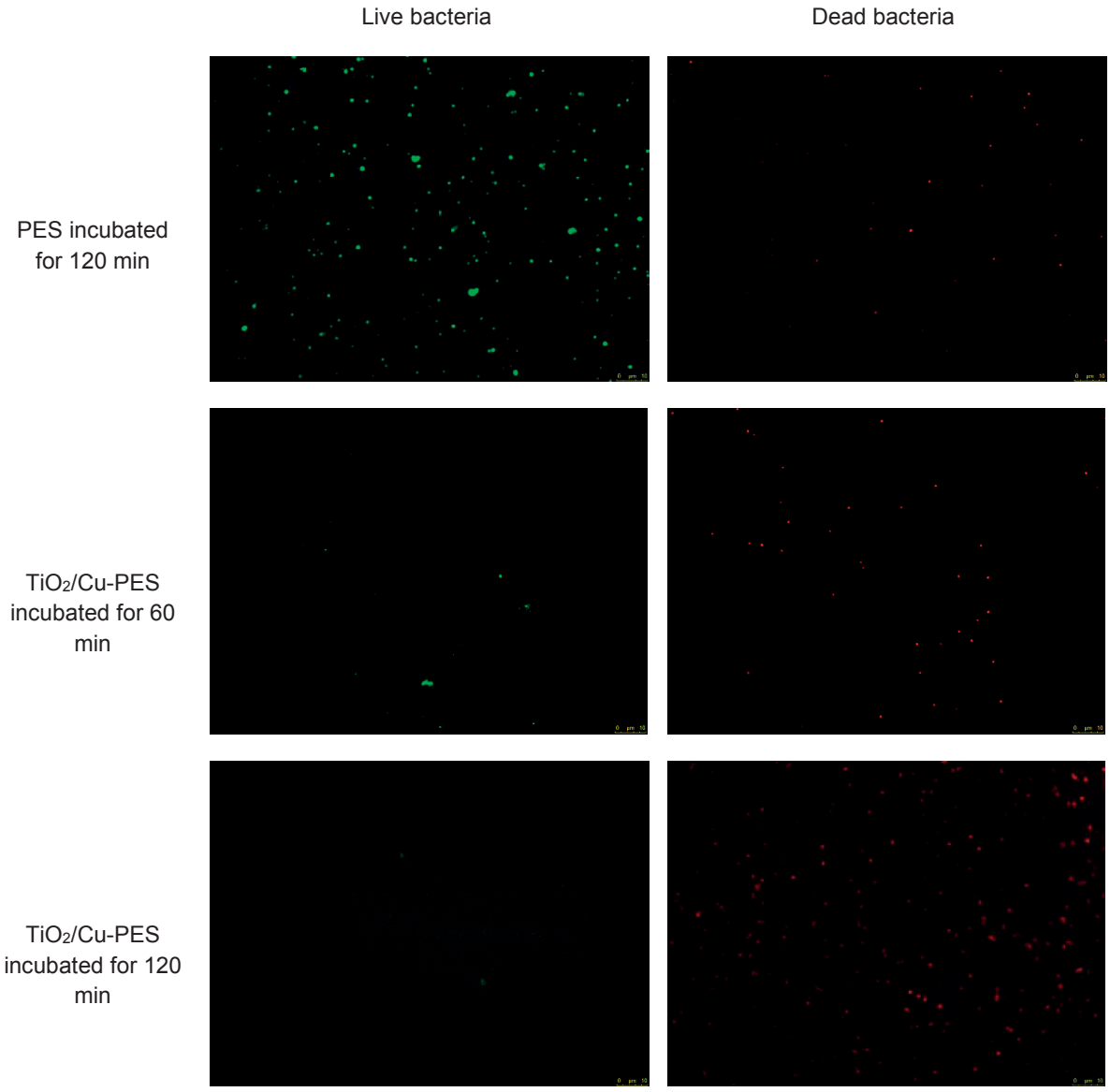

Annex 2. Optimization parameters prior to HIPIMS deposition.

Given Paramaters:

$U_{PulseOn}$	Voltage at one pulse
$I_{PulseOn}$	Current at one pulse
$t_{PulseOn}$	Time of one pulse
$t_{PulseOff}$	Time between pulses

Power of one pulse ($P_{PulseOn}$):

$$P_{PulseOn} = I_{PulseOn} \cdot U_{PulseOn} \quad [W]$$

Power of deposition (P):

$$P = P_{PulseOn} \cdot \frac{t_{PulseOn}}{\left(t_{PulseOn} + t_{PulseOff}\right)} \quad [W]$$

Example

Given Parameters:

$$U_{PulseOn} = 350\ V$$
$$I_{PulseOn} = 5\ A$$
$$t_{PulseOn} = 100\ \mu s$$
$$t_{PulseOff} = 1900\ \mu s$$

Calculation:

$$P = I_{PulseOn} \cdot U_{PulseOn} \cdot \frac{t_{PulseOn}}{\left(t_{PulseOn} + t_{PulseOff}\right)}$$
$$P = 5\ A \cdot 350\ V \cdot \frac{100\ \mu s}{(100\ \mu s + 1900\ \mu s)}$$
$$P = 5\ A \cdot 350\ V \cdot 100\ \mu s \cdot 0.0005\ \frac{1}{\mu s}$$
$$P = 5\ A \cdot 350\ V \cdot 100\ \mu s \cdot 0.0005\ \frac{1}{\mu s}$$
$$P = 87.5\ W$$

Annexe 3. Calibration of voltage for TiO_2 deposition as an example for HIPIMS calibration prior to deposition.

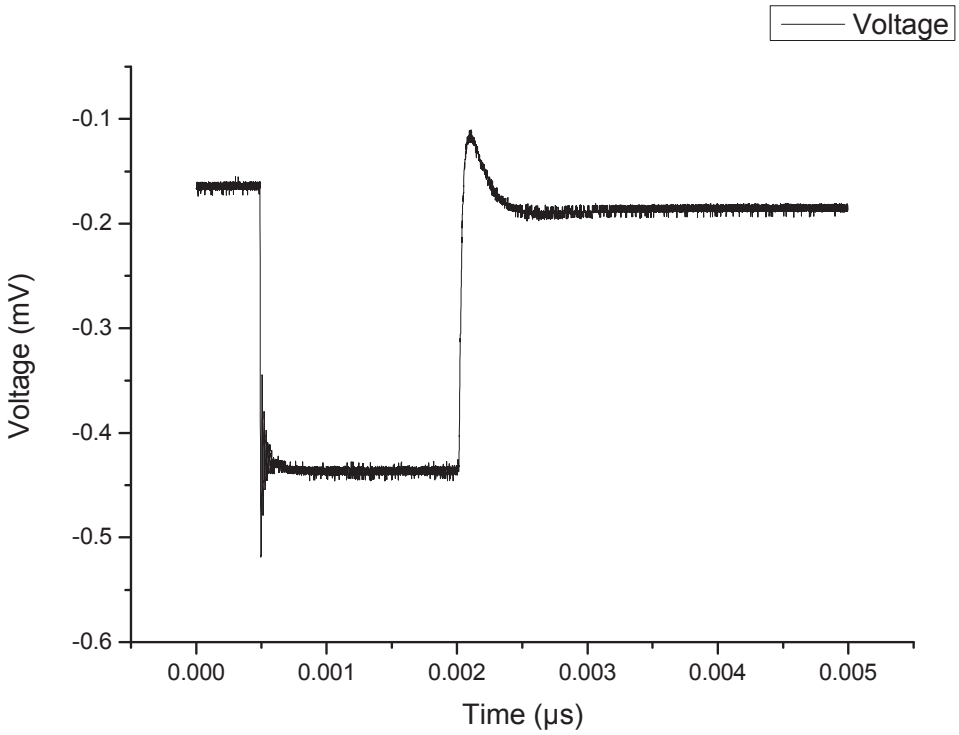

Annexe 4. XRD Patterns for Cu/CuO/TiO_2 films sputtered on polyester by HIPIMS at different times.

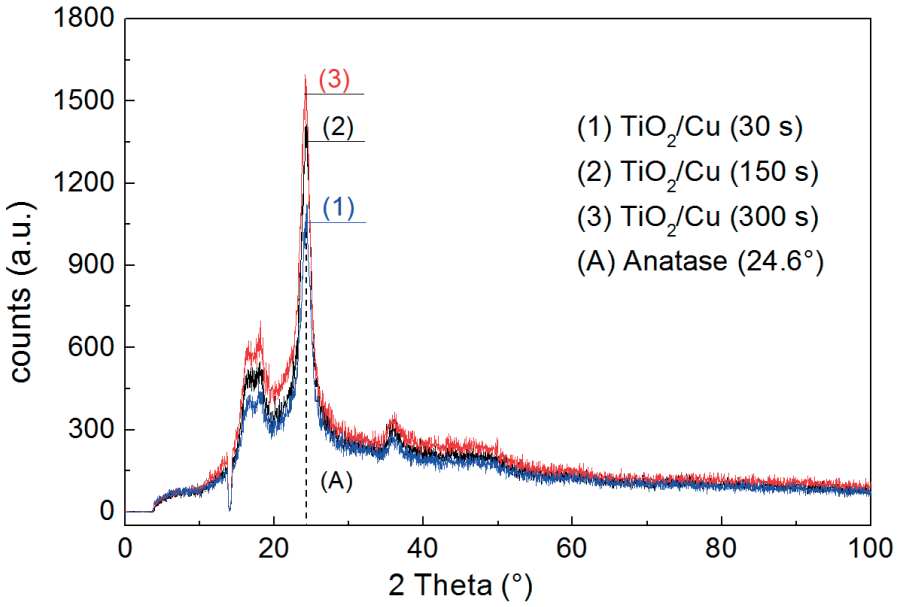

Annexe 5. Crystal phases of PE-TiO_2 sputtered: (1) pretreated with RF-air plasma for 15 min, sputtered for 1 min (2), no pretreatment sputtered for 5 min, (3) no pretreatment, sputtered for 1 min (4) pretreated with RF-air plasma for 15 min, sputtered for 8 min and finally (5) sputtered for 8 min without pretreatment.

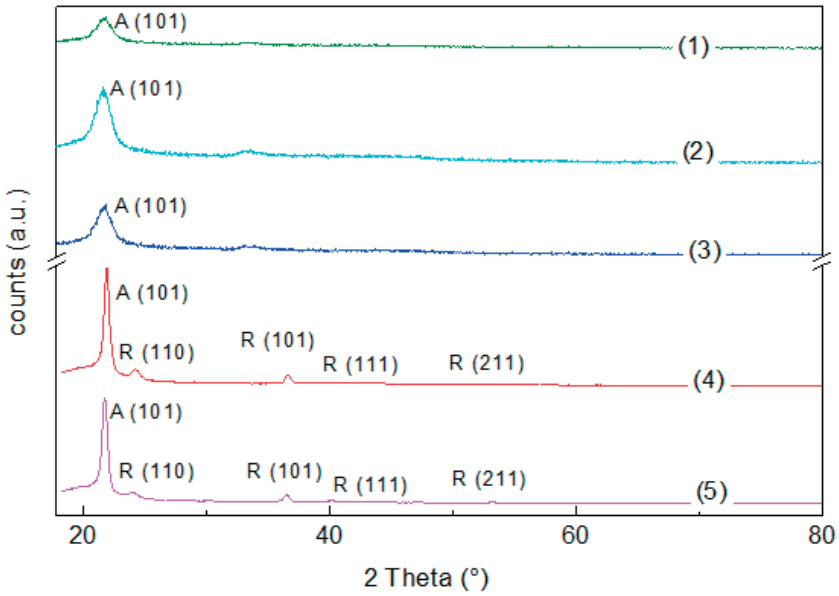

Dr. Sami Rtimi (Ph.D.)

Avenue du Tir Federal 92, 1024 Ecublens-Switzerland
Emails: sami.rtimi@epfl.ch , rtimi.sami@gmail.com

S. Rtimi is a photochemist with a strong background in microbiology and surface sciences and engineering. He was awarded a Ph.D. in Chemistry and Chemical Engineering (Antibacterial Materials for healthcare acquired infections prevention) from Swiss Federal Institute of Technology (EPFL). He started his carrier working on hospital wastewater treatment by solar photocatalysis. Since 2013, his work focuses on the development of fast antibacterial catalytic/photocatalytic ultrathin films. He is expert in coupling semiconductor nanostructures to degrade chemicals and microbiological pollutants at the solid-air-interface. S. Rtimi supervised undergraduates, Master students and actively helped his colleagues in their Ph.D. thesis.
Proficiency in French and English speaking and writing, mastering the practice of research by defining and optimizing experimental protocols. Sami have transverse leadership skills to coordinate experimental projects, coaching and team managing. He was "safety delegate" at work place (Cosec-2012-2016). He is organized, pragmatic, with excellent interpersonal skills and team oriented.

Addendum

A big majority of surfaces are susceptible to harbor pathogens in indoor environment (*houses, hospitals, schools*…) disturbing human comfort and health. Magnetron sputtering is used to apply adherent composite films on a substrate. I used this technique to depose nanoparticulate films leading to fast bacterial inactivation in the dark or under light irradiation on textile, polyethylene, and lastly on polyurethane 3D-catheters. The infection due to catheters is a major problem since it dessiminates bactertia directly to the blood vessels. The sputtering deposition of different metal/metal oxides uniform films on catheters is an innovative antibacterial approach. I recently reported at EPFL, for the first account until now, deposition on 3D geometry objects by modifying the magnetron sputtering unit (IP: TTO-EPFL ref 6.1319).

PROFESSIONAL MEMBERSHIPS

- Swiss Chemical Society- regular membership (Photochemistry section)
- European Society for Photochemistry
- European Society of Clinical Microbiology and Infectious Diseases (ESCMID)
- American Chemical Society (ACS)
- European Association of Research Managers and Administrators (EARMA)
- Royal Society of Chemistry (RSC)
- SciRev: Speeding-up Scientific Knowledge Production
- European Cooperation for Science and Technology (COST actions).

PEER-REVIEWED ARTICLES (* Stands for corresponding author**).**

1- A. Camarasa Mena, **S. Rtimi***, C. Pulgarin, J-C Lavanchy, J. Kiwi, Grafted semiconductors on PE-films leading to bacterial inactivation: synthesis, characterization and mechanism, Colloids and Surfaces A: Physicochemical and Engineering Aspects xx (2016) accepted

2- Sami Rtimi*, Cesar Pulgarin, Victor A. Nadtochenko, Fedor E. Gostev, Ivan V. Shelaev, John Kiwi, FeOx-TiO_2 Film with Different Microstructures Leading to Femtosecond Transients with Different Properties: Biological Implications under Visible Light, *Nature-Scientific Reports* xx (2016) accepted.

3- S. Achache, A. Alhussein, S. Lamri, M. François, F. Sanchette, C. Pulgarin, J. Kiwi and **S. Rtimi***, Sputtered Gum metal thin films showing bacterial inactivation and biocompatibility, Colloids and Surfaces B: Biointerfaces (2016) doi:10.1016/j.colsurfb.2016.07.007

4- Myriam K.S. Ballo, **Sami Rtimi**, César Pulgarin, Nancy Hopf, Aurélie Berthet, John Kiwi, Philippe Moreillon, José M. Entenza and Alain Bizzini, In Vitro and In Vivo Effectiveness of an Innovative Silver-Copper Nanoparticle Coating of Catheters to Prevent Methicillin-Resistant Staphylococcus aureus Infection, *Antimicrob. Agents Chemother.* doi:10.1128/AAC.00959-16

5- Alexander Gulin, Victor Nadtochenko, Artyom Astafiev, Valentina Pogorelov, **Sami Rtimi**, and Alexander Pogorelov, Correlating microscopy techniques and ToF-SIMS analysis of mammalian full-grown oocyte, *RSC-Analyst* 141 (2016) 4121-4129.

6- **Sami Rtimi**, César Pulgarin, Michael Bensimon, John Kiwi, New evidence for Cu-decorated binary-oxides mediating bacterial inactivation/mineralization in aerobic media, *Colloids and Surfaces B: Biointerfaces* 144 (2016) 222-228.

7- Myriam K.S. Ballo, **Sami Rtimi**, Stefano Mancini, John Kiwi, César Pulgarin, José Manuel Entenza, Alain Bizzini, Bactericidal Activity and Mechanism of Action of Copper-Sputtered Flexible Surfaces Against Multidrug-Resistant Pathogens, *Applied Microbiology and Biotechnology* (2016).

8- **Sami Rtimi***, Rosendo Sanjines, Cesar Pulgarin, John Kiwi. Quasi-Instantaneous Bacterial Inactivation on Cu-Ag Nano-particulate 3D-Catheters in the Dark and Under Light: Mechanism and Dynamics. *ACS Appl. Mater. Interfaces*, 8 (2016) 47-55.

9- **Sami Rtimi***, Rosendo Sanjines, Cesar Pulgarin, John Kiwi. Microstructure of Cu-Ag Uniform Nanoparticulate Films on Polyurethane 3D-catheters: Surface Properties. *ACS Appl. Mater. Interfac*es, 8 (2016) 56-63.

10- Stefanos Giannakis, Cristina Ruales-Lonfat, **Sami Rtimi**, Sana Thabet, Pascale Cotton, Cesar Pulgarin. Castles fall from inside: Evidence for dominant internal photo-catalytic mechanisms during treatment of Saccharomyces cerevisiae by photo-Fenton at near-neutral pH, *App.* Catalysis *B: Environmental* 185 (2016) 150–162.

11- **S. Rtimi***, S. Giannakis, M. Bensimon, C. Pulgarin, R. Sanjines, J. Kiwi, Supported TiO_2 films deposited at different energies: Implications of the surface compactness on the catalytic kinetics, *Applied Catalysis B: Environmental* 191 (2016) 42-52.

12- **S. Rtimi**, R. Sanjines, J. Kiwi, C. Pulgarin, M. Bensimon, I. Khmel, V, Nadtochenko, Innovative photocatalyst (FeOx-TiO_2): transients induced by Femtosecond laser leading to bacterial inactivation under visible light, *RSC-Advances* 5 (2015) 101751-101759.

13- Tommaso Nardi, **Sami Rtimi***, Cesar Pulgarin, Yves Leterrier, Antibacterial surfaces based on functionally graded photocatalytic Fe_3O_4@TiO_2 core-shell nanoparticles/epoxy composites, *RSC-Advances* 5 (2015) 105416 - 105421.

14- Stefanos Giannakis, **Sami Rtimi**, Efthymios Darakas, Antoni Escalas-Cañellas and César Pulgarin, Light wavelength-dependent *E. coli* survival changes after simulated solar disinfection of secondary effluent, *Photochemical & Photobiological Sciences*, 14 (2015) 2238-2250.

15- **S. Rtimi***, S. Giannakis, R. Sanjines, C. Pulgarin, M. Bensimon, J. Kiwi, Insight on the photocatalytic bacterial inactivation by co-sputtered TiO_2–Cu in aerobic and anaerobic conditions, *Applied Catalysis B: Environmental* 182 (2016) 277–285.

16- **S. Rtimi***, C. Pulgarin, R. Sanjines and J. Kiwi, Novel FeOx–polyethylene transparent films: synthesis and mechanism of surface regeneration, *RSC-Advances* 5 (2015) 80203-80211.

17- Audrey Bonnefond, Edurne Gonzalez, Jose Maria Asua, Jose Ramon Leiza, John Kiwi, Cesar Pulgarin, **Sami Rtimi***, New evidence for hybrid acrylic/TiO_2 films inducing bacterial inactivation under low intensity simulated sunlight, *Colloids and Surfaces B: Biointerfaces* 135 (2015) 1-7.

18- **Sami Rtimi**, Cesar Pulgarin, Rosendo Sanjines, Victor Nadtochenko, Jean-Claude Lavanchy, John Kiwi, Preparation and Mechanism of Cu-Decorated TiO_2–ZrO_2 Films

Showing Accelerated Bacterial Inactivation, *ACS Appl. Mater. Interfaces*, *7* (23) (**2015)** 12832–12839

19- **S. Rtimi**, C. Pulgarin, R. Sanjines, J. Kiwi, Accelerated self-cleaning by Cu promoted semiconductor binary-oxides under low intensity sunlight irradiation, *Applied Catalysis B: environmental* 180 (2016) 648-655.

20- **S. Rtimi**, M.K.S. Ballo, D. Laub, C. Pulgarin, J.M. Entenza, A. Bizzini, R. Sanjinés, J. Kiwi, Duality in the *Escherichia coli* and methicillin resistant *Staphylococcus aureus* reduction mechanism under actinic light on innovative co-sputtered surfaces, *Applied Catalysis A: General*, 498 (2015) 185-191.

21- O. Baghriche, **S. Rtimi**, A. Zertal, C. Pulgarin, R. Sanjinés, J. Kiwi, Accelerated bacterial reduction on Ag–TaN compared with Ag–ZrN and Ag–TiN surfaces, *Applied Catalysis B: Environmental*, 174–175 (2015) 376-382.

22- **S. Rtimi**, C. Pulgarin, R. Sanjinés, J. Kiwi, Kinetics and mechanism for transparent polyethylene -TiO_2 films mediated self-cleaning leading to MB dye discoloration under sunlight irradiation, *Applied Catalysis B: Environmental*, 162 (2015) 236-244.

23- Jelena Nesic, **Sami Rtimi***, Danièle Laub, Goran M. Roglic, Cesar Pulgarin, John Kiwi, New evidence for TiO_2 uniform surfaces leading to complete bacterial reduction in the dark: Critical issues, *Colloids and Surfaces B: Biointerfaces*, 123 (2014) 593-599.

24- John Kiwi, **Sami Rtimi**, Jelena Nesic, Cesar Pulgarin, Rosendo Sanjines, Michael Bensimon, Effect of surface pretreatment of TiO_2 films on interfacial processes leading to bacterial inactivation in the dark and under light irradiation, *Interface Focus* 5: 20140046.

25- **Sami Rtimi***, Rosendo Sanjines, Mariusz Andrzejczuk, César Pulgarin, Andrzej Kulik, John Kiwi, Innovative transparent non-scattering TiO_2 bactericide thin films inducing increased E. *coli* cell wall fluidity, *Surface and Coatings Technology*, 254 (2014) 333-343.

26- **Sami Rtimi**, Oualid Baghriche, Cesar Pulgarin, Arutiun Ehiasarian, Ralf Bandorf, John Kiwi, Comparison of HIPIMS sputtered Ag- and Cu-surfaces leading to accelerated bacterial inactivation in the dark, *Surface and Coatings Technology*, 250 (2014) 14-20.

27- **Sami Rtimi**, Rosendo Sanjines, Michael Bensimon, Cesar Pulgarin, John Kiwi, Accelerated *Escherichia coli* inactivation in the dark on uniform copper flexible surfaces, *Biointerphases*, 9 (2014) 029012-029018.

28- John Kiwi, **Sami Rtimi**, Rosendo Sanjines, Cesar Pulgarin, TiO_2 and TiO_2-Doped Films Able to Kill Bacteria by Contact: New Evidence for the Dynamics of Bacterial Inactivation in the Dark and under Light Irradiation, *International Journal of Photoenergy*, Volume 2014, Article ID 785037, 17 pages.

29- Francesca Petronella, **Sami Rtimi***, Roberto Comparelli, Rosendo Sanjinés, Cesar Pulgarin, M. Lucia Curri, John Kiwi, Uniform TiO_2/In_2O_3 surface films effective in bacterial inactivation under visible light, *J. Photochemistry and Photobiology A: Chemistry*, 279 (2014) 1-7.

30- **Sami Rtimi**, Oualid Baghriche, Cesar Pulgarin, Jean-Claude Lavanchy, John Kiwi, Growth of TiO_2/Cu films by HiPIMS for accelerated bacterial loss of viability, *Surface and Coatings Technology*, 232 (2013) 804-813.

31- **Sami Rtimi**, Cesar Pulgarin, Oualid Baghriche and John Kiwi, Accelerated bacterial inactivation obtained by HIPIMS sputtering on low cost surfaces with concomitant reduction in the metal/semiconductor content, *RSC Advances*, 3 (2013) 13127-13130.

32- **Rtimi S.**, Pulgarin C., Kiwi J., Innovative Cu and Cu/TiO_2 ultrathin adhesive films deposited by HIPIMS inducing accelerated inactivation of *E. coli*, MRSA under solar and actinic light, *European Cells and Materials* (2013).

33- **S. Rtimi**, C. Pulgarin, R. Sanjines and J. Kiwi, Innovative semi-transparent nanocomposite films presenting photo-switchable behavior and leading to a reduction of the risk of infection under sunlight, *RSC Advances*, 3 (2013) 16345-16348.

34- **S. Rtimi***, R. Sanjines, C. Pulgarin, A. Houas, J.-C. Lavanchy, J. Kiwi, Coupling of narrow and wide band-gap semiconductors on uniform films active in bacterial disinfection under low intensity visible light: Implications of the interfacial charge transfer (IFCT), *J. Hazardous Materials*, 260 (2013) 860-868.

35- **S. Rtimi***, M. Pascu, R. Sanjines, C. Pulgarin, M. Ben-Simon, A. Houas, J.-C. Lavanchy, J. Kiwi, ZrNO–Ag co-sputtered surfaces leading to E. coli inactivation under actinic light: Evidence for the oligodynamic effect, *Applied Catalysis B: Environmental*, 138–139 (2013) 113-121.

36- **Sami Rtimi***, César Pulgarin, Michael Bensimon, John Kiwi, Evidence for TiON sputtered surfaces showing accelerated antibacterial activity under simulated solar irradiation, *Solar Energy*, 93 (2013) 55-62.

37- **Sami Rtimi**, Oualid Baghriche, Rosendo Sanjines, Cesar Pulgarin, Michael Bensimon, John Kiwi, TiON and TiON-Ag sputtered surfaces leading to bacterial inactivation under indoor actinic light, *J. Photochemistry and Photobiology A: Chemistry*, 256 (2013) 52-63.

38- O. Baghriche, **S. Rtimi**, C. Pulgarin, C. Roussel, J. Kiwi, RF-plasma pretreatment of surfaces leading to TiO_2 coatings with improved optical absorption and OH-radical production, *Applied Catalysis B: Environmental*, 130–131 (2013) 65-72.

39- **S. Rtimi**, C. Pulgarin, J. Kiwi, RF-plasma and UVC pretreatment increasing the metal and semiconductor nanoparticles bacterial inactivation in the dark and under light irradiation, *European Cells and Materials* 26-suppl.6 (2013) 103.

40- **S. Rtimi**, C. Pulgarin, J. Kiwi, Innovative Cu and Cu/TiO_2 ultrathin adhesive films deposited by HIPIMS inducing accelerated inactivation of *E. coli* and MRSA under solar and actinic lights, *European Cells and Materials* 26-suppl.6 (2013) 26.

41- O. Baghriche, **S. Rtimi**, C. Pulgarin, R. Sanjines, J. Kiwi, Effect of the spectral properties of TiO_2, Cu, TiO_2/Cu sputtered films on the bacterial inactivation under low intensity actinic light, *J. Photochemistry and Photobiology A: Chemistry*, 251 (2013) 50-56.

42- O. Baghriche, **S. Rtimi**, C. Pulgarin, R. Sanjines, J. Kiwi, Innovative TiO_2/Cu Nanosurfaces Inactivating Bacteria in the Minute Range under Low-Intensity Actinic Light, *ACS Applied Materials & Interfaces*, 4 (2012) 5234-5240.

43- **S. Rtimi**, O. Baghriche, C. Pulgarin, R. Sanjines, J. Kiwi, Design, testing and characterization of innovative TiN–TiO_2 surfaces inactivating bacteria under low intensity visible light, *RSC Advances*, 2 (2012) 8591–8595.

44- **S. Rtimi**, O. Baghriche, R. Sanjines, C. Pulgarin, M. Ben-Simon, J.-C. Lavanchy, A. Houas, J. Kiwi, Photocatalysis/catalysis by innovative TiN and TiN-Ag surfaces inactivate bacteria under visible light, *Applied Catalysis B: Environmental*, 123–124 (2012) 306-315.

Patent: "Method and apparatus for coating nanoparticulate films on complex substrates" In the name of: Ecole Polytechnique Federale de Lausanne (EPFL), Inventors: Kiwi Juan, **Rtimi Sami**, Pulgarin César, Y/Ref.: 6.1319-PCT, O/Ref.: P2618PC00 / 0013-268 / bw-lm.

BOOK CHAPTERS:

45- Ed. Grisser, *Thin Film Coatings for Biomaterials and Biomedical Applications*, Chapter 16: Uniform, adhesive and low cytotoxic films accelerating bacterial reduction in the dark and under visible light. **Sami Rtimi**, Cesar Pulgarin and John Kiwi. WoodHead Publishing (Elsevier), 2016 ***ISBN***: 9781782424536.

46- Ed. Jinlian Hu, "*Active Coatings for Smart Textiles*". J. Kiwi and **S. Rtimi**, Environmentally mild self-cleaning processes on textile surfaces under daylight irradiation: Critical issues, Elsevier Limited (2016) Chapter 3. http://dx.doi.org/10.1016/B978-0-08-100263-6.00003-4.

47- Ed. Dominique Persano Adorno, Sergey Pokutnyi "*Advances in Semiconductor Research*", Nova Science Publisher, **Sami Rtimi**, Cesar Pulgarin, Rosendo Sanjines, John Kiwi, chapter 10: Titanium Dioxide Coupled with Small Band-Gap Metal Oxides Sputtered Films for Bacterial Inactivation on Textiles, (2015) ***ISBN***: 978-1-63321-788-1

48- Ed. Md. Ibrahim H. Mondal, *Textiles: History, Properties, and Performance*, **Sami Rtimi**, Cesar Pulgarin, Rosendo Sanjines and John Kiwi, Chapter 10: Innovative Ag-textile prepared by colloidal, conventional sputtering and HIPIMS including fast bacterial inactivation: critical issues. Nova Science Publisher Inc. (2014) ***ISBN***:978-1-63117-262-5.

49- Ed. A. Méndez-Vilas, "*Microbial pathogens and strategies for combating them: science, technology and education*", J. Kiwi, **S. Rtimi**, C. Pulgarin, Cu, Cu/TiO_2 and Ag thin films sputtered by up to date methods on non-thermal thin resistant substrates leading to bacterial inactivation, Formatex, Microbiology Book Series, ***ISBN***-13 Vol.1: 978-84-939843-9-7.

CONFERENCES AND PROJECTS MEETINGS:

50- The First International Conference on "New Photocatalytic Materials for Environment, Energy and Sustainability" **2016** (Gottingen, Germany), ***S. Rtimi****, C. Pulgarin, J. Kiwi*, Innovative Cu-decorated TiO_2-ZrO_2 Films Showing Accelerated Bacterial Inactivation and Self-Cleaning.

51- Smart and Green Interfaces Conference, **2016** (Athens, Greece) *John Kiwi,* ***Sami Rtimi****, Cesar Pulgarin*, Self-cleaning Processes by polymer/textiles sputtered with semiconductors under sunlight & mild environmental conditions.

52- Swiss Chemical Society-Photochemistry Section Annual Meeting September 8, **2015** (Zurich, Switzerland) ***Sami Rtimi****, Cesar Pulgarin, John Kiwi,* Innovative PE-TiO_2 flexible surfaces showing self-sterilizing and self-cleaning properties.

53- Workshop on strategies to reduce catheter-associated urinary tract infections, Thursday 2 July **2015** (Empa, St.Gallen, Switzerland) ***Sami Rtimi****, John Kiwi, César Pulgarin*, Preparation of combined metal oxides bactericidal surfaces for hospital acquired infection prevention: the case of catheters in the dark and under light.

54- 6th International conference on HIPIMS, June **2015** (Braunschweig, Germany) ***Sami Rtimi****, Cesar Pulgarin, John Kiwi*, Comparative study DCMS vs HIPIMS depositions of TiO_2-flexible surfaces showing self-cleaning properties

55- 15th Conference of the International Association of Colloid and Interface Scientists, May 24th-29th **2015**, (Mainz, Germany), *J. Kiwi,* ***S. Rtimi****, C. Pulgarin*, Biointerfaces leading to accelerated viability loss under light on colloidal TiO_2.

56- European Materials Research Society, E-MRS Spring Meeting, May **2015** (Lille, France), ***Sami Rtimi****, Cesar Pulgarin, Rosendo Sanjines, John Kiwi*, Innovative supported nanostructures involving highly resisting oxynitrides for antibacterial application.

57- Smart and Green Interfaces Conference April **2015** (Belgrade, Serbia) COST MP1106 Annual MC meeting, *J. Kiwi,* ***S. Rtimi****, C. Pulgarin* , Uniform, adhesive TiO_2 biointerfaces leading to accelerated viability loss under light and to cultivability loss in the dark.

58- D.Day 2014, Life Sciences Symposium from & for PhDs October **2014** (Lausanne, Switzerland), *M. K. S. Ballo,* ***S. Rtimi****, J.M. Entenza, J. Kiwi, C. Pulgarin, A. Bizzini*, Antimicrobial activity of copper -sputtered surfaces against multidrug - resistant pathogens,

59- Limpid EU project meeting January **2014** (Bangkok) *J. Kiwi,* ***S. Rtimi****, C. Pulgarin*, Critical Issues: a) Bacterial Inactivation by TiO_2 transparent non-scattering sputtered surfaces under light, b) by TiO_2-textiles in the dark.

60- Limpid EU project meeting January **2014** (Bangkok), *J. Kiwi,* ***S. Rtimi****, C. Pulgarin, R. Sanjines*, Cu/CuO and TiO_2-Cu/CuO Antibacterial Surfaces.

61- "Smart and Green interfaces" - 4th COST MP1106 Annual meeting, April 22nd–24th, **2014** (Marseille, France), ***S. Rtimi****, J. Kiwi, C. Pulgarin*, Solar light-induced antibacterial activity

under mild environmental conditions by pretreated polyethylene-TiO_2 thin films. Critical issues.

62- 5th International conference on HIPIMS 2-3 July **2014** (Sheffield, England) ***Sami Rtimi,*** *Cesar Pulgarin, Arutiun Ehiasarian, Ralf Bandorf and John Kiwi*, Ag- and Cu-flexible surfaces leading to fast bacterial inactivation in the dark: comparative study DCMS vs HIPIMS depositions.

63- ICBBA-2014, 2nd International Conference on Biological & Biomimetic Adhesives 6-9 May **2014** (Istanbul, Turkey) ***S. Rtimi,*** *C. Pulgarin, J. Kiwi*, Problems related to *E.coli* adhesion on uniform adhesion prepared low temperature hindering bacterial inactivation. Critical issues.

64- Workshop on antimicrobial and antibacterial surfaces, Innovative surfaces, 30.6.**2014** (Bern, Switzerland) ***Sami Rtimi,*** *Cesar Pulgarin and John Kiwi*, Preparation and evaluation of TiO_2 uniform, and adhesives films able to inactivate bacteria in the minute range.

65- **BioMicroWorld2013**, V International Conference on Environmental, Industrial and Applied Microbiology, 2-4 October **2013** (Madrid, Spain) ***S. Rtimi,*** *C. Pulgarin, J. Kiwi*, Metal-semiconductor sputtered surfaces leading to an accelerated bacterial loss of viability under light irradiation,

66- **BioMicroWorld2013**, V International Conference on Environmental, Industrial and Applied Microbiology, 2-4 October **2013** (Madrid, Spain), *John Kiwi; Cesar Pulgarin;* ***Sami Rtimi***, TiO_2 polyethylene films (PE) pretreated by RF-plasma and UVC leading to bacterial inactivation under light with hydrophobic-hydrophilic conversion.

67- European Materials Resaearch Society, 27-31 May **2013** (Strasbourg, France), ***S. Rtimi,*** *O. Baghriche, R. Sanjinés, C. Pulgarin, J. Kiwi*, Ag-TiN and Ag-ZrN Bactericide Nanocomposites Deposited by Magnetron Sputtering; Photocatalysis/Catalysis inactivation of *E. coli*.

68- PSS2013-The Photocatalytic and Superhydrophilic Surfaces Workshop, PSS2013, 12th/13th December **2013** (Manchester Museum, England), *J. Kiwi,* ***S. Rtimi,*** *C. Pulgarin, R. Sanjines*, RF-Plasma and UVC Pretreatment of Transparent non-Scattering Uniform Surfaces Sputtered by TiO_2 Implications for Bacterial Inactivation.

69- ISSIB-2013, The 4th International Symposium on Surface and Interface of Biomaterials 24-28 September **2013** (Roma, Italy), ***S Rtimi,*** *C Pulgarin, J Kiwi*, RF-plasma and UVC pretreatment increasing the metal and semiconductor nanoparticles bacterial inactivation in the dark and under light irradiation.

70- ISSIB-2013, The 4th International Symposium on Surface and Interface of Biomaterials 24-28 September **2013** (Roma, Italy), ***S Rtimi,*** *C Pulgarin, J Kiwi*, Innovative Cu and Cu/TiO_2 ultrathin adhesive films deposited by HIPIMS inducing accelerated inactivation of *E. coli*, MRSA under solar and actinic light.

ACKNOWLEDGED EFFORT

71- Laura Suárez, Cesar Pulgarin, Christophe Roussel, John Kiwi, Preparation, kinetics, mechanism and properties of semi-transparent photocatalytic stable films active in dye degradation, *Applied Catalysis A: General*, 516 (2016) 70-80.

72- Amela Groso, Alke Petri‐Fink, Barbara Rothen‐Rutishauser, Heinrich Hofmann and Thierry Meyer, Engineered nanomaterials: toward effective safety management in research laboratories, *J. Nanobiotechnol* (2016) 14:21

73- Laura Suárez, Huiyu Dong, Cesar Pulgarin, Rosendo Sanjines, Zhimin Qiang, John Kiwi, Innovative Photo-Fenton catalysis by PE-FeOx films leading to methylene blue (MB) degradation: kinetics, surface properties and mechanism, Applied Catalysis A: General, 519 (2016) 68-77.